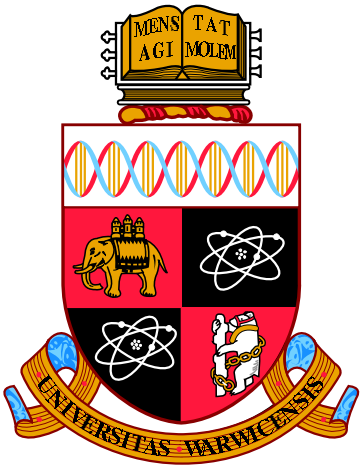

Developing Force Measurement Techniques for Cell Mechanics and Adhesion

by

Tianrong Jin

Thesis

Submitted to the University of Warwick

for the degree of

Doctor of Philosophy

School of Engineering

October 2016

WARWICK
THE UNIVERSITY OF WARWICK

Contents

List of Tables

List of Figures

Acknowledgements

Foremost, I am very thankful to my supervisor Dr Isaac Kuo-Kang Liu for his support and guidance throughout the time as his student. I have been incredibly lucky and profoundly grateful to have a supervisor who cared so much about my research and who responded to my questions and queries so promptly and perceptively. In particular, I thank him for his help and comments on the paperwork burdens.

My sincere thank also goes to Dr Richard Siow and Dr Li Li from King's College London for our fruitful collaboration and their time in teaching me skills required for cell culture and biological experiments. Their insightful guidance has been invaluable concerning the collagen gel based cell contraction experiments. Moreover, thanks are also due to our collaborators Dr Claire Hills and Prof. Paul Squires from the University of Lincoln (previous from School of Life Science, University of Warwick) for their help with AFM cell-to-cell adhesion experiments.

This PhD project is fully funded by the bursary programme from School of Engineering, University of Warwick and I would like express my gratitude for its financial and technical support. Also, it has been a great pleasure to received help from Dr Eleftherios Siamantouras for his kind assistance during the design of cell mechanics tester. I would also like to thank Dr Nathaniel Shiers for his comments on revising this thesis.

I owe a debt of thanks to my parents, Zhonghua Jin and Peiling Ying for their years and years emotional support and unconditional love. In particular, I would like to thank my mother for pushing me when I experienced ups and downs during my study in UK.

Last but not least, my special thanks are reserved for my fiancée, Anyi Zou for her continued tolerance, support, encouragement and painstaking care during writing the thesis. I cannot stop being amazed and inspired by her curiosity of science and exploration of unknown. I also thank her in advance for not crying when she reads this. It is to her that I would like to dedicate this thesis.

Tianrong Jin

University of Warwick,

July, 2016

Declarations

I hereby declare that the work on this thesis, submitted in partial fulfilment of the requirements for the degree of Doctor of Philosophy at the University of Warwick, presents my own work and has not been previously submitted to any other institution for any degree, diploma or other qualification. The contribution of collaborative work has been specifically acknowledged. All sources of information have been acknowledged by means of references and bibliography. Published work is contained in the Appendix.

Parts of this thesis have been published by the author:

- Tianrong Jin, Li Li, Richard CM Siow, and Kuo-Kang Liu. Collagen matrix stiffness influences fibroblast contraction force. Biomedical Physics & Engineering Express 2, no.4, (2016): 047002. doi: 10.1088/2057-1976/2/4/047002
- Tianrong Jin, Li Li, Richard CM Siow, and Kuo-Kang Liu. A novel collagen gel-based measurement technique for quantitation of cell contraction force. Journal of the Royal Society Interface 12, no.106 (2015): 20141365. doi: 10.1098/rsif.2014.1365
- Claire E. Hills, Tianrong Jin, Eleftherios Siamantouras, Issac KK Liu, Kieran P. Jefferson, and Paul E. Squires. *'Special K'* and a loss of cell-to-cell adhesion in proximal tubule-derived epithelial cells: modulation of the adherens junction complex by ketamine. PloS One 8, no.8 (2013): e71819. doi: 10.1371/journal.pone.0071819

Parts of this thesis have been presented by the author:

- Tianrong Jin, Richard C. Siow, Li Li and Kuo-Kang Liu. Collagen matrix stiffness influencing on fibroblast contraction force. Frontiers in Bioengineering and Biotechnology. 10^{th} World Biomaterials Congress, Montréal, Canada, 17^{th} May - 22^{nd} May, 2016.doi: 10.3389/conf.FBIOE.2016.01.01917

- Tianrong Jin, Richard C. Siow, Li Li and Kuo-Kang Liu. A new gel-based sensing technique for quantitative measurement of cell contraction force. 8^{th} IEEE EMBS PGBiomed International Student Conference, University of Warwick, Coventry, UK, 15^{th} - 17^{th} July, 2014

- R.C. Siow, T. Mughal, T. Jin, L. Li, M. Parsons, I.K.K. Liu and G.E. Mann. Transforming growth factor-β_1 modulates redox signalling, migration and contractility in human aortic adventitial fibroblasts. Society for Free Radical Research International, Kyoto, Japan, 2014.

- Tianrong Jin and Kuo-Kang Liu. Nano-Mechanical study of biological cells. Physics of Living Matter 8^{th} Edition, Cambridge, UK, 19^{th} - 20^{th} September, 2013.

Abstract

Cellular force is essential in maintaining the normal function of a biological cell. The primary goal of this study is to develop experimental methods to quantitatively determine forces generated from cell contraction and cell-to-cell adhesion. A novel method has been developed to measure the cell contraction forces exerted within a cell-embedded collagen matrix. The technique provides a 3D cell-matrix model which allows estimation of the cell contraction forces over a certain period of time. It was found that embedded fibroblast cells are able to cause a shrinkage of their surrounding matrix due to cell contractility. Tailored equipment which has ultimate force and displacement resolutions of 10 nN and 100 nm respectively has been constructed to accurately determinate the elasticity of cell-embedded collagen matrix. In combination with a mathematical model, the cell contraction force can be calculated based on the geometric parameters of the collagen matrix before and after the shrinkage. Reagents of agonist (histamine) or antagonist (ML-7) have been used to stimulate or block the fibroblast contraction force. They both show the effect of altering the stiffness of an extracellular matrix which is critical in the determination of cell contraction forces. More importantly, the analysis of the measured data based on a non-linear mechanical model have also confirmed that the elasticity of the extracellular matrix will influence the fibroblast contraction force.

Cell-to-cell adhesion is an intricate interplay of mechanical, chemical and electrical signals between cells. A novel method based on Atomic Force Microscopy Single Cell Force Spectroscopy (AFM-SCFS) has been applied to examine cell-to-cell adhesion of human kidney proximal tubule HK2 cells. Ketamine was used to evoke early changes in expression of proteins (E-cadherin, N-cadherin and β-catenin) central to adherens junctions that lead to the loss of cell-to-cell adhesion force. The results provide strong evidence that the illicit substance Ketamine has major impacts on renal function and the loss of intracellular adherent energy. Overall, both cell contraction and cell-to-cell adhesion experiments demonstrated that the changes of biological states evoke protein interactions which would ultimately lead to the biomechanical alterations. Therefore, characterising the changes of mechano-biological properties can provide new insight into the investigation of physiological and pathological issues.

Abbreviations

ADP	Adenosine Diphosphate
AFM	Atomic Force Microscopy
AFM-SCFS	Atomic Force Microscopy Single Cell Force Spectroscopy
ANOVA	Analysis Of Variance
ATCC	American Type Culture Collection
ATP	Adenosine Triphosphate
BFP	Biomembrane Force Probe
BMI	Body Mass Index
CCD	Charge Coupled Device
CGCA	Collagen Gel Contraction Assay
DAG	Diaglycerol
DAQ	Data Acquisition
DMEM	Dulbeccos' Modified Eagle's Medium
EDL	Electrical Double Layer
E-Modulus	Elastic Modulus
FA	Focal Adhesion
FCS	Fetal Calf Serum
F-D	Force-Displacement
FPCL	Fibroblast-Populated Collagen Lattice
h	hour(s)
HAoAF	Human Aortic Adventitial Fibroblasts
HRFS	High Resolution Force Spectroscopy

ICCJ	Interactive Control Centre Joystick
IP3	Inositol Triphosphates
kg	kilogram
MA	Micropipette Aspiration
min	minute(s)
ml	millilitre
MLC	Myosin Light Chain
MLCK	Myosin Light Chain Kinase
MTC	Magnetic Twisting Cytometry
mm	millimetre
mM	micromolar
MN	Micro-Needle
mN	micro Newton
mPAD	micro-fabricated Post Array Detector
MT	Magnetic Tweezers
NI	Nano-Indentation
nm	nano metre
nN	Nano Newton
OT	Optical Tweezers
PBS	phosphate-Buffered Saline
P-value	value of statistical significance
R^2-value	coefficient of determination
SCC	Source Code Control
SD	Substrate Deformation
s.e.m	standard error of the mean
TFM	Traction Force Microscopy
μN	Micro Newton

Chapter 1

Introduction to cell mechanics

1.1 Introduction

Over the past few decades, the way of thinking about life science questions has been undergoing a radical and revolutionary transformation. The subject of biology has been transformed from a qualitative and observational discipline into a more quantitative one in terms of all aspects of works from DNA level to organ level. Many sub-disciplines have been emerging and demanding an interdisciplinary integration among biology, statistics, mathematics, physics, engineering and computer science. As a result, biophysics and biomechanics are becoming increasingly important in contribution to the conventional biology and physics.

With the advancement of imaging technology, there is a desperate need for probing the mechanical properties of biological samples from tissues to molecules. In particular, many established cellular processes and diseases can be shifted in paradigm by understanding the role of mechanical forces. For example, the forces triggered by the cellular processes can initiate cell adhesion, migration, proliferation and contraction [118]. Similarly, mechanical loading, including fluid shear and cell

stretching, can also serve as an extracellular signal which regulates cells' phenotype [35]. Moreover, interfering with cell sensing process has been proven to relate to several pathological phenomena, such as cancer, atherosclerosis and osteoporosis [35, 76, 133]. Therefore, all these cell behaviours associated with mechanical forces have led to the study of cell mechanics [145]. The term cell mechanics here specifically refers to the study that uses tailored engineering tools to investigate mechanical behaviours of cells.

The primary goal of this chapter is to introduce some diseases that are associated with cell mechanics and adhesion. Due to the size and complex characteristics of biological cells, there are several challenges in measuring their mechanics and adhesion which will be introduced in the following sections. In Chapter 2, a number of state-of-the-art experimental techniques have been surveyed and reported in detail. Chapter 3 describes the nano-bio-mechanical tester developed for measuring cell mechanics in terms of hardware and software configurations. Chapter 4 describes the nano-bio-mechanical tester in combination with a mathematical model that has been used to quantify the contraction force of single cells *in vitro* using fibroblasts embedded in a collagen gel matrix. Further results of extra-cellular matrix regulating the fibroblast contraction force are presented in Chapter 5. Chapter 6 describes a novel method to measure cell-to-cell adhesion force by using Atomic Force Microscopy (AFM) force spectroscopy. Finally, some more important conclusions that can be drawn from this research and a number of recommendations of how this research topic can be further developed are given in Chapter 7.

1.2 Cell mechanics and human diseases

Most of our understanding of health and disease is based on the mechanism of biology and biochemistry. However, a significant level of attention has been shifted

towards thinking about the mechanics of cells in relation to some common diseases such as cancer, hypertension, and diabetes. For instance, cancer cells often exhibit a different elasticity compared to healthy cells and blood vessel cells change contractility subject to the high blood pressure [38]. Not only does this imply that the physiological system has a mechanical mechanism to maintain the fundamental structure, but also suggest that the human cellular system will respond to biomechanical stimulation. Understanding human pathological phenomena would often require the understanding of cell mechanics. The following list shows some typical examples that elaborate how biomechanics at the cellular level directly impacts the human physiological system and further leads to pathological disease.

- In the process of hearing, external environment generates physical loadings (sound waves) that are potentially perceived by the human ears. Sensing elements (*i.e.* inner ear bones, cilium and cochlea) will conduct a large number of biochemical and biomechanical events, for instance, wave causes the vibration of inner ear bones and calcium ions will flow into the cilia due to the opening mechanism of tip links. The cilium will then convert these mechanical loadings into biochemical signals so that human brain can interpret those signals through nerve impulses. In the process, the sound waves as an external loading stimulates the actin filaments between two adjacent cilia. It is essential that the cilia should maintain the right mechanical characteristic in order to handle the deflection caused by the sound wave [114].

- Infection is another common example of how foreign genetic information is delivered into the human immune system. The very first step for the virus infection is to destroy the cell's intrinsic protection, *i.e.* membrane, by mechanically disrupting the normal cell activities. However, cell membranes have their protection mechanism, called endocytosis. During one type of endocytosis of foreign genetic cargo (*i.e.* receptor-mediated), the receptor of designated

cells flows to bind the ligands of a virus. The virus would eventually be enveloped into the cell. During the whole process, the behaviours of cell adhesion, folding and pinching, are mechanically important for both cargo delivery and cell protection [85].

- Breathing and heart beating are also interesting examples to show how mechanical contractile forces play a major role in physiology processes. The airway smooth muscle cells and epithelial cells conduct cyclic stretches in order to maintain breathing pressure. Moreover, stretching forces generate feedback signals for basement membrane to monitor the breathing conditions. If the smooth muscle cells are hypersensitised by airborne pathogens, the cells will keep in hypercontractility condition, which will ultimately cause asthmatic attack [104]. The mechanical dysfunction of cardiac myocytes directly relates to the arrhythmogenesis with congestive heart failure. The calcium fluxes regulate the switches of myofilaments which lead to the activation of myocytes contraction [9].

- Cancer cells exhibit metastasis largely owing to the decrease of cell-to-cell adhesion forces. The cancer cells, in the process of remaining metastatic, will detach from the tumour and relocate to a new site to grow. Cell migration, detachment and reattachment are all involved with mechanical events. The tumour, as a whole, will also regulate itself with surrounding environment, such as hardening connective tissues and redirecting blood vessels, to create a more comfortable and nutritional growing environment [20].

- Skeletal structure is one of the most noticeable systems in the human body that constantly endures mechanical loadings. Evidence show that bone cells are likely to remain healthy if bones are continually under mechanical stimulation [131]. Osteoporosis contributing to fragility and higher risk of fracture is more likely to take place in the individuals who have less exercise. It means

that most of the osteoblasts have their sensing elements to detect physical movements. With more usage of the cells, it is likely that the target cells will have faster metastasis.

Overall, the cell is a dynamic system which interacts and adapts towards external microenvironment continuously to maintain a healthy state. With all these active evidence in our living system, the importance of investigating mechanical behaviours of biological cells cannot be ignored. It is clear that the systems not only have a mechanical function which support the physiological environment, such as blood vessels and heart pump blood and skeleton supports body, but also actively respond to the mechanical loading, for example, bones reinforce and degrade due to mechanical forces.

1.3 Contraction and adhesion

Intracellular contraction force, cell-to-cell adhesion and cell-to-substrate adhesion force are vital for many biological processes; for instance, wound healing, cell regeneration, inflammation, and cancer. Among these processes, the most fundamental behaviour which includes both cell contraction forces and adhesive forces is cell migration (locomotion). Cell locomotion consists of four continuous steps: *i*) protrusion, *ii*) adhesion, *iii*) translocation, and *iv*) release as shown in Figure 1.1. Cells may undergo more than one step at any point of time.

The first phase is called protrusion. In this step, the polymerisation of actin filaments at the leading edge of the cell controls the formation of lamellipodium and filopodium. The veil-like lamellipodium and finger-like filopodium both contain rich cross-linked actin bundles. It is well-acknowledged that the actin polymerisation propels the change of membrane configuration and mediates the protrusion of

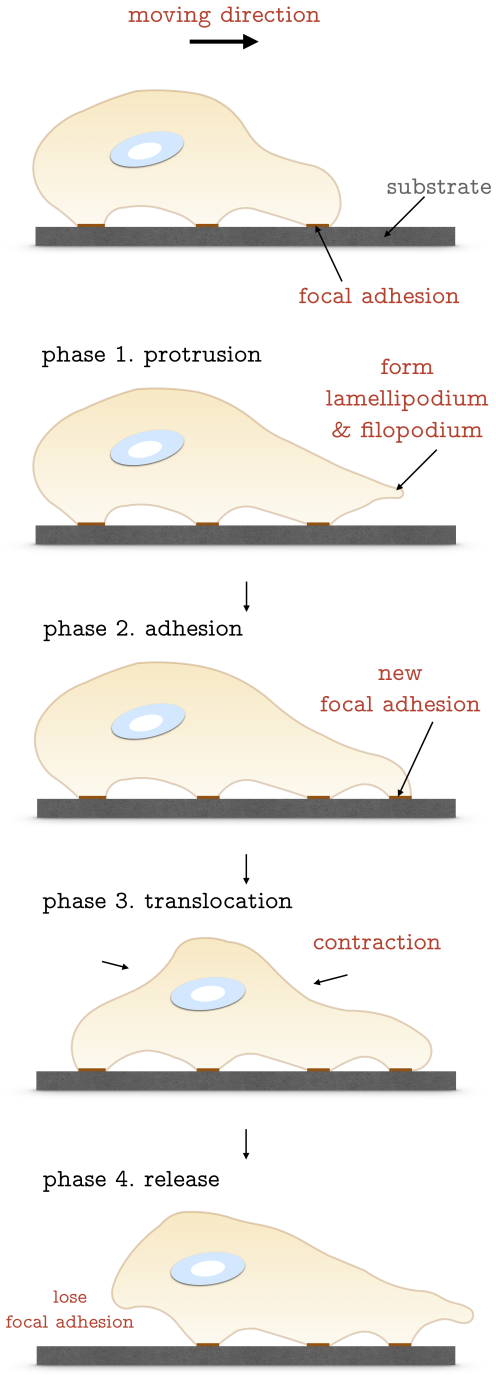

Figure 1.1: Schematic diagram of cell locomotion. The moving direction in this case is towards right. The steps include protrusion, adhesion, translocation and release.

lamellipodium [130]. The second step is adhesion when the cell membrane moves forwards and a new configuration of cytoskeleton is quickly assembled. There will be a new assembly point from the membrane firmly attached to the substrate. The cell and substrate develop new focal adhesion (FA) points and generates adhesion forces. The adhesion force causes the cell to firmly anchor to the substrate and leads to the third step, *i.e.* translocation. During this procedure, the cell moves towards the direction where new FA points are generated. Intracellular contraction force is then created. The mechanism of how contraction forces are generated will be introduced later in Section 1.3.1. Actin-myosin interaction dominates the process. The very last step of this cyclic activity is the release of the rear end FA. The loss of adhesion force combined with contraction force generated in phase three collectively pushes the cell to move forward.

1.3.1 Cellular contraction force

Mechanism of cell contraction force

The mechanism of cell contraction was firstly reported in 1954 by two separate research groups [70, 71]. They have proposed the sliding filament theory which explains the model of multiple muscle proteins sliding towards each other to generate contraction force. Huxley has modified the model by stating that the filament sliding occurs by cyclic attachment and detachment of myosin on actin filaments. Contraction forces are generated when the myosin pulls the actin filament towards the centre of cells [72]. The theory was recently validated and regarded as the 'cross-bridge' model based on the actomyosin interactions [44, 142].

Briefly, the model considers actin filaments and myosin, residing in most of the cellular systems, to be responsible for the cell contraction. Myosin acts as a molecular motor to convert chemical energy ATP to mechanical energy for contrac-

(a)

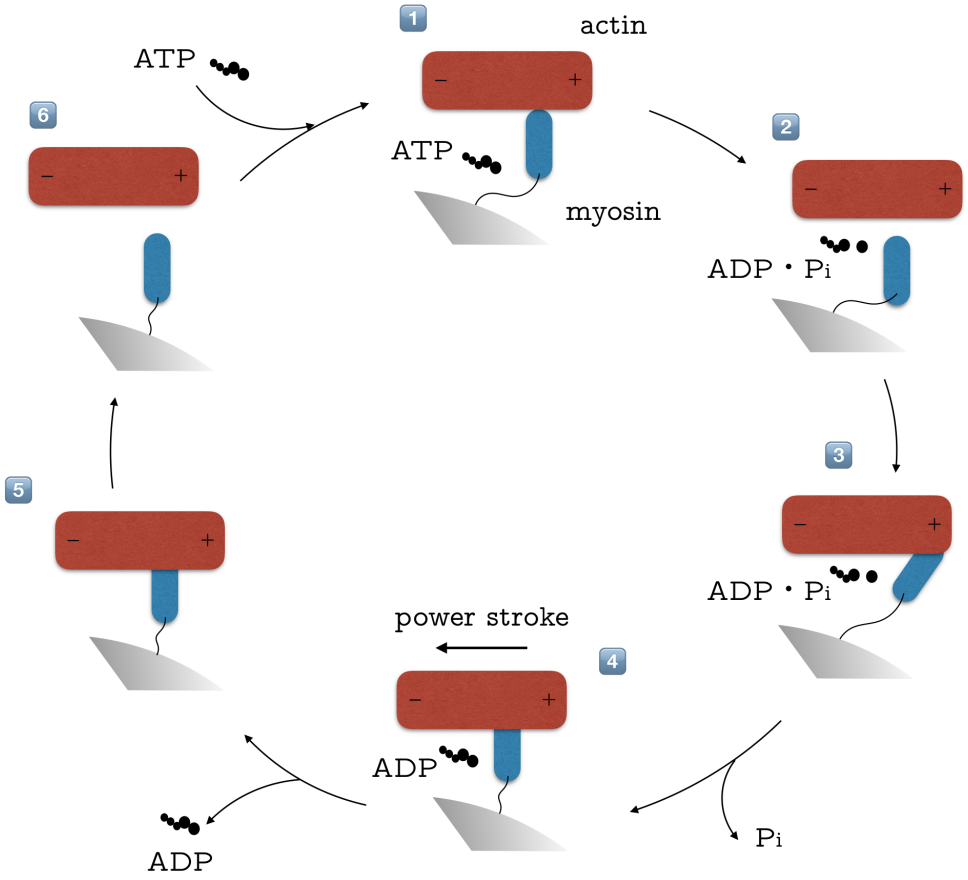

(b)

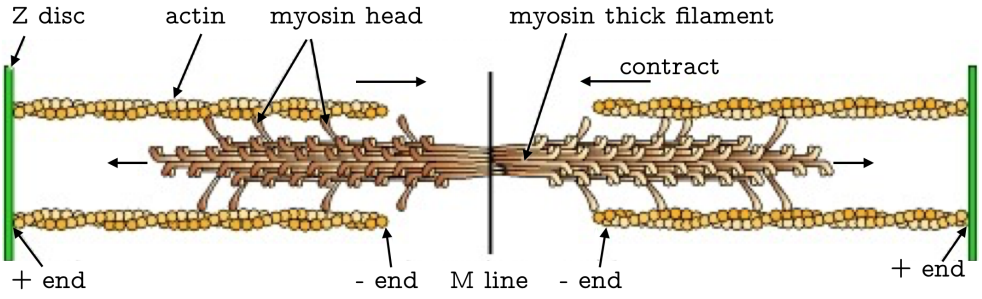

Figure 1.2: (*a*) Schematic diagram of the myosin configuration cross-bridge model. In the cyclic model, the actin molecule slides from right to left. (*b*) The organisation of a sarcomere that constitutes the basic contractile unit.

tion whilst the actin filament as part of the cytoskeleton structure is responsible for driving the entire cell entity in motion. Figure 1.2a shows a schematic of actin-myosin's cyclic process illustrated by the cross-bridge model. The cycle starts at the top where actin and myosin are tightly bonded in the absence of ATP/ADP (adenosine triphosphate/adenosine diphosphate). The phase is also known as *rigor* state (phase 1). After ATP moves in and bonds with myosin, the hydrolysis of ATP makes the myosin start to release from the actin filament (phase 2). The release of chemical energy from ATP induces myosin to change conformation and become a *cocked* configuration (phase 3). In this state, the neck region of myosin moves towards the (-) area. The displacement is around 5 nm. The hydrolysis product (ADP and P_i) remain attached to the myosin's head. In between phase 3 and phase 4, the release of phosphate is activated by the actin and triggers a 'power stroke'. In the process of the 'power stroke' (phase 4), the myosin drags the actin filament to move, in this case, left. The mechanical forces and physical displacement of cell entity are generated in phase 4. In phase 5 and 6, at the release of spent molecule ADP, the system returns to the original state and completes the cycle.

The cross-bridge model explains the interaction between one actin and one myosin molecule. Inside cell entity, several hundreds of myosin molecules are staggered and interlocked at their long α-helical tails as Figure 1.2b shows. F-actin was derived from G-actin polymerisation and formed a polar configuration. The '+' and '-' represent the *barbed* and *pointed* ends of the actin polymer. The entire length of one F-actin filament is around 36 nm and there are limited binding sites for myosin's head to attach to. The overall movement of a myosin head is limited to 5 nm. Hence, in each full twist of z-disc, it is impossible for every myosin molecule to reach far enough to a binding site. In fact, only very few myosin heads are able to grab a binding site as Figure 1.2b shows. The overall productions of myosin molecule sliding contributes to the cell contraction.

Modulation of the cell contraction force by the matrix

Human cells rely greatly on their surrounding matrices to maintain the vitality and the function of the human tissue. Cells naturally adhere to extracellular matrices, which constitutes a mechanically stable and elastic micro-environment. Many biological cells, such as fibroblasts, epithelial and endothelial cells, have the ability to reconstruct the mechanical properties of their surrounding microenvironment [110]. This behaviour has been widely studied in regenerative medicine and tissue engineering. The mechanism helps the human body to recover from damaged tissue by cell proliferation and differentiation towards the formation of a new healthy tissue. In the meantime, when cells anchor to the extracellular matrices, physical behaviours will be triggered to probe the mechanical properties of their encompassing territories. For example, focal adhesions link the actin-myosin cross-bridge inside the cell with a number of extracellular matrix proteins outside the membrane and regulate the transmitting signals during contraction [8, 51]. It has also been shown that the FA is mechano-sensitive and regulated by the external force in terms of size, shape and composition [50, 170]. Hence, FA is the mediator that transmits and converts forces into biochemical signals to regulate cell contractions. The extracellular matrix changes its mechanical property constantly and subtly. Therefore, ECM generates mechanical signals continuously which are probed by FA and translated to the cells. Meanwhile, cells generate contraction force after the signals are perceived which results in the conformation changes of extracellular matrices and affects neighbouring cells. The overall structure forms the intercellular feedback loop. In addition, mechano-sensing of the extracellular matrix is synergistically controlled by many subcellular signalling molecules such as integrins and cadherins [1].

1.3.2 Cellular adhesion

Cell adhesion is a fundamental mechanism whereby cells are organised and formed in tissues and organs. Cell adhesion also can be regarded as a complex system whereby cells translate various interactional genetic information in response to biochemical signals and finally form our organs and tissues. Cells change adhesion energy continuously to maintain their stability and activity [10]. The form of this behaviour is presented as cell mobility and contractility. There are two forms of adhesion interactions that are widely studied: cell-cell adhesion and cell-ECM adhesion. Cadherins and integrins have been implicated in the control of cell adhesion and the maintenance of cell structure. Cadherins mainly mediate cell-cell adhesion in terms of compaction and rearrangements whilst integrins regulate cell-ECM adhesion on spreading and motility. E-cadherin in epithelium has been mostly studied in the cadherin family. It is a transmembrane Ca^{2+}-dependent homophilic adhesion receptor. Cadherin can link two adjacent cells directly by multivalent linker molecules. In the process of cadherin mediated cell-cell adhesion, α-catenin and β-catenin are formed to link actin and to transmit signal, respectively. Hence, signals generated by the adhesion receptors contribute to the regulation of cell-cell adhesion. Moreover, adhesion receptors, cytoskeleton and signal pathways conjointly regulate the tissue morphogenesis. Integrin also belongs to the family of transmembrane proteins that tightly bind with the plasma membrane and intracellularly connect to the cell cytoskeleton. The process of cell motility and major enzymatic activities are vital for regulating cell-ECM interactions. Integrins are dimers which are composed of α- and β-subunits [73]. For example, $\alpha_5\beta_1$ integrin is a fibronectin receptor which has isoform of α_5 subunit and β_1 subunit. Integrins would assemble into the focal adhesion with a highly regulated mechanism however the exact role of each component has not yet been well defined.

1.4 Multi-scale biomechanics

Cells organise themselves in biological systems by proliferation, migration, and differentiation. In each of the processes, different biomechanical behaviours are involved. These include cell-cell adhesion and contraction which decide how cells assemble themselves into tissues or escape from them. The deep down molecular level mechanics such as actin-myosin induced protein movement enable to refine larger scale of study such as cell contractility. The cell-level or so-called micro-scale studies also relate to the mesoscale behaviours; for example, cell contractility can be further studied in terms of its effect on cell migration in extracellular matrix. Moreover, mesoscale behaviours would result in the macro-scale (tissue) phenomena. For example, cell migration and contraction are directly linked with skin wrinkling, ageing and wound reorganisation [165]. In all, macroscopic tissue level activities are induced by the single molecule protein mechanics. The multi-scale coordination and regulation form the entire physiology system. Amazingly, our body invents the mechanism and regulates interactions with minimum consumption of energy.

Mechanics is the subject that studies the quantitation method of physical materials which are subjected to force and displacement. Biomechanics has been applied to study the mechanical properties of biological systems, such as human organs, tissues and cells. Nano-biomechanics is a special type of biomechanics in terms of the scale of measurement. The macroscopic biomechanics is always based on the assumption that the material is homogeneous in composition and the size of test probe is always negligible. However, this is not normally true as the biological sample is usually a mixture of a large number of different proteins and composites. The latest development of force and displacement measurement technology allows the investigation into small groups of protein, such as the research topics of nano-measurement, nano-fluids and nano-fabrication [146]. By extracting the pa-

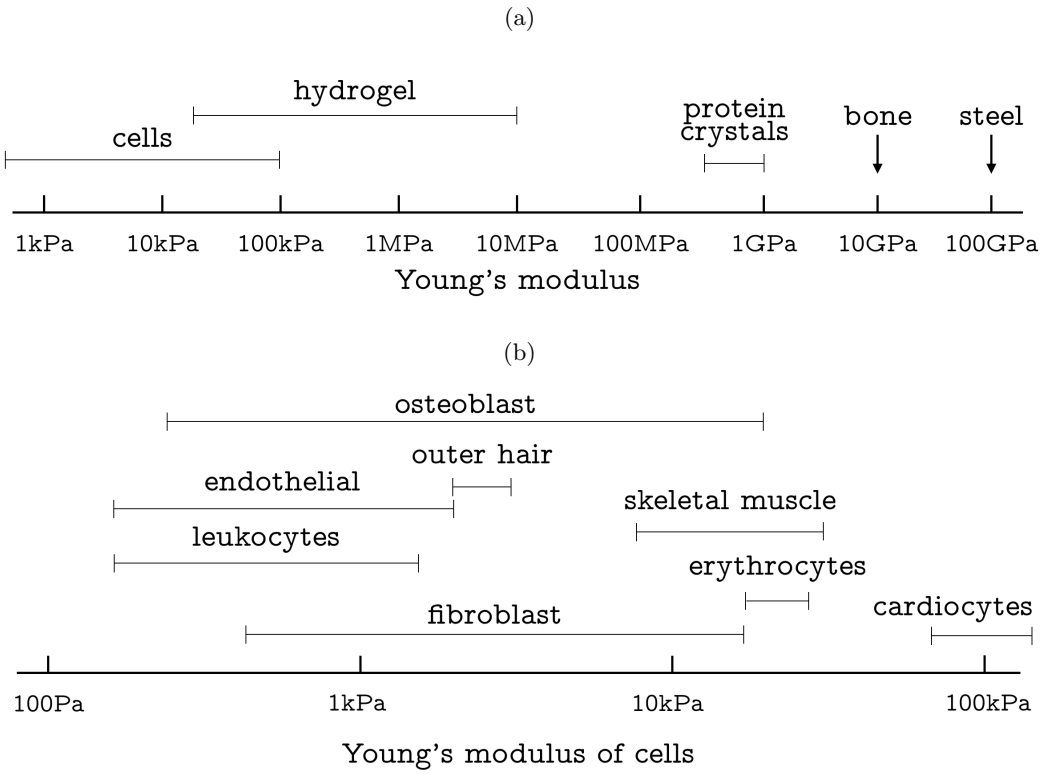

Figure 1.3: (*a*) Young's modulus of different bio-materials (adapted from [4]). (*b*) More cells that Young's modulus specifies according to the review [155].

rameters of force and displacement, in combination with mathematical models, it is now possible to analyse mechanical properties of the materials or samples. The work offers to provide new insight into observing the biological and pathological phenomena. Thanks to the advancement in nano-fabrication and microscopy, people can further manipulate cells and molecules at force and displacement of less than a piconewton (pN) and a nanometre (nN) respectively. The results can provide us with unique mechanical parameters, such as Young's modulus, rigidity, Poisson's ratio, compressibility, contractility and viscoelasticity. Young's modulus (or elasticity modulus) attracts the most interest in studying biomechanics. Young's modulus of cells can be calculated *in vitro* by acquiring a Force-Displacement (F-D) curve using different nano/micro-mechanical testers. Suitable mechanical models for cells are subsequently applied to mathematically fit the F-D curve. A comprehensive review has introduced many mechanical models including Hertz, JKR, Lifshitz, and Tatara theories [101]. Figure 1.3a shows common elastic modulus of bio-materials. Cells are the least elastic material in the diagram. This enhances the difficulties of measurement and determination. Figure 1.3b shows elastic moduli of different cells which have been examined by Atomic Force Microscopy (the measuring technique will be introduced in Chapter 2 and Chapter 6).

1.5 Grand challenges in cell mechanics

As we have described in this chapter, biomechanics is related to many physiological and pathological processes. The cell is a complex system where each protein has specific tasks. Nano-biomechanics studies provide a methodology for working at atomic, molecular, sub-cellular, and cellular-level in order to understand mechanical structures and create new materials that have functions similarly to our human body. However, comprehensive analysis of biomechanics for human cells is extremely

difficult. It includes cytoskeleton, membrane and cell entity. Moreover, biological cell is a viscoelastic material which means fluid-like and solid-like behaviours both exhibit in the system. In order to probe the mechanical properties of cells, sophisticated mechanical measuring devices are required. Higher resolution, faster speed, less noise, feedback control processes are necessary for this type of study. During the measurement, any changes in temperature and humidity would affect the experiment as the size of protein and cell is extremely small. In addition, primary samples from the human body have variations concerning BMI (body mass index), genetic disease, age and gender. It often requires statistical assessment of any mechanical testing results. Furthermore, experiment situation *in vitro* is relatively well controlled whilst *in vivo* testing could be affected by many potential complications from physiological environments. Basic fundamental mechanics can solve most of the cell mechanics questions, however, there is still many to be done by using advanced mechanical analysis. On top of this, much research in this area requires extensive collaboration. This research normally involves the development of nanomechanical testing devices, building mechanical/mathematical models, creating platforms/procedures for testing and validation, biological hypotheses and exploration, animal testing, and clinical trials.

Chapter 2

Cellular force sensing techniques

2.1 Introduction

To date, various nano-/micro- mechanical testers exist in the area of experimental analysis of biological samples. Several comprehensive reviews [99, 100, 133, 156] have reported the development of state-of-the-art biomechanical tools and their current applications along with many advanced mechanical models. Selecting a suitable mechanical tester requires the estimation of the size of samples and the measuring capacity. Figure 2.1 shows the typical force and displacement range in the study of biomechanics. Force is in the range from 1 nano-Newton (10^{-9} N) to 1 micro-Newton (10^{-6} N) for cell mechanics study whilst the force to manipulate protein and molecule is required in the range of pico-Newtons (10^{-12} N). In this study, the focus is mainly laid on the contraction and adhesion measuring techniques.

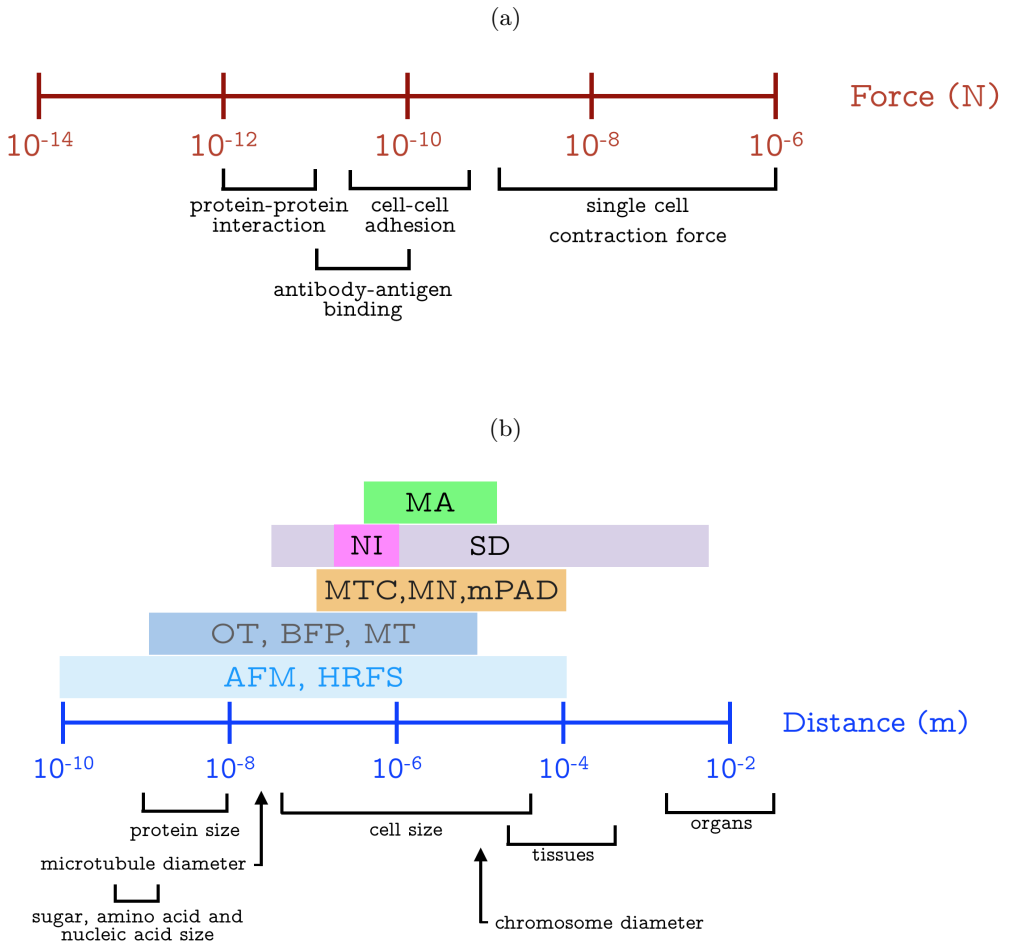

Figure 2.1: Force (a) and distance (b) range of common biological events. The experimental technique in abbreviation with its corresponding testing range. MA - Micropipette Aspiration; NI - Nano-Indentation; SD - Substrate Deformation; MTC - Magnetic Twisting Cytometry; MN - Micro-Needle; mPAD - micro-fabricated Post Array Detector; OT - Optical Tweezers; BFP - Biomembrane Force Probe; MT - Magnetic Tweezers; AFM - Atomic Force Microscopy; HRFS - High Resolution Force Spectroscopy. Adapted from [99, 156].

2.2 Mini-review of contraction force measurement technique

Cellular contraction forces are normally measured indirectly by probing the cell-embedded or cell-populated matrices. Measurement of forces generated by cells can be performed on cell populations or single cells. The original technique to study contraction force generated by a cell population was invented by Bell *et al* [6]. Fibroblasts were embedded in the collagen gels. Cell contraction force was indicated by the magnitude of gel radius or volume shrinkage. The technique was improved by Delvoye *et al* to accurately determine contraction force using the technique known as culture force monitor (CFM) [32]. Briefly, in the method, strain gauges are attached to the edge of cell-embedded collagen gels so as to acquire contraction force generated by the cells continuously. To obtain single cell contraction force, Harris *et al* developed a method by laying the cells onto elastic substratum, called 'Traction Force Microscopy (TFM)' [57, 58]. The traction forces that each cell exerts will deform the substrate and create visible wrinkling. On the surface, the cell traction force can be determined by the number of wrinkles at micrometre level. Owing to the increasing interests in the mechanics of cell locomotion, strengths and adhesion, several new single cell techniques have been developed to quantify the contraction force, such techniques including optical traps [87], micro-needle/micropillar arrays [147] and micro-machined substrata [49].

2.2.1 Collagen gel-based contraction assay

Cell-embedded collagen matrix provides a unique way to study the mechanical interactions within the 3D culture. Such interaction was not easy to examine on a normal *in vitro* cell culture because the culturing areas are fixed on a monolayer. When cells are evenly distributed inside a collagen matrix, the traction forces generated

by cells exist in the collagen matrix at all directions. Meanwhile, collagen fibrils will develop isometric tension to retain their original shape and resist deformation. The tension would consequently load on the cells and generate reciprocal interactions. As the collagen fibres are linked, traction forces are propagated throughout the collagen matrix resulting in global remodelling and contraction. This mechanism of cell-embedded collagen matrix is similar to the *in vivo* homeostatic response. Soft connective tissues are under enormous endogenous tension caused by their resident cells where contraction force is generated upon the extracellular matrix. Many researchers have used the method to determine the mechanism of how cells regulate the contraction. The recipe and the protocol of collagen gel contraction assay can be found in the literature [120].

Several models have been developed for different cell-embedded collagen contraction assays. Figure 2.2 illustrates the difference of the three major types of collagen matrix contraction models. Figure 2.2a shows most commonly used model. When cells are evenly seeded into the collagen matrix, it takes 20 - 60 minutes for gels to polymerise in a 37 ℃ incubator. Collagen gel will then be immediately dislodged from the surface of a Petri dish. A gel will be floating and mainly have radius reduction which can be observed from the top view of the Petri dish. The common expressions of the magnitude of contraction are represented by the percentage of gel reduction before and after the measurement period. Here a list of some research that has used cell-embedded collagen matrix based techniques to measure the cell contraction events [3, 12, 29, 42, 65–68, 74, 77, 111, 121, 129, 132, 144, 150, 153, 169, 173]. Figure 2.2b represents anchored cell contraction assay. Compared with the floating contraction array, an anchored gel contraction assay will mainly have thickness/height reduction as the bottom side of collagen matrix is adhered tightly with Petri dish. The tension in this type of model will be distributed anisotropically. Figure 2.2c is the modification of the previous methods. This method was developed by Tomasek

Table 2.1: Selected cell-embedded collagen gel-based studies which pertain to the listed disease/disorder categories.

Disease/disorder category	**Selected References**
Cardiovascular Disease	[29, 153]
Aging	[121]
Growth Factor (TGF-β1)	[12, 42, 65, 150]
Wound Healing	[12, 67, 68, 74, 129, 153, 173]
Eye disease	[3, 111, 132]
Respiratory system diseases	[42, 66, 169]
Platelet disorder	[144]
Oral health	[77]

et al [152]. Stress will be developed during the period when the gel was anchored to the dish. After dislodging from the dish, stress will be eliminated. Many researchers have used this method to study the difference between pre-stressed and relaxed cells [39, 89, 125] and to investigate environmental stress effects on the cells.

Significant efforts have been made to correlate cellular studies performed by collagen gel-based contraction with the pathology of the disease. In an effort to elaborate the breadth and depth of disease-related research since Bell *et al* invented the method, a few selected disease categories with their literature references are listed in Table 2.1. A number of review articles related to collagen gel based contraction assay advances in biochemistry and biophysics have been published [1, 27, 35, 52, 55, 91, 95, 96].

The main cell type to study cell contraction force is (myo)fibroblast derived from skin, lung and blood vessels. (Myo)fibroblast are deeply embedded in the cellu-

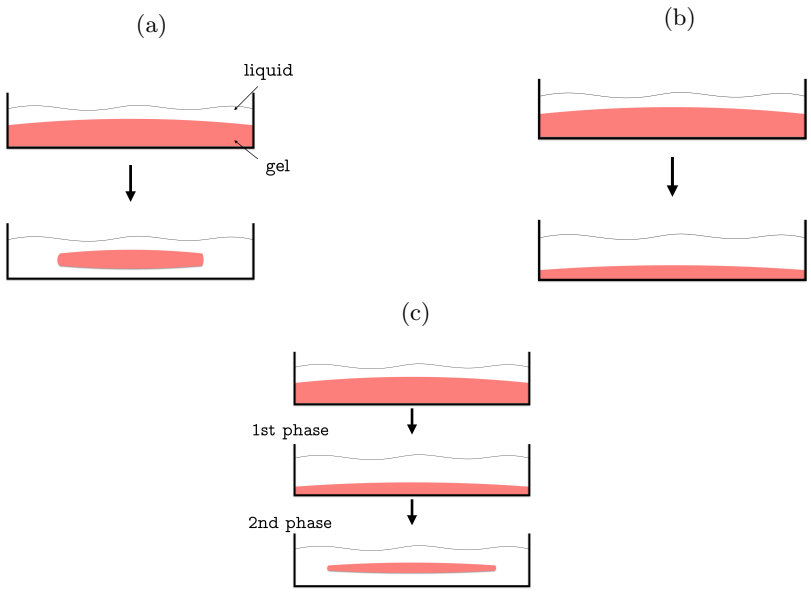

Figure 2.2: Models for cell-embedded collagen matrices for testing magnitude of contraction. (a) Floating matrix contraction: cell-embedded collagen matrix was dislodged immediately after collagen matrix polymerised. (b) Anchored matrix contraction: during entire contraction period cell-embedded collagen matrix was not dislodged from the surface of Petri dish. (c) Stressed contraction method: the first phase of contraction, collagen matrix was attached to the plate to enhance the internal stress. In the second phase, the collagen matrix is dislodged and stress released.

lar matrix where they secrete, differentiate, quiescence, and proliferate to maintain the homoeostasis of their matrix physiological functions. The growth factor *in situ* will enhance their adhesion, signalling, sequestration or activation [28]. In terms of pathological situation, the interaction between fibroblast and matrix has direct impacts on wound healing, ageing and skin defect.

The commonly-used method for detecting cell contraction is measuring the percentage shrinkage of collagen gel area [6]. A long focal camera is placed on top of the culture plate. The focus is tuned to the point at the centre of the plate. It is recommended that the lid of the culturing plate is removed to acquire a better view. As the culturing plate (*e.g.* Petri dish, multi-well plate) is often transparent, the background colour is often advisable to be black or a darker shade. To assure that camera focus is at the centre of the plate when taking the image, it is advisable to inspect whether the distances between outer rim and inner rim are constantly equal along the periphery as Figure 2.3 shows. The collagen radius/diameter is often calculated by referencing culturing area of the Petri dishes. In this case, the culturing area is normally shown as the green circled area in Figure 2.3b. It is advocated that the images of the culturing area should be calibrated before the testing. Hence, the actual gel radius (r_{gel}) can be calculated by the following equation:

$$r_{gel} = \left(\frac{P_{gel}}{P_{dish}} \cdot \frac{S_{dish}}{\pi} \right)^{\frac{1}{2}} \tag{2.1}$$

where P_{gel} and P_{dish} represent the pixels of collagen gel and Petri dish (culture area) captured in the images, respectively. S_{dish} represents the area of culturing surface which normally shows in the product information of Petri dishes. The overall numbers of pixels in the images are the representation of measuring area of specific region.

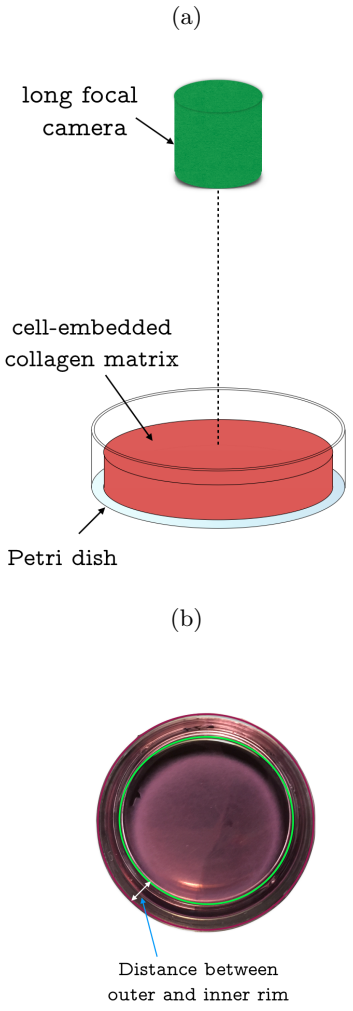

Figure 2.3: (*a*) Schematic diagram of long focal microscope to measure collagen gel diameter in Petri dishes. (*b*) Example images for measuring the collagen radius. It is necessary to keep the distance between outer and inner rim constant to ensure the focus is at the centre of Petri dish.

2.2.2 Culture Force Monitor (CFM)

The methods mentioned above for measuring geometric changes of cell-embedded collagen gel give a simple solution to quantify cellular contractility. However, these approaches have an intrinsic drawback, that is when the contraction force is relatively small, the representation of radius changes does not significantly show adequate sensitivity. To overcome this challenge, Delvoye *et al* [32] invented an approach to monitor the overall contraction forces generated from embedded cells by attaching the strain gauges to collagen edges. The method has successfully improved the sensitivity limited by measuring gel radius alone. The method is known as Culture Force Monitor (CFM) [32]. Figure 2.4 shows the schematic diagram that explains the basic principle of how CFM works. In typical CFM systems, cell-embedded collagen gel is normally attached to the plates to restrain the gel's movement. The strain gauge is connected to one of the plates while the other plate is attached to a x-y stage that adjusts and provides the gel with a minimum initial strain. The entire system is then placed in a 37 ℃ incubator for online monitoring.

The alternative type of CFM system is based on the free-floating collagen matrix. There are two-needled strain gauges directly connected to the collagen matrix. It measures the isometric contraction by each pointing the other through the centre of the collagen matrix. This set-up provides the maximum sensitivity for the force transducer. It is able to detect the contraction force for the gel displacement down to 0.5 mm which is a barely noticeable change [36].

Since the discovery of CFM, various research groups have been devoted to modifying the method and applying it to numerous cell types with related biological events, such as cell morphology [37, 47], tensional homoeostasis [15, 19, 137], collagen stiffness effect [83, 105, 172] and growth factor/agonist effect [18, 86]. Besides these applications, significant improvement has been made to increase the CFM efficiency.

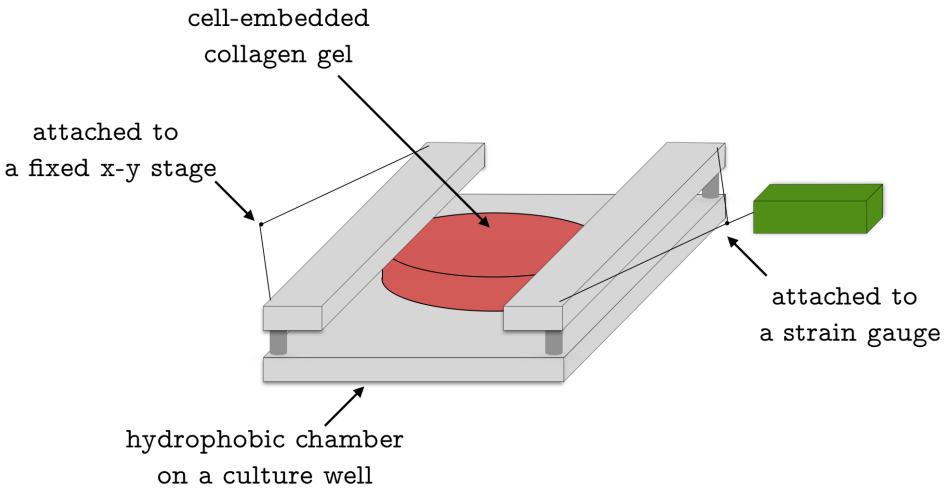

Figure 2.4: Schematic diagram of a traditional culture force monitor. The cell-embedded collagen matrix is placed in a hydrophobic chamber where two plates are locked and attached to the edge of the gel. One side of the plate is fixed to a x-y stage at the bottom of the culture plate. The other plate is attached to a strain gauge to measure overall contraction force that the cell generates.

Wang and co-workers have reported a multi-station CFM [18, 19, 127] which is able to measure multiple biological samples simultaneously. This improvement saves a significant amount of time to examine a patch of cells *in vitro* and facilitates the statistical analysis. CFM can also be used as a tool to pre-stress the cell-embedded collagen gel [83, 105], to mimic the stressed environment *in vivo*, and to remodel the matrix materials. Since one of the plates is fixed to the x-y stage underneath, instead of reaching the minimum initial strain, the mechanism can be used to stretch the collagen matrix for an extended period before cells start to contract. In this process, embedded cells are stretched and elongated. This pre-treatment provides a solution for long/short period pre-stressed cells relaxation experiments.

2.2.3 Traction Force Microscopy (TFM)

In 1980, Harris *et al* [57] found the interesting fact that when cells are cultured on a very thin silicon substrate, the cell traction force generates a visible wrinkling on the substrate surface due to the locomotion. Initially, these wrinkles were used to estimate how many traction forces cells generated. It also can be applied to determine if a specific area of cells are contractile [58, 90]. However, this approach has limitations for determining the specific amount of forces and directions of cell contraction, although a few modifications have been made to adjust the measurement technique [16, 49, 123]. Pelham and Wang [126] first invented the method of using polyacrylamide material as a deformable substrate and putting cells dyed with fluorescent labelling antibodies onto the substrate to examine cell locomotion. Still, the method is not calibrated to determine the actual traction force. Munevar and co-workers [117] have improved the technique by seeding large numbers of fluorescent micro-beads in the polyacrylamide substrate. Given the value of the elastic modulus of the substrate, traction forces of cells on the substrate can be estimated by tracking the displacement of fluorescent micro-beads. Figure 2.5 illustrates the

calibrated traction force microscopy and its sequence of image processing.

As cells can be seeded onto or in the polyacrylamide substrate, the technique has broadened the application of various cell types, both adherent and non-adherent cells. Those types include fibroblast (3T3[1]) [97, 117, 157], smooth muscle cells [151, 158], osteoblast [26], keratocyte [34], dictyostelium [75] and HeLa cells [159]. Mostly, TFM is used to determine the magnitude of single cell contraction force [31, 107, 122, 168] during locomotion [33], migration [21, 103, 116] and development [30, 94]. Moreover, TFM can be used as a tool to elucidate many pathological events caused by the traction force, such as apoptosis [157], cancer [134] and hypertensive heart disease [106]. In addition, TFM has been applied further to investigate cytoskeletal changes [22, 75, 103], focal adhesion [8, 122] and cell shape changes [97]. Recently, scanning confocal microscopy [45, 46, 84, 92, 93, 107] has been combined with TFM to perform a three-dimensional force scanning for single cell traction. The technique has provided a number of advantages. For instance, TFM is able to determine single cell traction force in a quantitative manner. The cell-gel interactions can also be seen and quantified. Various selections of fluorescent microbeads allow for control of the area where cell traction events take place. However, this also leads to the disadvantage of the technique, which is that the resolution of contraction force entirely depends on the accuracy in gel elasticity measurement and camera spatial resolution. The measurement of elastic modulus of polyacrylamide substrate according to the report [102] is done by dropping a steel ball onto the substrate. Young's modulus (Y) was determined by the modification of Hertz contact theory as the following equation:

$$Y = \frac{3(1-\nu^2)\cdot f}{4\cdot d^{3/2}\cdot r^{1/2}} \tag{2.2}$$

[1] 3T3 refers to 3T3 protocol of transferring every 3 days and cell density at 3×10^5cells/20cm^{2}dish.

(a)

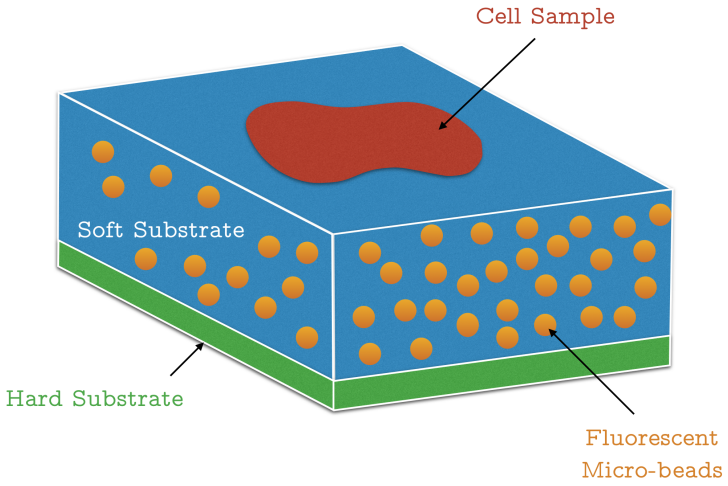

(b)

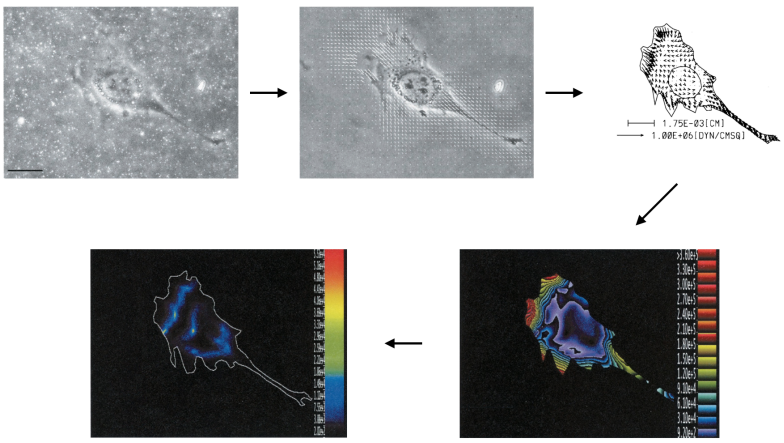

Figure 2.5: The working principle of traction force microscopy. (*a*) Schematic diagram of widely used traction force microscopy. Cell sample is placed on top of polyacrylamide substrate where fluorescent micro-beads are embedded. The entire gel matrix are placed onto a culturing plate (*i.e.*, Petri dishes). (*b*) The typical TFM image analysis process (modified from [117]). Scale bar, 20 μm.

where Poisson's ratio (ν) is assumed to be 0.3, f is the force that steel ball generated on the substrate (steel ball is 7.2 g/cm^3), d is measured indentation depth and r is the radius of the steel ball. As substrate deformation indirectly determines the traction force of the cell, it is necessary to examine the Young's modulus of polyacrylamide substrate every time before the traction experiment. Secondly, the stiffness of the substrate will influence the contractility of cells onto/within the matrix. Cells have the ability to sense the substrate stiffness so as to remodel themselves to accommodate and compensate their behaviours, such as contraction [59]. Thirdly, the camera resolution will also influence the measurement of traction force as the micro bead movement is traced under the microscope. Lower resolution will lead to the centres of beads not being accurately tracked. Three-dimensional characteristic layers of gel would result in a difficulty for the camera to focus on different intersecting surfaces.

2.3 Atomic force microscopy

Binning *et al* in 1986 invented a powerful tool, Atomic Force Microscopy (AFM), to initially probe the mechanical property of surfaces in atomic scale [11]. Until recently, AFM has been broadly and extensively used as a bio-analytical tool to probe and manipulate the cellular dynamics, to analyse mechanical properties from tissue to molecule, and to map the topography of micro-substance. AFM belongs to the category of Scanning Probe Microscopes (SPM) which many review articles have introduced through its applications [13,69,162] since it began to be used in the 1980s.

Atomic Force Microscopy aims to detect the attractive or repulsive force by a tip connected to the cantilever. The basic components of an AFM are illustrated in Figure 2.6, which consists of a cone tip, a cantilever, a laser beam, a photodetector

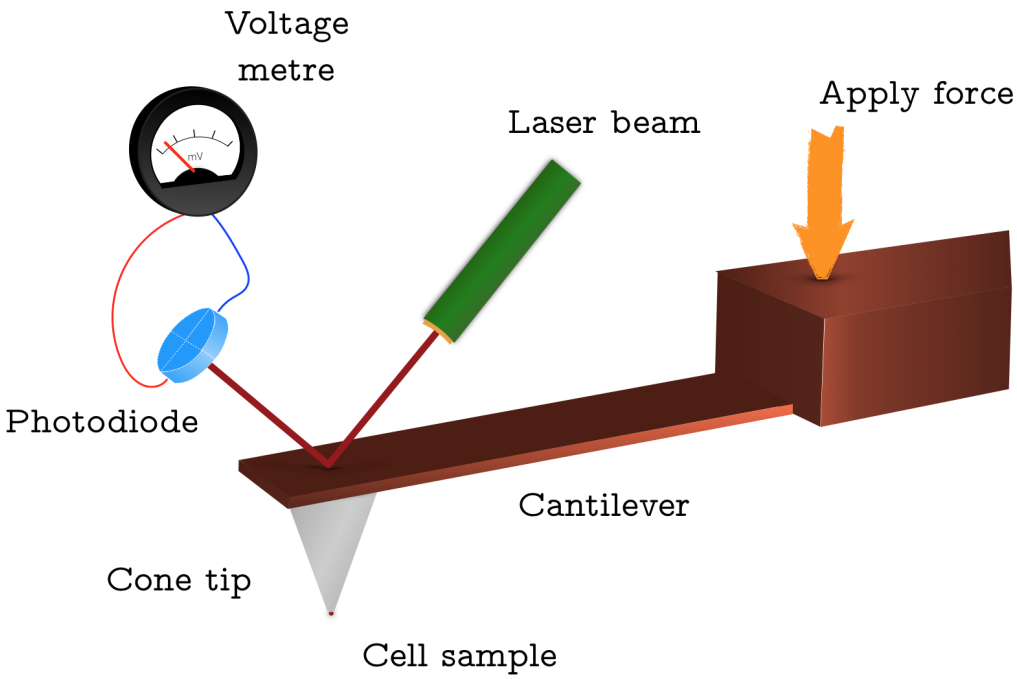

Figure 2.6: Basic constitution of Atomic Force Microscopy. During testing, signals are sent to move the system along z-axis. A laser beam was launched, reflected on the cantilever, and received at the photodetector. The voltage metre is able to detect the deflection of the laser on photodetector so as to determine the force magnitude. The cantilever is mounted with a cone tip at the front to probe the biological samples.

diode, and a z-axis piezo-stage. The output of the system would be the voltage versus z-axis displacement. The micro-fabricated cantilever tip requires remounting and calibration every time before the experiment as each tip has a distinctive stiffness of silicon or silicon nitride probe. The final output is plotted as force versus displacement. Various shapes of the front tip can be mounted with the cantilever, for instance, cone, pyramidal, spherical or flat shape tip.

Atomic Force Microscopy was originally designed to determine the Young's moduli of biological samples and to generate high-resolution images of surface topography. Both applications share the similarity of testing procedures. At the start of testing, the cantilever tip and laser beam are calibrated (calibration procedure can be found in chapter 6.2.2). Force-Displacement curve is generated on one specific position of the sample drawing approaching and retraction of the tip. Mechanical models will be used to fit the curve in order to find out the Young's moduli of the sample. If AFM is programmed to generate multiple Force-Displacement in one specific area, a surface image can be mapped to each measurement point. AFM has been used to test single molecules [41, 115, 140], nucleus [56, 64], cytoskeleton [128, 135], ECM stiffness [141, 149, 160] and cell elasticities [24, 25, 139].

The major challenge in AFM measurement technique is to determine the point of contact. When the tip approaches the sample very closely but not in contact, electrostatic force, electrical double layer (EDL) force, van der Waals force, and chemical force ($e.g.$ hydrogen bonding) affects the determination of actually contacting position, especially when AFM is used to manipulate molecules and nanomaterials. Furthermore, the shape of tip and point of contact would ultimately affect the nature of Force-Displacement curve. Results vary by using different commercial AFM.

2.4 Aims and objectives

The primary aim of this study is to examine cellular contraction force of fibroblast and adhesion force of HK2 cells in a quantitative manner. More specifically, to examine the contraction force of fibroblast, the study develops a novel biomechanical testing platform to examine the mechanical property of bio-materials. The model is based on the modification of cell-embedded collagen matrix. A 3D static contraction model is developed to characterise the contraction force *in vitro* (Chapter 4). As the model is based on the cell-embedded collagen matrix, the matrix effect on the fibroblast contraction is also discussed (Chapter 5). Furthermore, the study also focuses on the AFM single cell force spectroscopy to characterise cell-to-cell adhesion force (Chapter 6). The main objectives are listed as follows:

- To develop a cell contraction model based on the fibroblast-embedded collagen matrix.
- To develop and test micro-indentation instrumentation to examine the mechanical characteristics of collagen gel matrices.
- To examine cell contraction force of fibroblast based on the cell-embedded collagen matrices.
- To quantify the agonist triggered single cell contraction force.
- To investigate matrix stiffness effect on fibroblast contraction force by the micro-mechanical testing method.
- To examine Ketamine-induced loss of cell-to-cell adhesion energy by a new approach derived from AFM single cell force spectroscopy.

Chapter 3

A novel nano-biomechanical tester

In this chapter, a novel instrumentation of a biomechanical tester will be described. There will be an overall introduction to metrology and industry, followed by a detailed description of each component including their specifications, calibration procedures and integrated software development. It aims to provide repeatable procedures for the design and building of the novel instrument.

3.1 Introduction to micro-mechanical metrology

In the modern engineering discipline, the fabrication and manufacture of sensors have a tendency to minimise the size of products. The accuracy and resolution of instruments, however, have increased to meet the requirement of the highly-precise design of materials, such as biomaterial. It can be predicted that the sub-μm or even nanometre precision could become popular since the emergence of interdisciplinary research, such as nano-biomechanics and nanomaterials. Finer details are required

for investigation, including shape, surface roughness, porosity, and Young's modulus in the precision engineering.

Nano-technology has followed the success of micro-technology. Research in nanoscale has been undergoing tremendous growth since the nanoscale has become increasingly important for advanced bioscience and biotechnology. For example, materials like polymers, metals, and ceramics used for medical purposes have been characterised in nanometres. In regards to the biomechanical metrology, a majority of measurements are aimed to perceive detailed parameters of molecules, cells or tissues, such as stiffness, elasticity, and viscosity. To acquire the mechanical property of a target substance, depth-sensing indentation testing can provide useful information related to the deformation behaviour of materials.

Metrology is regarded as the key step in any manufacturing process. Basic metrology provides the dimension, geometries and other standard parameters of measurement. More sophisticated quantification of property metrology could be realised since the measurement precision has improved. In the last three decades, several state-of-the-art metrological tools have been developed to characterise mechanical properties of non-biological/biological materials at micro/nano-scale including:

- Scanning probe microscopy,
- Optical coherence tomography,
- Optical diffraction microscopy,
- Digital holography,
- Micro-computer tomography.

These micro/nano-dimensional metrological tools give a clear outline of in-

terferometric solutions to acquire basic static parameters of materials. However, modern technology has capabilities to measure the dynamic properties of materials, such as electrical, thermal, magnetic and mechanical characteristics. In this chapter, a novel biomechanical tester will be introduced to broaden a means to detect mechanical properties of biological samples. The tester is mainly used to characterise biological cells and tissues. Its hardware and software designs will be described in the following system calibration and experimental procedures.

3.2 Hardware design

3.2.1 Force transducer

General information

The major function of the system is to detect a force-depth curve of a single biological cell so as to determine the deformation behaviour, stiffness, elasticity and viscoelasticity. The main part of the system is the force sensing element. The force transducer used for detection was based on the capacitance changes of capacitors which were mounted with a cantilevered fused silica beams. Figure 3.1 shows the electronic configuration of the force transducer (400A - 407A series from Aurora Scientific Inc. Canada). As the charges of two capacitors (C_{force} and $C_{reference}$) are equal, it implies that no reacting force is applied from outside. Only while the indenter is in contact with the target materials does the subtraction of C_{force} and $C_{reference}$ become non-zero, which means the system will generate current proportionately to the detector circuitry block. The current signals are then converted into the voltage signal by the block (differential trans-impedance amplifier). After a difference amplifier and a buffer amplifier, the signal will flow through as linearised voltage output as Figure 3.1 shows.

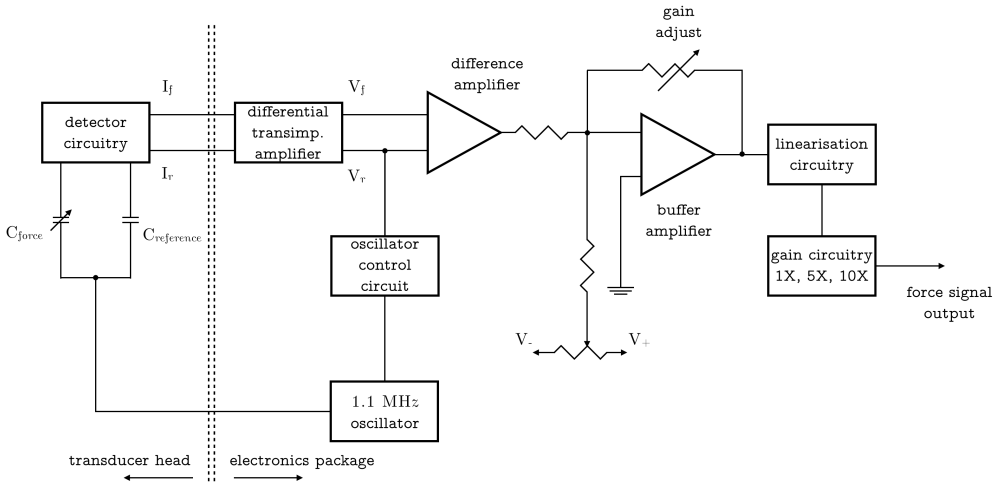

Figure 3.1: Schematic diagram of force transducer electronic block.

It is worth pointing out that before the current signals are passed to the block of a differential amplifier, the 1.1 MHz oscillator is also driven by the signals. This function allows the system to be thermally stable. When the temperature changes occurred the reference capacitor, the current signal will increase simultaneously. Hence, the voltage through the oscillator control block is affected by the current variation, which will then cause the control block to reduce the oscillation amplitude in order to finish the compensation of temperature for the sensing element.

The transducer (406A) can provide force resolution of 10 nN, which is the best force resolution compared with other modes in the 400A - 407A series (see Table A.2 in the appendix). The model offers a force sensitivity of 0.05 mN volt^{-1} which is ideally and sufficiently for individual cell/tissue characterisation.

Meanwhile, a satisfactory cylindrical flat indenter was mounted upon the lower head of the force transducer. Figure 3.2 shows the top and side view of the force transducer with its dimensions. There are three possible coupled forces directions that will be applied to the transducer. Arrow $a-a$ entails the ideal sensing

(a)

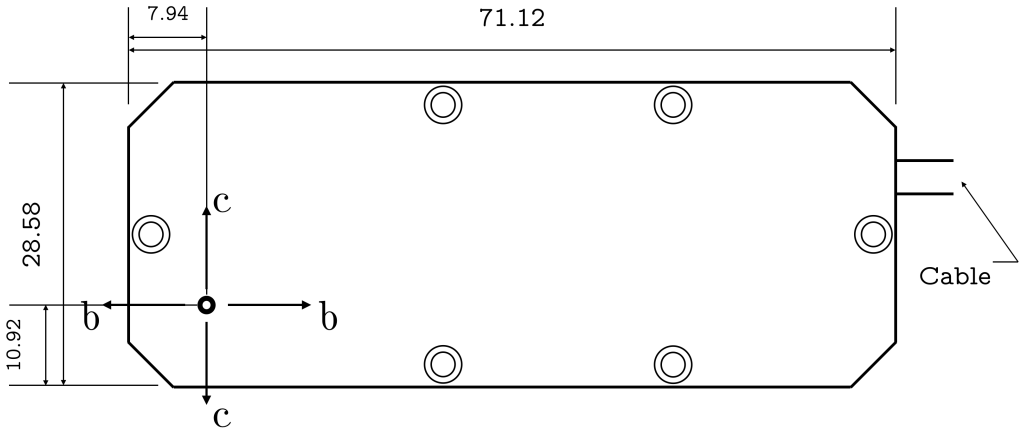

(b)

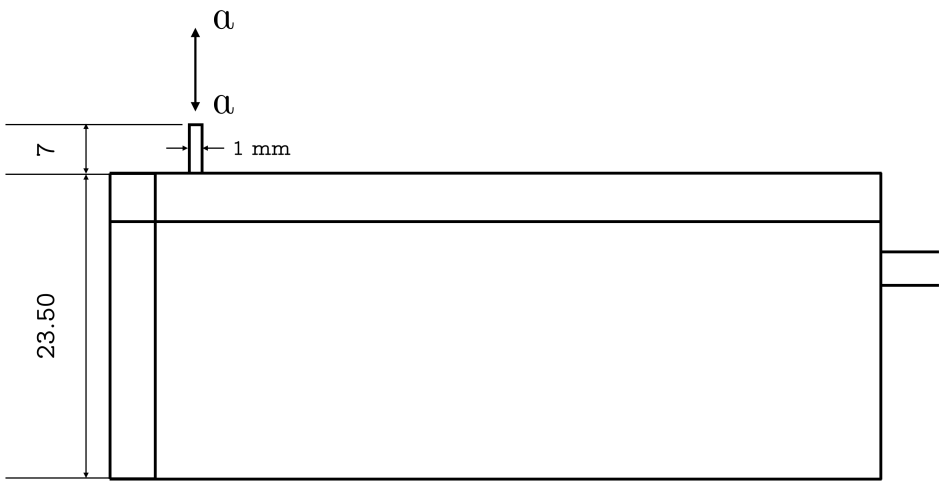

Figure 3.2: Schematic view of force transducer. (*a*) top view; (*b*) side view. Length in unit mm.

direction of force transducer. Forces on arrow $b - b$ or $c - c$ will not be sensed by the force transducer. The indenter, therefore, should be aligned with arrow $a - a$ so that the full output from the force transducer can be perceived while deforming the target objects.

Cylindrical flat punch

A modified indenter tip is the key to sensing the applied force onto the materials. Not only the tip surface will affect indenter in contact with samples, but also modelling indentation process will be difficult if the shape of the tip is not smooth. As shown in Figure 3.2b, the force transducer is mounted with a fine glass probe with 1 mm diameter and 7 mm in length. However, the probe is tubular which means that is not suitable to indent soft materials. A lid was required to cover the hollowed-out probe so that the entire cylindrical punch formed. The reason to use a cylindrical flat punch is because the fabrication and installation process is simple which only requires a flat lid to mount with force transducer whilst other types of lid such as cone or spherical ones comes with a special mounting process which does not fit with the current system set-up. The flat lid will be the part in contact with the samples during experiments. Since the force transducer is very sensitive and fragile, any overloaded force will damage the force transducer. A precise procedure was carefully designed to assemble a circular lid onto the hollow cylindrical probe.

Hard non-reflective polymer material was chosen to fabricate the lid. The reason for choosing the hard polymer is that the material is easily acquired and the surface is relatively smooth compared with metal. The mechanical strength is strong enough to compress the cells without self-deformation. One of the most prominent advantages is that polymer is easily carved and shaped. The probe on the force transducer as shown in Figure 3.2 dictates the lid should be a circular shape. The

diameter should be slightly larger than 1 mm. The probe covered with a wider radius lid could physically prevent the contamination towards the force transducer. Since a flat polymer lid is used as the cover to the indenter in the system, the indenter generally works as a cylindrical flat punch. Other possibilities like spherical and cone shaped indenters were also considered options. However, the fabrication and mounting procedure of them will most likely damage the force transducer.

After selecting the appropriate material and shape, the next step was to attach the lid onto the probe. Two major factors were considered in the process of glueing the lid. Firstly, the procedure should not harm the force transducer. It was planned to gradually move the probe downwards to be in contact with the binding agent and then firmly attach it to the tip. Secondly, due to further experiments being performed at a temperature approximately 37 ℃ and in aqueous solution, the binding agent should be stable at this temperature. Otherwise, the lid might detach from the probe during the experiment. Wax was the recommended material for the binding agent. The melting point is around 60 ℃ and it is an ideal material to resist liquid medium.

The procedure of mounting the lid onto the force transducer can be described in three stages:

Firstly, the force transducer should be mounted properly with the step motor stage and lid cut into a round shape with proper diameter. Prepare a heating ring on the x-y stage and heat up the temperature exceeding the wax melting point. The wax should be completely melted into liquid. Move the force transducer with x-y-z direction until it touches the wax. Then move back to the beginning position and wait till the wax nearly solidified. The residual wax on the probe was selected as the binding agent.

Secondly, place the well-cut lid on the x-y stage. Identify the contacting

position between the probe and lid from computerised software. Use the inverted microscope to validate the position. It also needs to make sure that the probe and lid are centrally aligned. Here, it is worthy of notice that changing the focus length of the microscope may provide a clearer look at both probe and lid so as to micro-adjust the central position.

Thirdly, lift up the force transducer in the z-axis direction. Small adhesion force from the wax may help to keep the lid bonded to the probe, but the adhesion force was not enough. The lid was well-attached and properly positioned. The heating ring was placed on the x-y stage again. Then lift downwards the force transducer for the second time to the touching point with x-y stage. Open the heating ring until the temperature of the wax reaches the melting point. Next, the lid was at the right position and wax has melted. The melted wax can be seen under the microscope. It was necessary to give a small displacement downwards (approximately 5 μm) to make sure that the lid was firmly attached. Then turn off the heating ring and wait until the room temperature reached. Hold the contacting status for about 5 minutes.

During the holding process, it can be observed that the forces will be changing continuously. It was because the temperature drops perpetually, which leaded to the x-y stage deformation. Hence, it was a good practice to keep the force constantly (over 300 μN) to make sure that the lid was stationary.

Finally, the lid was successfully attached. Next move upwards the force transducer. During experiments, the lid was fixed without detachment or shift. If the lid was contaminated or broken during the experiment, it was fairly easy to change the lid only by melting the wax and lift up the force transducer and do the process again with a new lid. Figure 3.3 shows the side and top view of the tip after the lid is attached on the force transducer.

(a)

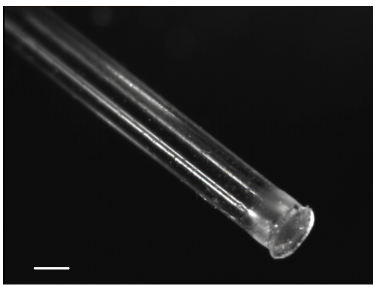

(b)

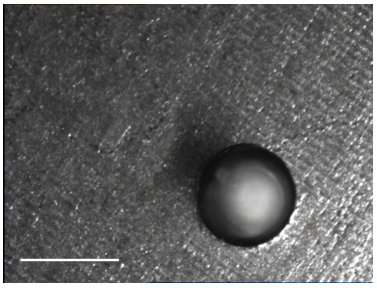

Figure 3.3: Schematic diagram of force transducer probe with the lid. (a) side view (b) top view. Scale bar, 1 mm.

3.2.2 Motorised stages

A precise motorised stage is one of the key components to generating micro- or nano- level translation. Step moving resolution directly dictates the accuracy of the displacement during measurement. In the project, the system copes with three-dimensional displacements so as to locate precisely the target materials/cells. With the aid of a CCD camera and visual lens, it is easy to locate the cell by sending commands to the system. Essentially, the x-y axis and z-axis step motorised stage will assist to move the Petri dish and force transducer respectively to the targeted positions. The resolution for x-y and z axis stage are 100 nm.

There are three major factors for a good stage, which are metric accuracy, resolution and repeatability. Fundamentally, the requested value should match with the actual value to a maximum extent, that is, metric accuracy defined in linear

motion devices. The reproduction of same output is another important factor for routine measurement which is defined by the repeatability. The resolution of the x-y stage is the original design from the factory. The specification and performance of the stages will be introduced in the calibration section 3.4.2.

xy-axis stage

The motorised x-y control system includes an Interactive Control Centre Joystick (ICCJ)(PS3J100 Control Centre, Prior Scientific), a modular system (ProScan™III, Prior Scientific) and a high precision motorised stage (H117-series ProScan™, Prior Scientific) as shown in Figure 3.4. ICCJ is a central position controlling accessory, which has an instant response to user's manipulation. The screen has a feedback to the intricate operation. For example, the stage can move diagonally because the x-axis servomotor underneath the stage can be triggered for only x-axis motions. The cubic black box is integrated with a modular system. The box controls stages of two directions and operates them simultaneously, *i.e.* with zero delays. The size is extremely small with the footprint of only 177×177 mm^2. If the stage system cooperates with fluorescence microscopy, the cubic box can be similarly used to control the excitation filter wheel. The third component is the x-y stage which is manipulated by the modular system. This stage is specifically designed to be integrated with inverted microscopes. With the travel range of 114×76 mm (in x and y directions respectively) and 400 steps for a single resolution, the x-y stage is ideal to achieve motions at micro-scales.

z-axis stage

The z-axis stage was directly connected with the force transducer and controlled the indentation depth. It was also required to deliver high resolution, metric accuracy

Figure 3.4: Schematic diagram of Prior Scientific xy-axis stage and its controlling units.

and repeatable measurements. Step motor linear stage (UTS 100CC, Newport) with its motion controller (ESP 301, Newport) is employed. The whole unit has long travelling range of up to 100 mm with maximum speed of 40 mm sec^{-1}. The resolution and minimum incremental motion are 0.1 μm and 0.3 μm respectively. It can bear 20,000 hours loads of 5 kg and 30% duty cycle.

3.2.3 Data acquisition

The system obtains the force and displacement reading from separate routes. The motorised stage was connected with host PC via USB 2.0 communication link, which was simply plug-and-use pattern. The serial port setting is introduced in the software design session (Chapter 3.3). The signal coming from the force transducer was a form of analogue input. The data would then be transferred into a computer via terminal I/O block, which was a 68-pin terminal block with SCC expansion slots (National Instrument, UK) connected with E-series DAQ (Data Acquisition) device

Figure 3.5: Schematic diagram of Newport z-axis stage. Left is controlling unit (ESP 301) and right is z-axis motorised linear stage (UTS 100CC)

as shown in Figure 3.6b. The SCC-68 block connector has four SCC modules for integrating multiple input signals. The connection of force transducer into PC host can be summarised in following three steps.

1. Find the output cable from the transducer (from 'OUT' dot to the terminal block on Figure 3.6a). Expose one end of the cable and attach them to NO. 68 and 24 on SCC-68, which refers to AI 0 and AI GND as shown in Figure A.4 in the appendix. The signals can then reach the breadboard area for I/O signal connection. This terminal has integration with computerised DAQ software that can simply acquire force transducer's readings. The next step is to connect with the PC host.

2. Attach the SCC-68 to the computer using MIO connector as Figure 3.6b shows. The cable connects 68 pins terminal block with 100 pins E-series PCI receiver (PCI-6036E, National Instrument, UK). The PCI receiver has sixteen 16-bit data acquisition channels and streams to disc at rates up to 200 kilo samples sec^{-1}. The number of channels and streaming rate is sufficient for force signal acquisition.

3. Finally, Figure A.2, A.3 and A.4 in the appendix show the name of each port for the application of data acquisition. The Labview controlling panel can easily discover the corresponding connection panels and mechanism, which will be introduced later in software design session.

In terms of the power supply of the connector block, if the SCC-68 was connected to the computer via PCI-DAQ board, there would automatically be +5 V power provided by the DAQ device that would be sufficient for low-power consumption use. The voltage would be distributed to all components in the connector block. However, if the power supply was not enough or there is a shortage of voltage due to an unstable computer PCI card, users can optionally use the SCC-68 power supply module to generate the power. The external power supply module shown in the

(a)

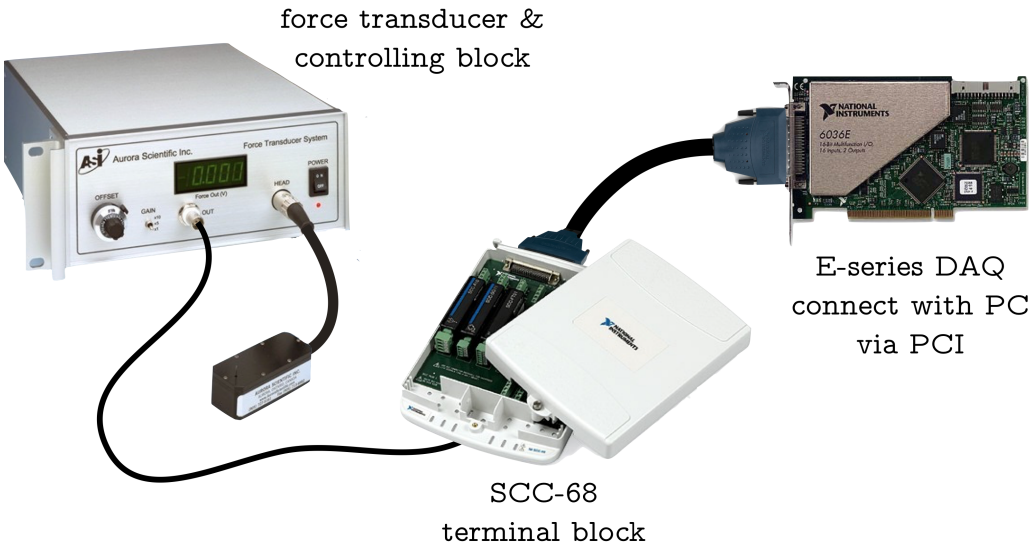

(b)

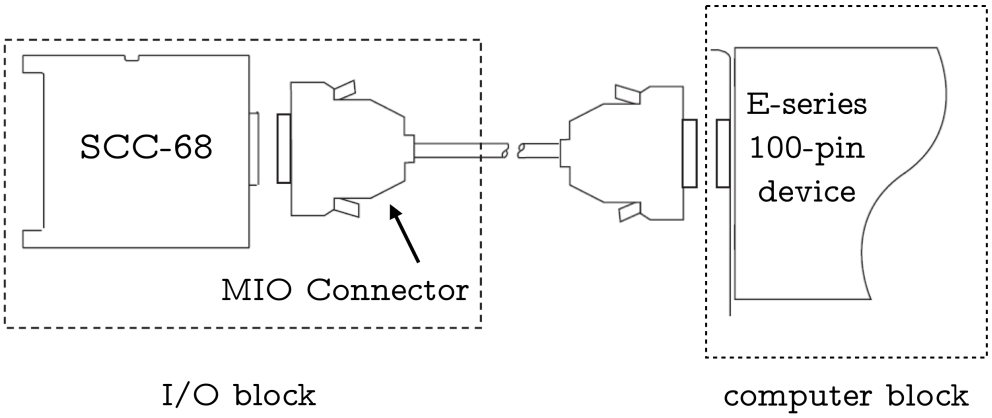

Figure 3.6: I/O connection pathway of acquiring data from force transducer. (a) Analogue voltage signals generated from force transducer are transmitted and converted into PC via controlling block, terminal block and DAQ. (b) Connection of I/O block and computer host.

Figure A.3 item 4 will be an alternative to support the system. The external power supply cable was required and the maximum input voltage should be limited to 15 volts. Exceed voltage would have a negative influence on the circuit and damage the device.

3.3 Software design

After the hardware was properly built, it was necessary to design the software to control the individual components from different manufacturers to work in coordination. The ultimate aim of the software programming was to develop a stable hardware controlling and data recording system. The only component needing to be manipulated was the z-axis stage. There were two primary parameters that were required to be logged that are the displacements from z-axis and forces from the force transducer. The data were recorded as a data matrix and displayed as plots by the software.

Labview (National Instruments, UK) is a programming language for system designing. The essential difference between Labview and other assembly languages is that Labview is completely based on the graphical programming (referred to as 'G'-language), also called data-flow language. Each programme is regarded as a VI (Virtual Instrument). Inside, users create different graphical block diagrams to realise action in demand and then pull those blocks together by drawing logical wires between them. Graphical block diagrams aim to represent the different parameters, algorithms, functions, DAQ (data acquisition) ports and so on. The 'wires' are used to propagate variables. While creating the block diagram and connector nodes, a corresponding front panel can be generated. The front panel serves as the user interface for defining initial values, monitoring progress and displaying outputs.

The natural advantage of graphical programming is that it can clearly show the data flow and the sequence of operating for each modular block. The language is designed to use for data acquisition, instrument control and automation where monitoring during a process is a critical requirement. In terms of the control interface, users can easily change the parameters and input instructions while the software is running. It is specifically applicable for the experiments requiring constant measurement, for example, the force and displacement measurement in the project. The initial input parameters and signals can be sent to the backstage from the front controlling interface. The algorithm and sequences are working in the backstage. All the novel designs and principles will be introduced in this chapter.

For the software design, Figure 3.7 shows the schematic diagram of general data flow and connection ports. The virtual instrument refers to the central Labview programme. A force transducer was connected via PCI/DAQ port. DAQ assistants were embedded with Labview software as shown in Figure A.5 and A.6, which cooperates with SCC-68 terminal connector. Users were able to extract force transducer inputs with specified sampling frequency and output format (continuous). Reading force input was relatively more straightforward compared to z-axis controlling and logging as the data flow from the transducer to PC was a one-way direction. The virtual instrument only reads voltage signal without sending instructions back.

However, the major challenge was to control and acquire data from z-axis stage. The virtual instrument should be capable of sending instructions to the device at the some time as receiving the readings from z-axis stage. The default communication interface of the ESP 301 controller was through 4-pin USB 2.0 connector located on the rear panel. Table 3.1 suggests the allocation of pins to provide power and transmit data. Due to the characteristic of dual channel communication, it was possible to control and receive data at the same time. The USB interface should be configured properly before the device starts communication. Labview se-

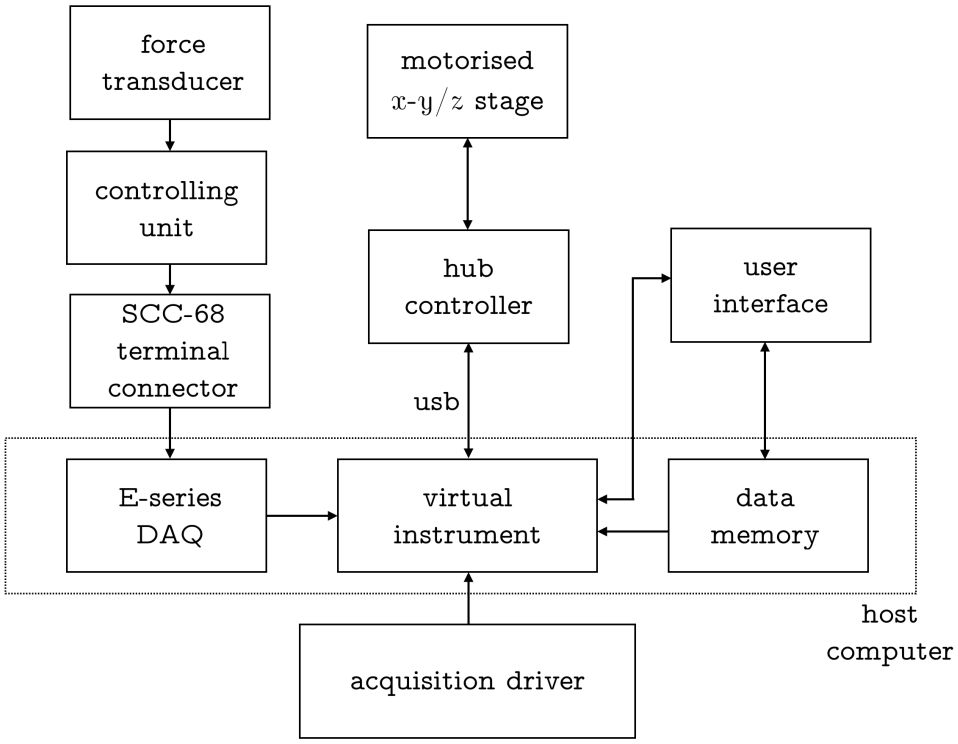

Figure 3.7: Data flow of system input and output. The blocks inside the dashed-box are host PC components. The arrows indicate the direction of data flow and controlling mechanism.

Table 3.1: USB 2.0 pin-to-pin allocation for data transduction

Pin No.	**Function description**
1	VCC+
2	Data out
3	Data in
4	GND

rial port sub-VI was established for communication. The system only works with 32-bit Windows-7 (Microsoft, US) operating system. The configuration was fixed at the 921,600 baud rate, 8 bits data, 1024 buffer size, no parity and 1 stop bit as shown in Figure A.7. The serial port number was found by checking the device manager in Windows OS.

The software was designed block by block. The aim was to manipulate the z-axis stage to a preset position and then move back to the initial value while recording displacement and force values. This moving pattern was called loading and unloading. According to user's manual of ESP 301 motion controller, the command pattern was specified by simply sending command syntax to the controller. Depending on the command, the system decodes and decides the motion. In Labview, 'concatenate strings function' palette is selected as the package to deliver a command to the controller.

Figure 3.8 introduced the experimental procedure and the sequence of how the software works. The first step was to recognise the initial value and starting point. Command 'DH' - referred to as define home is used to set the current position as home. After setting the motor speed by command 'VA' (setting velocity), the indentation depth was keyed in by command 'PA' (move to absolute position).

The software then initiated the next block which contains two parts of commands, namely the reading loop and the indentation. The indentation was monitored by a continuous query loop to check if the position is reached by command 'MD' (read motion done status). Meanwhile, a reading loop was recording the system time and current position from the serial port. The unloading part was similar to the loading procedure despite their opposite directions in displacement. To move reversely, the system was only required to recognise the 'home' position as the destination. After integrating the data acquired from the force transducer, the software was ended by the stop motion command 'ST'.

3.4 System calibration

The calibration of each component of the nano-biomechanical tester is introduced in this chapter. It mainly aims to verify the components' accuracy compared with factory defaults so as to validate the experimental data. The basic calibration procedure is to compare a known standard physics value with the output measured from the system. Forces from the transducer are determined by the mass of paper strips. Displacements of the motorised stage are calibrated by a laser distance meter. The calibration devices all have higher resolution than each component of the tester to ensure the overall performance of individual parts in the system. In this section, every component of the system will be calibrated and explained with real experimental data.

3.4.1 Calibration of force transducer

The purpose of calibrating the force transducer was mainly to determine linearity, sensitivity and repeatability. It is worth noting that the calibration of force trans-

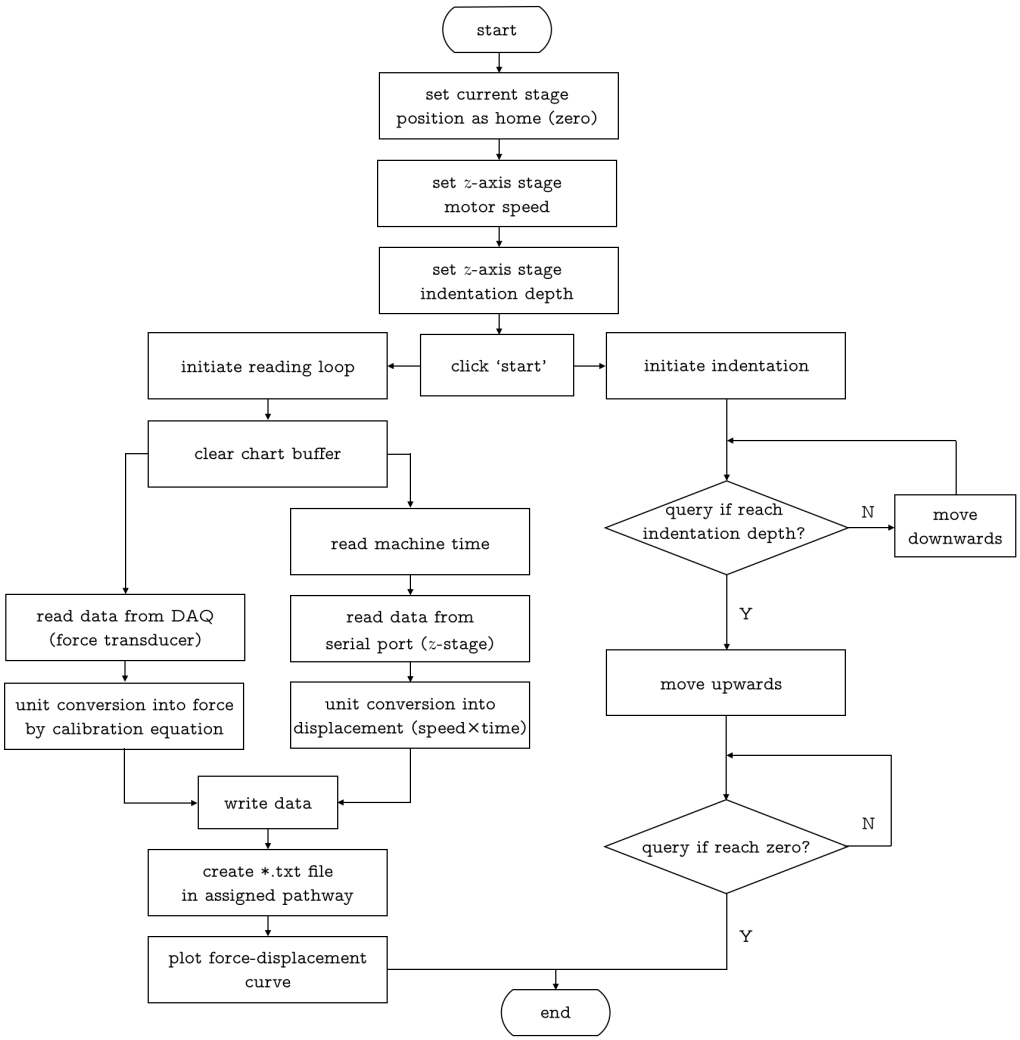

Figure 3.8: The flow chart for basic experimental procedures of acquiring mechanical properties of samples.

ducer should be the last procedure before any experiment so as to eliminate the risk of contamination. Frequent calibration of the force transducer was also required as the sensitivity can be affected by environmental changes such as temperature, humidity and duration of using the device. The calibration was performed right before each experiment to ensure the reliability of the experiment.

The calibration of the force transducer was undertaken by placing a known mass on the tip of transducer and recording the output voltage. The minute paper strips were used as the known scales (model 1702, Sartorius). Figure 3.9 shows the labelled paper strips. Their mass was measured on an accurate and calibrated scale twice as shown in Table A.4. The average loading force can then be calculated as the mean of two measurements as indicated in the following equation:

$$\text{loading force } (\mu\text{N}) = \text{average mass (mg)} \times 9.81 \text{ (N kg}^{-1}) \tag{3.1}$$

The estimated masses of paper strips, therefore, were used as the reference masses. The masses were placed on the force transducer to perform calibration. Here, it is worthy of notice that the paper scraps needed to be placed horizontally to eliminate any unbalanced force that would have caused inaccuracy in force transducer. Nevertheless, the central point should be found firstly and then be placed with the piece of paper on the force transducer. The paper strips should be cut into a square shape so as to find the central point straightforward. The output voltage is then recorded as Table A.4 shows.

Linearity and sensitivity

Table A.4 shows the mass measurement of paper strips versus the corresponding force output when the papers are placed on the transducer. Both mass and voltage have two readings that are obtained individually. The second set of data is acquired

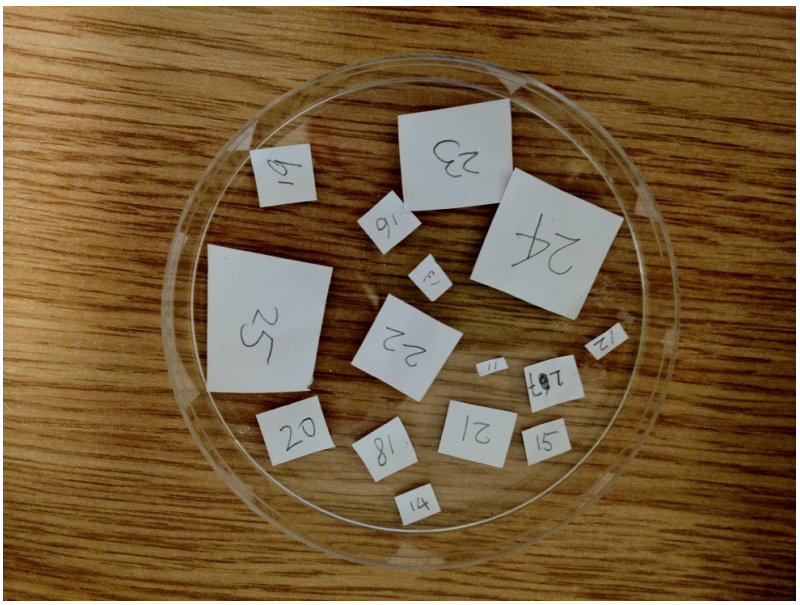

Figure 3.9: Labelled paper strips for calibration of force transducer.

after the completion of the first one. The linearity calibration was designed to obtain the relationship between output voltage and input mass. As Figure 3.10a shows, the black dots represent the measuring data. By using linear regression fitting, the goodness of fit reaches 0.9983 for R squared value and P value less than 0.0001. It, therefore, can be decided that the force transducer are in ideal linearity response. The fitting model can be represented as the following equation:

$$\text{Output voltage (volts)} = 0.02565 \times \text{Loading force } (\mu\text{N}) - 0.2622. \tag{3.2}$$

Figure 3.10b plots the residual between the fitted line and measured data. The residuals are in the range of $\pm$ 0.4 volts. Compared with maximum output 10 volts, the residuals ($\pm$ 4%) are in the acceptance range. After rearranging Equation 3.2, the sensitivity of force transducer can be calculated accordingly as 38.9863 (μN volt^{-1}) based on the Equation 3.3. From Table A.2, the sensitivity of factory default is shown as 50 (μN volt^{-1}). However, the real sensitivity can be determined based

(a)

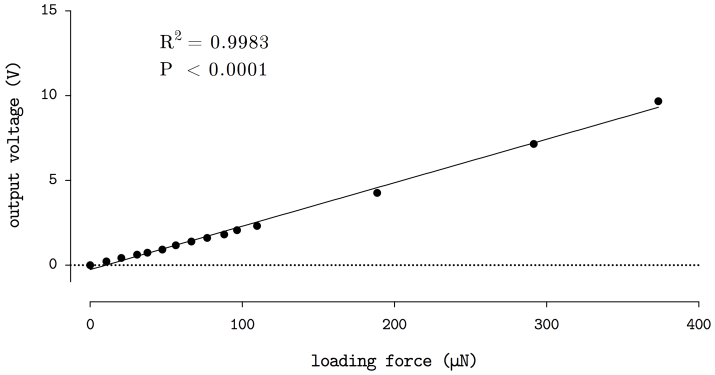

(b)

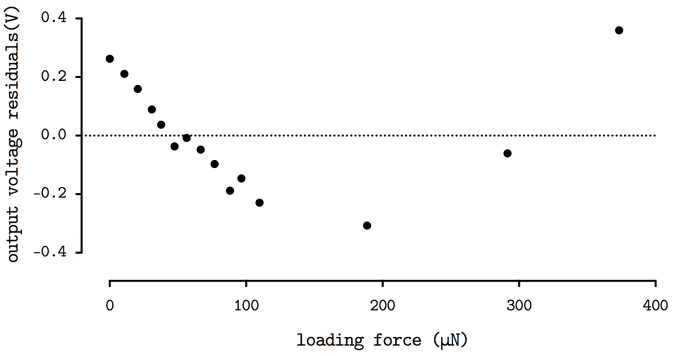

(c)

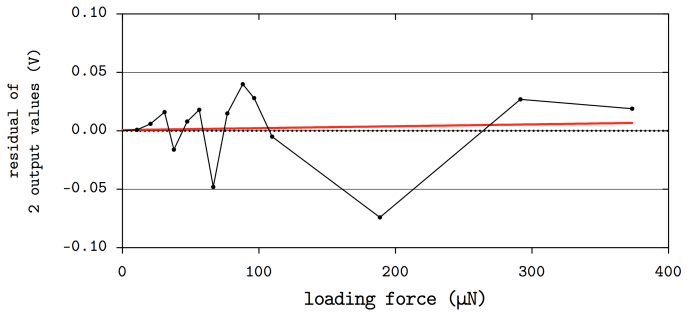

Figure 3.10: Performance of force transducer in linearisation. (a) Output voltage at different loading forces. Numbers are from Table A.4. R^2-value and P-value in (a) were calculated based on the linear regression model. (b) Residuals between output voltage and linear fitting against loading force. (c) Residuals of 2 output readings against average loading force. The red line suggests the linear regression fitting of residuals.

on the calibration as follows.

$$\text{Sensitivity} = \frac{\text{Loading force } (\mu\text{N})}{\text{Output voltage (volts)}} = \frac{1}{0.02565} = 38.9863(\mu\text{N volt}^{-1}). \quad (3.3)$$

Repeatability

Figure 3.10c provides the residuals of two output readings from Table A.4 against the average loading force. All residuals are within the range of ± 0.1 volts along with the slope of the linear fitted line close to zero, which clearly suggests the repeatability of force measurement can be trusted.

3.4.2 Calibration of z-axis stage

The aim of calibration of the z-axis motorised stage was to determine the accuracy of displacement. The standard of assessing a motorised stage is based on its resolution, metric accuracy, and repeatability. The calibration procedures will be introduced accordingly. Figure 3.11 shows the calibration set-up. The stage was placed on a horizontal anti-vibration table. The laser transmitter (XL-80, Renishaw, UK) produces a stable laser beam and was used to detect the distance between itself and measurement optics. The measurement optics was tightly mounted on the stage. The laser detector was well calibrated and its measurement resolution (1 nm) was two orders higher than the resolution of the UTS 100CC motorised stage (100 nm). The calibration procedures can be concluded as the determination of the metric accuracy, hysteresis and repeatability.

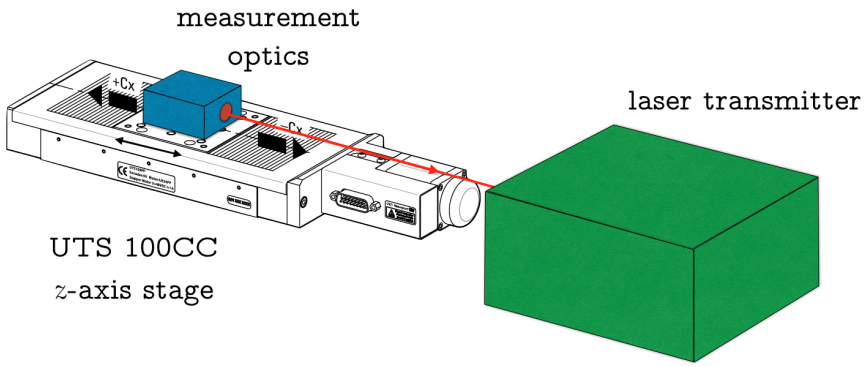

Figure 3.11: Schematic view of z-axis motorised stage calibration set-up.

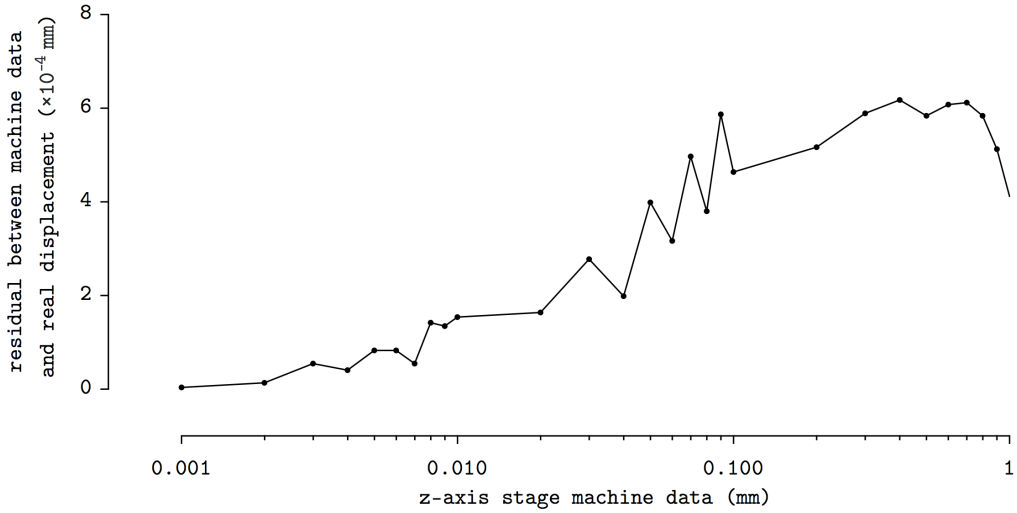

Figure 3.12: Performance of z-axis stage in its metric accuracy. The residuals between the machine data and real displacement are plotted against the device output. The x axis are plotted at scale of $\log_{10}$.

Metric accuracy

The first step of calibration was to measure the metric accuracy of z-stage. The results were concluded in Table A.3 which represented three different incremental precisions of 0.001 mm, 0.01 mm and 0.1 mm. The residuals between real detection and the machine data were calculated and plotted on Figure 3.12. From the diagram, it can be seen that the residuals between real data and machine controlled data were all less than 7×10^{-4} mm. A smaller amount of displacement will lead to less deviation, which was acceptable to the system. The mean of residuals was within 0.15% of the average machine output, which clearly shows the performance of its metric accuracy.

Hysteresis

The hysteresis effect on the system occurs when displacement exerts in two directions. One of the planned experiments was called the loading and unloading experiment, which means the z-axis stage will move forward and then recover back to the original position. The calibration of the hysteresis effect becomes crucial as this may directly affect the accuracy of measurement. Two sets of calibration experiments are performed with the various incremental precisions of 0.0002 mm and 0.002 mm as concluded in Table A.5. It shows that the hysteresis effect indeed exists in the system. With a higher amount of incremental steps, there will be greater hysteresis effect. However, the residuals plotted on Figure 3.13 shows that the hysteresis effect is relatively small compared with the resolution of motorised stage. Hence, the hysteresis effect was reasonably negligible.

(a)

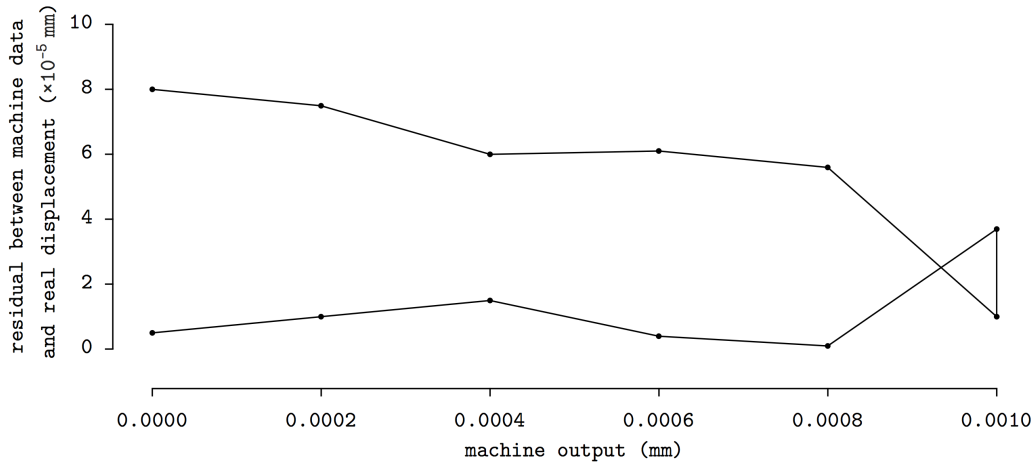

(b)

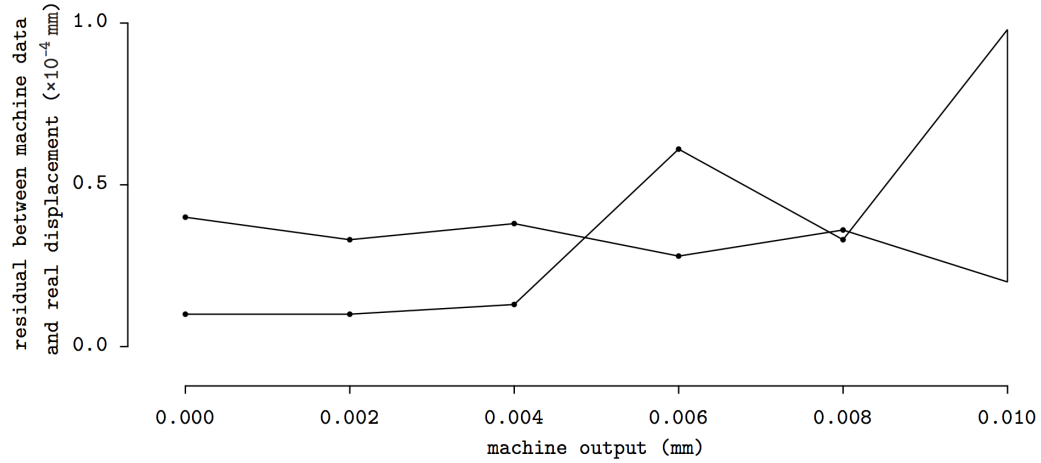

Figure 3.13: Performance of z-axis stage in its hysteresis. The residuals between machine data and real displacement are plotted against the device output at different increment step (a) 0.0002 mm; (b) 0.002 mm.

Repeatability

Repeatability of the motorised stage decides if the system can perform repeatable experiments in a short period. The repeatability examination was completed by moving the stage from home to a given distance five times. The data can be found in Table A.6. Figure 3.14 shows average residuals ± deviation between the machine data and real displacement. All residuals are within the range of 2.5×10^{-5} mm. The data again suggests that the errors are in the acceptable range (higher than manufacturer resolution) and the system is capable of performing repeatable experiments.

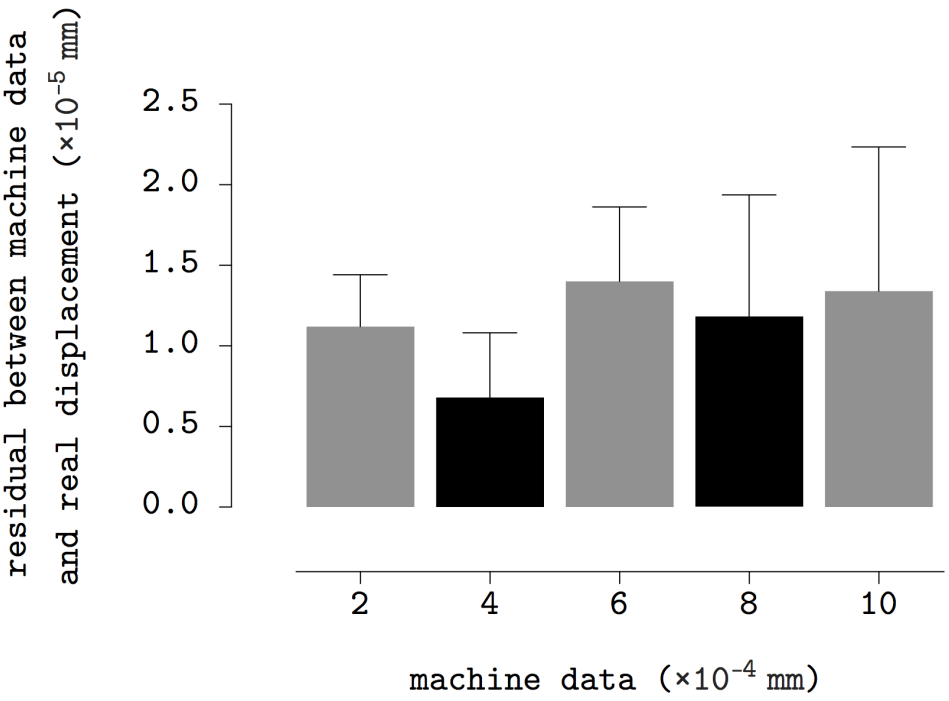

Figure 3.14: Repeatability examination of z-axis stage. Data denotes the mean ± s.e.m of residual between system outputs and real displacements.

3.5 Experimental setup

As shown in the Figure 3.15, the system is mainly comprised of a force transducer (406A, Aurora Scientific Inc.) attached with a cylindrical flat punch or indenter (*ca* 1 mm in diameter), z-axis step motor linear stage (UTS 100CC with ESP301 Motion controller, Newport), xy-axis stage (ProScan™III, Prior Scientific) and a temperature control heating plate (Temp. Control, iBidi). All components are mounted on an inverted microscope (TE2000-S, Nikon) and controlled by Labview software (National Instrument). The system has ultimate force and displacement resolutions of 10 nN and 100 nm respectively. The force transducer senses the force via the cylindrical indenter. Mechanical properties of collagen gels were measured by the detailed system. Nanoindentation of collagen gel was performed at controlled indentation speed. Force and displacement were recorded simultaneously during the loading/unloading indentation cycles. The whole system was placed on an anti-vibration table (Wentworth Laboratories Ltd.).

After the system was built and calibrated, it was necessary to set up a standard experimental protocol and make all components work in coordination. Figure 3.16 illustrates the standard experimental procedure to characterise mechanical properties of biological samples.

The mechanical characterisation of biological samples will be performed *in vitro*. Hence, the very first step is to establish a physiological environment that is similar to the human body. The heating plate (Temp. Control, iBidi) was used to generate a 37 ℃ environment where sterile Petri dishes are placed on top. Biological samples are cultured in a 37 ℃ and 5% CO_2 humidified incubator so that the Petri dishes and samples are preheated before experiments. To maintain the low CO_2 environment, during testing, all samples are immersed in the DMEM CO_2-independent medium. The use of CO_2-independent medium was necessary since the

(a)

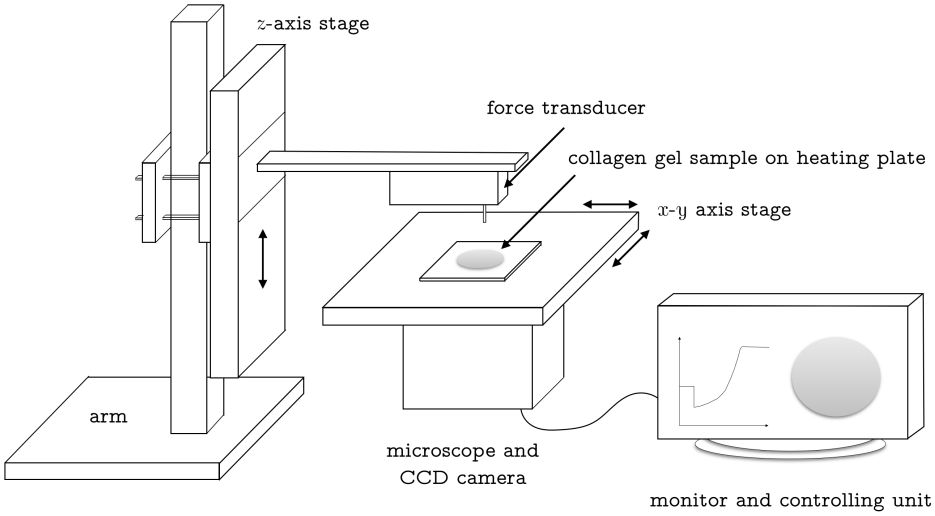

(b)

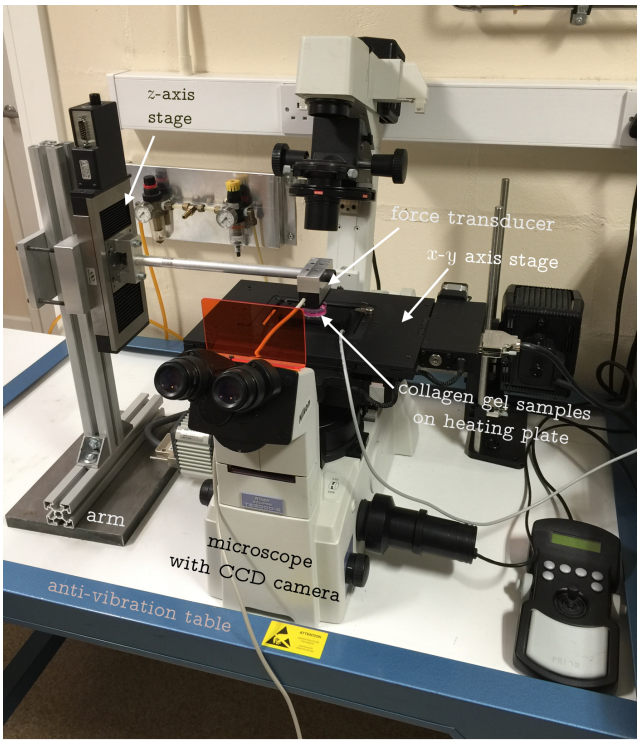

Figure 3.15: (*a*) Schematic of depth-sensing nano-indentation system for force-displacement measurement. (*b*) Image of nano-indentation system.

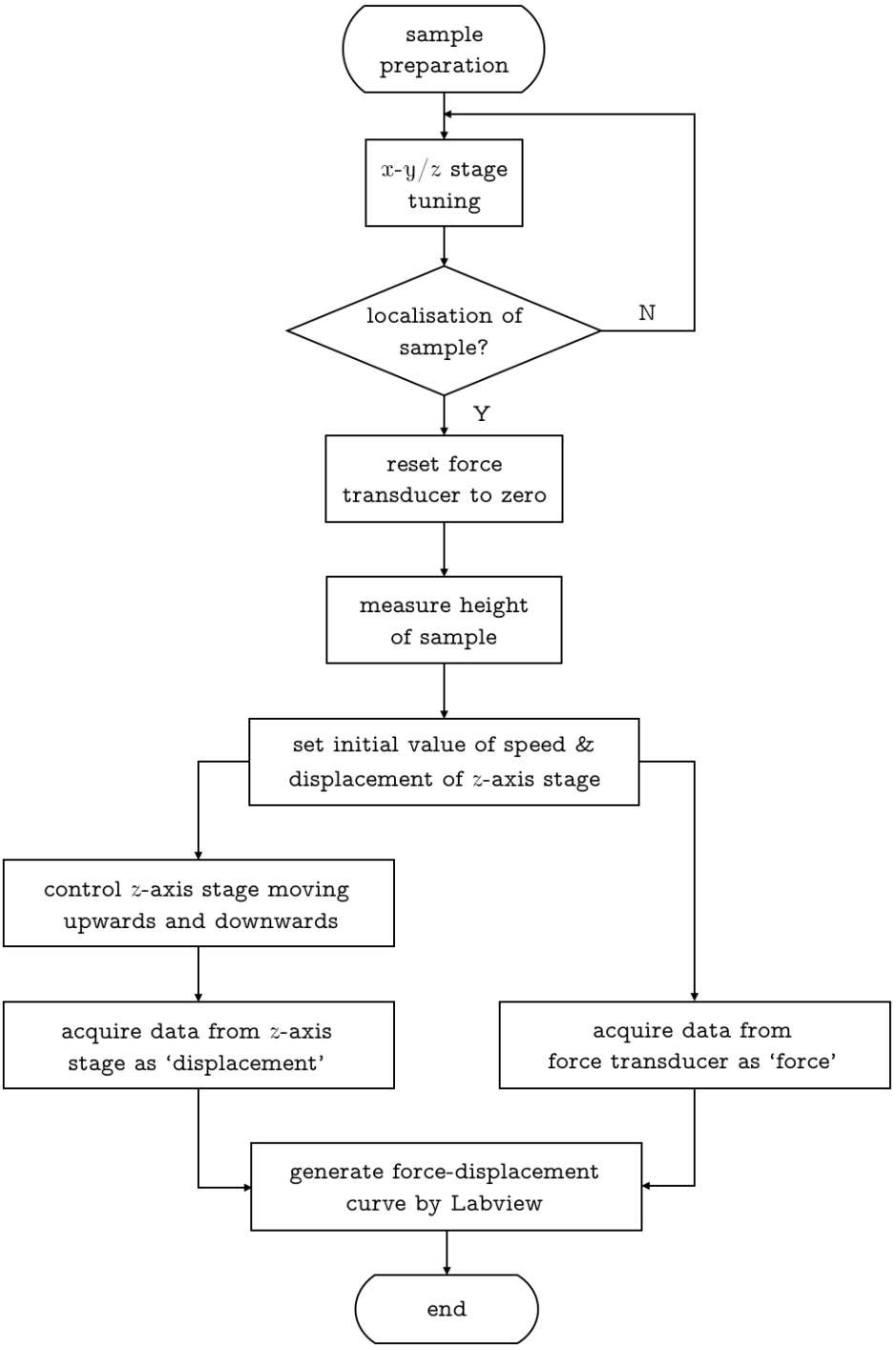

Figure 3.16: The flow chart for basic experimental procedures of acquiring mechanical properties of samples.

mechanical testing of biological samples was performed in the microscope without a CO_2 chamber. All experiments must be finished within a two hour period as the cells will become degraded from normal conditions. All cell culturing procedures and protocols are described in appendix A.

The next step was xy/z-stage tuning. It aims to deploy the Petri dish to the view of the microscope by moving the xy-stage. Similarly, positioning the force transducer to target biological samples. The procedures should be operated manually and repeatedly. The localisation requires the combination of microscopy and force spectroscopy. Cell samples should be fluorescently stained so as to visualise under the microscope since light through condenser was blocked by the force transducer. In the project, cells were stained by fura-2 AM, a ratio of metric calcium dye excited by 340/380 nm of light and 510 nm emission. The cells were pre-incubated with furo-2 AM for 30 minutes before being washed twice with PBS.

After force transducer and cells samples were aligned by checking under the microscope, force spectroscopy software was used to perform localisation of cell samples. The force transducer was moved downwards to approach the cell samples. A force curve is generated simultaneously to observe the approaching process. The increment displacement step of z-axis stage should be limited to 50 μm in order to prevent potential damage to the force transducer. A similar procedure can be applied to approach the surface of the Petri dish. The subtraction between the positions of the Petri dish base and indenter-cell contact point implies the average height of cell samples. The very last step before the measurement was to reset force transducer to zero manually.

The loading and unloading software introduced in Chapter 3.3 was used to perform the mechanical measurement. The initial speed and indentation depth for approaching depends on the height of samples. Normally, the entire period of

loading and unloading should be in the range of 90 to 120 seconds. The speed and depth can be calculated accordingly. The software will then control z-axis stage to move downwards and upwards. The data recording proceeds separately to acquire displacement and force signals. Finally, the system will generate Force-Displacement curve in Labview and create a text file for further data analysis.

Chapter 4

Measurement of fibroblast contraction force

Thanks to the development of nano-biomechanical test (see Chapter 3), cell contraction force of fibroblast can be measured based on an improved assay of cell-embedded collagen matrix. In parallel, a theoretical model has been established to calculate cell contraction force based on gel elasticity, thickness and radius. Histamine (100 μM) was used to stimulate human aortic adventitial fibroblast contraction while the myosin light chain kinase inhibitor ML-7 (25 μM) was used to inhibit cell contraction. The collagen matrix used in the model provides a physiological environment for fibroblast contraction studies. The study demonstrates that histamine can elicit a significant increase in contraction force of fibroblasts embedded in collagen, while the Young's modulus of the gel decreases due to the gel degradation.

4.1 Introduction

The collagen contraction assay was firstly reported by Bell *et al* [6] and has been described as fibroblast-populated collagen lattice (FPCL). The mechanism for fibroblast contraction is mediated by the control of myosin light chain (MLC) phosphorylation status through the action of MLC kinase (MLCK) [40]. As reviewed by Dallon and Ehrlich [27], raised intracellular calcium levels leads to calmodulin-dependent MLCK activation, which results in MLC phosphorylation and actin-myosin cross-bridge formation and filament sliding.

Human aortic adventitial fibroblasts (HAoAF) are resident in the adventitia of the aorta and they have been employed in experimental models of arterial remodelling and restenosis [153]. Histamine is an agonist that elicits increases in intracellular calcium and is released by basophils and mast cells during inflammatory responses. It acts on cells via a family of G protein-coupled histamine receptors, histamine receptor H1 through H4. Several studies have shown that human fibroblasts express H1 receptor and can be activated via histamine binding, resulting in phospholipase C activation and production of inositol triphosphates (IP3) and diacylglycerol (DAG) [79, 98]. The increase of IP3 causes calcium release from the internal stores and consequently triggers fibroblast contraction via activation of MLCK [66].

Several approaches have been developed to measure cell contraction forces *in vitro*; among these, collagen gel contraction assay (CGCA) and traction force microscopy (TFM) are the most common techniques. For the both methods, cell contraction forces are measured indirectly based on measurement of the deformation of the matrix surrounding the cells, such as a cell-embedded collagen gel or cell-seeded polymer substrate. However, the CGCA technique is used for the measurement of forces in populations of cells, while TFM is more suited for the measurement of

forces in single cells.

When CGCA is used for assessing contraction forces, cells are embedded within the collagen matrix, which provides cells with a physiological environment. Collagen is a key component of the extracellular matrix that facilitates cell migration and contraction [1]. Cell embedded collagen gels are easily constructed and the measurement of their contraction is straightforward. Conventional techniques used to measure collagen gel contraction rely on imaging only the gel area from a top-view. The estimation of contraction is often expressed by the area changes of the gels between the beginning and end of the treatment or cell contraction period [77, 167]. To improve the measurement of cell contraction kinetics for time-dependent changes, time-lapse-video-based imaging techniques have been developed to record changes in gel areas continuously while the cells contract [119]. Although the versatility of the CGCA method facilitates general use, it does not provide quantification of cellular contraction forces, since the mechanical properties of the collagen matrix will dictate the measurement accuracy of the cellular contraction forces. The elasticity of the disk-shaped collagen gel can be influenced by the cell treatments and the same amount of gel radius shrinkage may result from very different cellular contraction forces. Moreover, in the normal physiological environment, cells do not merely contract in a two-dimensional manner, therefore measuring the radius of gel disc only from the top view will not provide an accurate assessment of the magnitude of cellular contraction.

Alternatively, TFM was developed to measure single cell contraction forces by observing the underlying elastic polymer substrate (*e.g.* polyacrylamide gel) embedded with multiple fluorescence microbeads [17, 33, 168]. A number of mathematical models have been developed to facilitate the estimation of contraction force based on the relative motion of the beads. However, the stiffness of the gel substrate can be altered by cell differentiation and biochemical treatments during the measurement

and this may affect the accuracy of the force measurement. More importantly, it is more technically challenging to obtain results using the TFM method and measurements do not provide a true physiological model because the assessment of cellular contraction based on a 2D surface, instead of a 3D gel matrix.

To improve the accuracy of CGCA force measurements, a culture force monitor (CFM) system was developed by attaching strain gauges at the edges of a cell-embedded collagen gel to directly assess cell contraction [19, 32, 36, 37, 47, 86]. Cellular contraction force can be measured continuously without the influence of the elastic variation of collagen gel. Single cell contraction force can thus be approximately estimated by the measured force divided by the total number of the embedded cells. However, the measurement was only limited to a random uniaxial stress as the strain gauges could only measure the contraction in single directions.

Having taken into account the variation in the elasticity of the collagen matrix, we re-designed the collagen gel based assay technique to quantify cell contraction forces with a significantly higher degree of accuracy. The method essentially correlates the relationship between gel deformation and embedded cell contraction force. The elastic modulus and thickness of each collagen gel were routinely quantified by a bespoke nanoindentation tester and the data were used as input parameters for a simple mathematical model that correlates cell contraction force with gel properties, including radius, thickness, and elasticity, which varied throughout the different treatments. The single cell contraction force can also be determined providing that total cell number embedded in the gels are known. In this study, we have also applied the new gel-based sensing technique to investigate the contraction force of HAoAF treated with the agonist histamine or following co-treatment with ML-7, a well-established inhibitor of MLCK, to attenuate fibroblast contraction.

4.2 Material and methods

4.2.1 Cell culture

Cryopreserved Human Aortic Adventitial Fibroblasts (HAoAF) were purchased from PromoCell GmbH at passage 2. Cells were cultured at 37 ℃ in a 95% air/5% CO_2 atmosphere using phenol red-free Dulbecco's modified Eagle's medium (DMEM) supplemented with Fetal Calf Serum (FCS, 10%), penicillin (100 IU ml^{-1}), streptomycin (100 µg ml^{-1}) and L-Glutamine (2 mM). Cells at passage 7 to 9 were used in all experiments.

4.2.2 Collagen gel contraction assay

Collagen gel assay

Confluent HAoAF cultures were detached from flasks using trypsin/EDTA and cell number determined using a haemocytometer. After centrifugation, cells were re-suspended in DMEM containing 10% FCS at densities of between 0.5×10^6 and 2.5×10^6 cells ml^{-1} and mixed with culture medium containing collagen I (rat tail, Corning, EU) on ice at a ratio of 1:9, resulting in the final solution containing 1.76 mg ml^{-1} collagen type I, 2 mM L-glutamine, 100 IU ml^{-1} penicillin, 100 µg ml^{-1} streptomycin and 5% FCS. The pH level of the mixture is balanced by the 1M NaOH and 0.5M $NaHCO_3$. The cell suspension was transferred into 35 mm Petri dishes (1.2 ml $dish^{-1}$, achieving cell densities between 0.06×10^6 and 0.3×10^6 cells gel^{-1}) and incubated in a cell culture incubator for 20 minutes to polymerise the gel before addition of a further 1.5 ml DMEM containing 5% FCS. After incubation for 16 hours, the culture medium was replaced with fresh DMEM containing 5% FCS and collagen gels were dislodged from the edge of the dish using a sterile spatula. Gel

thickness and elasticity measurements were conducted 48 hours later. In experiments to address the effects of histamine on cell contraction, fibroblasts were re-suspended in DMEM containing 10% FCS at a density of 1.8×10^6 cells ml^{-1} (achieving a cell density of 0.216×10^6 cells gel^{-1}) and incubated for 16 hours before treatment of cells in the presence or absence of the myosin light chain kinase inhibitor ML-7 (25 μM) for 30 minutes. Some dishes were then stimulated with the agonist histamine (100 μM) to elicit cell contraction. Collagen gels were then immediately dislodged from the dish using a sterile spatula with gel thickness and elasticity measurements conducted 5 hours later.

Experimental measurements

A depth-sensing nanoindentation tester (Figure 4.1a, details see Chapter 3.5) was developed to quantitatively measure the thickness and Young's modulus of the cell-embedded collagen gel, which were used as input parameters to estimate contraction force (see Section 4.3.2). When the thickness and elasticity were measured, collagen gel was plated in the 35 mm Petri dishes with no culturing medium on the heating plate at 37 ℃. Ten random positions were picked and measured to generate ten different Force-Displacement (F-D) curves for analysis. The gel indentation was performed at a controlled speed of 40 μm sec^{-1} to generate the Force-Displacement curve.

The thickness of the gel was measured based on the displacement difference between the gel's top surface and the Petri dish surface, while the gel elasticity was measured based on the analysis of the indentation F-D curves. The first 25-30% of the curve was extracted to determine Young's modulus (E) by fitting a non-linear strain dependent elasticity model as shown in Figure 4.1b. In parallel, a computerised camera has been used to measure the radius of the disk-shaped

(a)

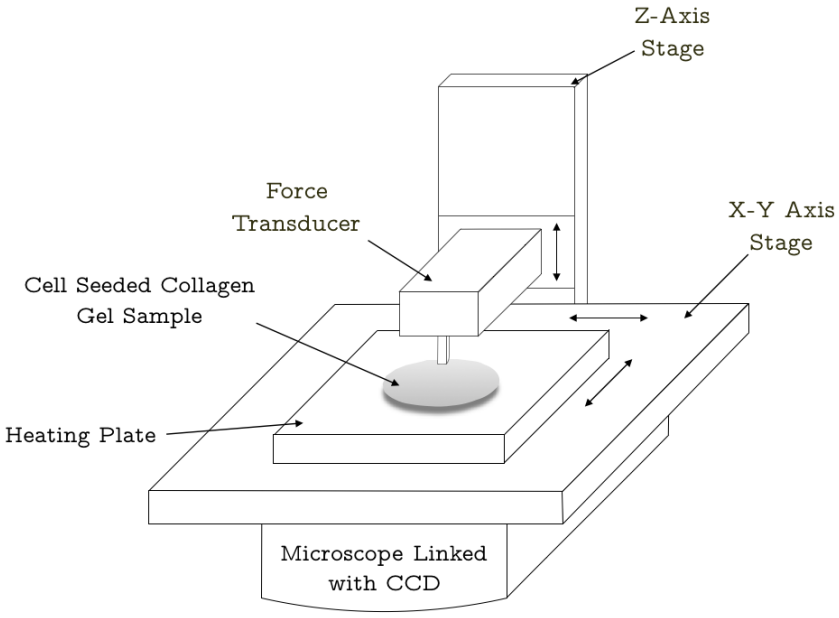

(b)

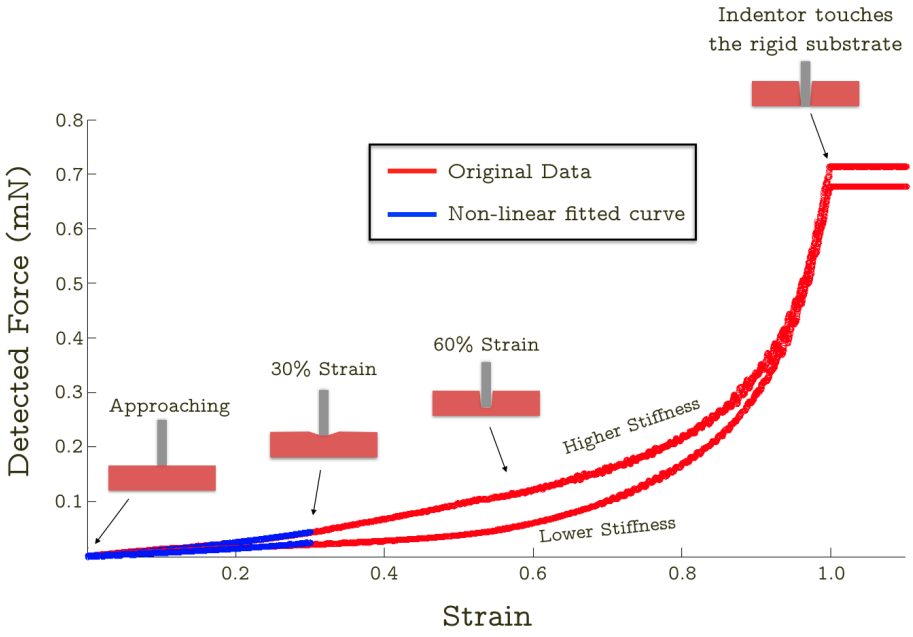

Figure 4.1: (*a*) The schematic setup of bio-nano-indentation tester. (*b*) Typical loading Force-Displacement curves of collagen gels with higher and lower stiffness indented by a flat punch.

hydrogel, from the vertical top view, and the radius change before and after cell contraction can be determined by referencing the culturing area of Petri dishes. The measurement accuracy of the radius was up to 1 μm.

4.3 Mathematical modelling

4.3.1 Young's modulus of collagen gel

The Young's modulus of collagen gel is modelled by employing non-linear strain dependent elasticity [148]:

$$E = E_0 \cdot \frac{1 - \bar{\epsilon} + \frac{\bar{\epsilon}^2}{3}}{(1 - \bar{\epsilon})^2} \tag{4.1}$$

where E_0 is the Young's modulus (E) at strain $\bar{\epsilon} = 0$. To estimate the Young's modulus, it is necessary to find a suitable connection between F-D curve and the modulus. When a cylindrical punch indents a flat elastic substrate (collagen gel), a linear relationship derived from Hertz contact theory can be express as [80]:

$$E^* = \frac{F}{2rD} \tag{4.2}$$

where E^* is reduced modulus of collagen gel, r is the radius of cylindrical indenter, D is the displacement or depth of indenter into the collagen gel surface, and F is the force measured by the force transducer. For two elastic bodies in contact, the reduced modulus can be also described as following according to Hertz contact theory [60]:

$$E^* = [\frac{1 - \nu^2}{E} + \frac{1 - \nu_i^2}{E_i}]^{-1} \tag{4.3}$$

where ν is the Poissons ratio and E is the Young's modulus of indented collagen gel. The subscript i refers to the properties of cylindrical indenter. The values of ν are in the range of 0.42-0.48, which were calculated based on the measured radii and

thicknesses of the collagen gel disks before and after contraction. The indenter is regarded as perfectly rigid, *i.e.*, $E_i = \infty$, and thus combining (4.1), (4.2) and (4.3), the following equation can be derived:

$$F = E_0 \cdot \frac{2rh}{1-\nu^2} \cdot \frac{\bar{\epsilon} - \bar{\epsilon}^2 + \frac{\bar{\epsilon}^3}{3}}{(1-\bar{\epsilon})^2} \tag{4.4}$$

For the strain $\bar{\epsilon}$ can be approximately calculated as the ratio of the displacement of indenter to the measured thickness of the collagen gel, H, *i.e.*, $\bar{\epsilon} = D/H$. Hence, by using non-linear least square regression to fit $F(\bar{\epsilon})$ with D based on the Equation (4.4), the Young's modulus E_0 of collagen gel can be estimated from each measured F-D curve.

4.3.2 A theoretical model to measure contraction force

A simple theoretical model has been developed to estimate cell contraction force (F^*) based on the force balance between cell contraction and gel deformation. As shown in Figure 4.2, thickness (h_0 and h_1) and radius (r_0 and r_1) of a disk-shape collagen gel at the beginning and end of contraction. The Young's modulus E of collagen gel is described by the linear elastic mechanics as:

$$E = \frac{\mathrm{d}\sigma}{\mathrm{d}\varepsilon} \tag{4.5}$$

where $\mathrm{d}\sigma$ and $\mathrm{d}\varepsilon$ represent stress and strain respectively, generated by cell contraction to the gel. During the entire contraction process, the contraction force acts perpendicularly on the circumference surface which area can be expressed as $2\pi r \cdot h$. Hence the stress $\mathrm{d}\sigma$ can be calculated by radial contraction force $\mathrm{d}F$ per unit area

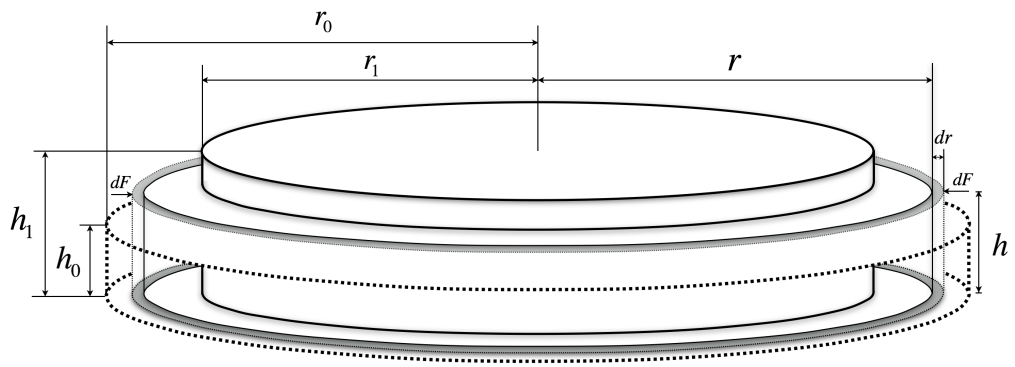

Figure 4.2: Schematic of theoretical model for collagen gel before and after contraction.

as the equation:

$$\mathrm{d}\sigma = \frac{\mathrm{d}F^*}{2\pi r \cdot h} \tag{4.6}$$

where r and h are the immediate radius and thickness of collagen gel. Correspondingly, the strain $\mathrm{d}\varepsilon$ can be expressed as the deformation of collagen gel at radial direction.

$$\mathrm{d}\varepsilon = \frac{\mathrm{d}r}{r} \tag{4.7}$$

Hence, combing the equation (4.5), (4.6) and (4.7), Young's modulus E_0 can be expressed as:

$$E = \frac{\mathrm{d}\sigma}{\mathrm{d}\varepsilon} = \frac{\mathrm{d}F^*}{2\pi h \cdot \mathrm{d}r} \tag{4.8}$$

Here, the average thickness can be expressed as $h = \dfrac{h_0 + h_1}{2}$ if the gel thickness change is approximately linear during the contraction process. After rearranging the equation (4.8) with integration, the final overall contraction force therefore can be presented as:

$$F^* = \int_{r_1}^{r_0} \mathrm{d}F^* = \int_{r_1}^{r_0} \pi E(h_0 + h_1)\mathrm{d}r = \pi E_0(h_0 + h_1)(r_0 - r_1) \cdot \frac{1 - \bar{\epsilon} + \dfrac{\bar{\epsilon}^2}{3}}{(1 - \bar{\epsilon})^2} \tag{4.9}$$

The model simply correlates the overall cell contraction force F^* with the measured material parameters, including Young's modulus, thickness, and radius of collagen gel. Single cell contraction force is approximately calculated as the overall contraction force divided by the counted cell numbers.

4.4 Results

4.4.1 Young's modulus of collagen gel

Typical indentation curves and their corresponding non-linear fitting curves are represented in Figure 4.3a. First 25% of indentation depth to the gel thickness (*i.e.*, strain up to 0.25) is selected to estimate Young's modulus of collagen based on the minimum least square fitting of the equation (4.4) with the experimental force-strain data. Figure 4.3b shows the Young's modulus for HAoAF-embedded collagen gels for controlled gel and treated gel at the cell density of 0.216×10^6 (cells gel^{-1}). After the treatment with histamine, the Young's modulus of collagen gels were decreased by 41.2% compared with the untreated ones, while treatment with ML-7 shows the gently inhibitory effect of decreasing elasticity (*ca* 59.3%).

4.4.2 HAoAF contraction force after histamine and ML-7 treatment

The images shown in Figure 4.4b and c demonstrate the shrinkage of the HAoAF-embedded collagen gels treated by histamine with/without ML-7 compared with the untreated gel (Figure 4.4a). The shaken gel sizes/radii can be calculated by counting the pixels of the gel images referencing the culturing area of Petri dishes. By substituting the measured radius, Young's modulus and thickness of collagen gels into the equation (4.9), HAoAF contraction force can then be estimated. Figure

(a)

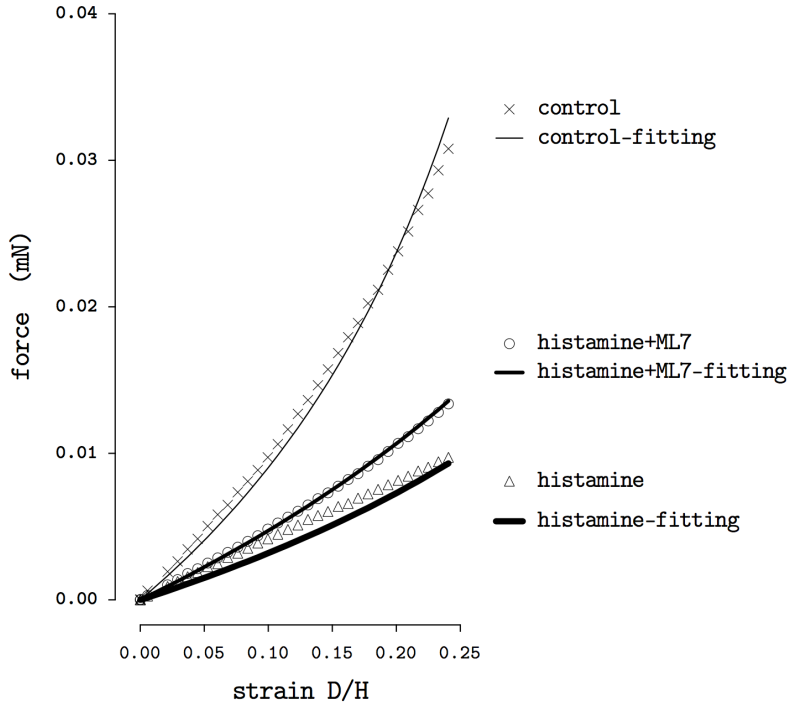

(b)

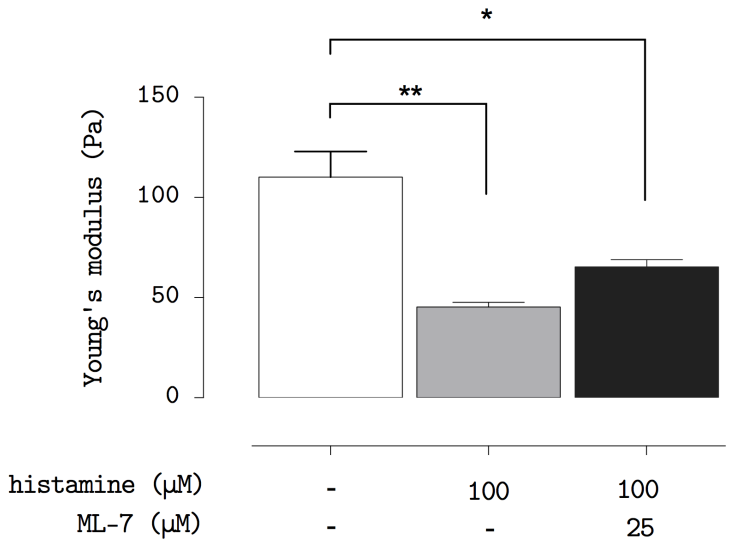

Figure 4.3: (a) Typical Young's modulus fitting of collagen gel contraction measurement from force-strain curve. (b) Data denote mean ± s.e.m of Young's modulus of collagen gel with/without histamine and ML-7 from three independent measurements ($N = 3$). P-value was calculated using One-Way ANOVA with Bonferroni Post-Hoc test. $^{**}P < 0.05$, $^{*}P < 0.5$.

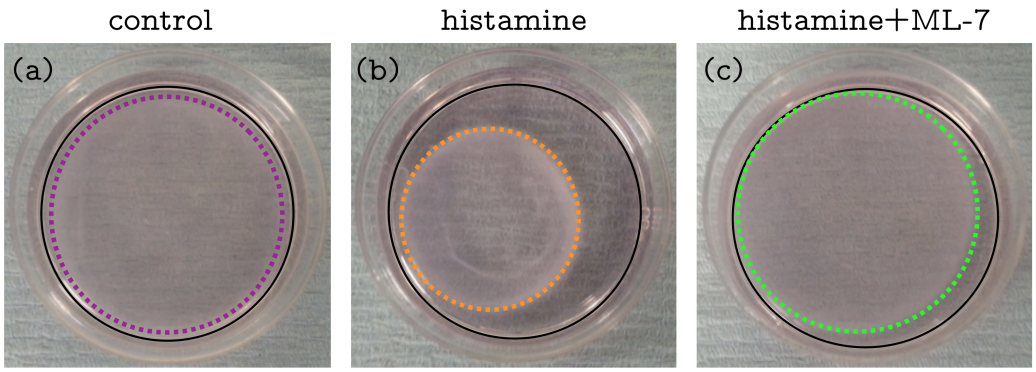

Figure 4.4: Photographs of the typical HAoAF embedded collagen gel after treatments. (a) controlled collagen gel, (b) agonist histamine (100 μM) stimulated collagen gel, (c) Histamine stimulated collagen gel with the presence of myosin light chain kinase inhibitor ML-7 (25 μM). The areas circled with black solid lines in (a), (b) and (c) represent the culturing areas of 35 mm Petri dishes. The areas circled with coloured dash lines in (a), (b) and (c) denote the sizes of collagen gels, which were calculated by referencing the culturing area of Petri dishes.

4.5 shows that when cells were treated with histamine (100 μM), there was a nearly three-fold increase of contraction forces from 0.3 ± 0.04 to 0.89 ± 0.02 mN of overall contraction force. In the meantime, single cells contraction forces were calculated by the overall contraction force divided by the total number of cells embedded in collagen gel. The single cell contraction forces correspondingly increases from 1.41 ± 0.4 nN to 4.15 ± 0.5 nN when histamine was added. The myosin light chain kinase inhibitor ML-7 (25 μM) attenuated the increase of contraction forces by 60%.

4.4.3 Cell density effects on contraction force

In the study, a constant volume of collagen gel was embedded with different cell numbers to examine whether cell density could potentially have an influence on single cell contraction force. As shown in Figure 4.6, the gel contraction forces determined for three different cell densities, *i.e.*, 0.06, 0.12 and 0.3×10^6 (cells gel^{-1}), have been measured after 48 hours. The result shows that the overall contraction force calculated as determined by linear regression increases in a linear manner with

(a)

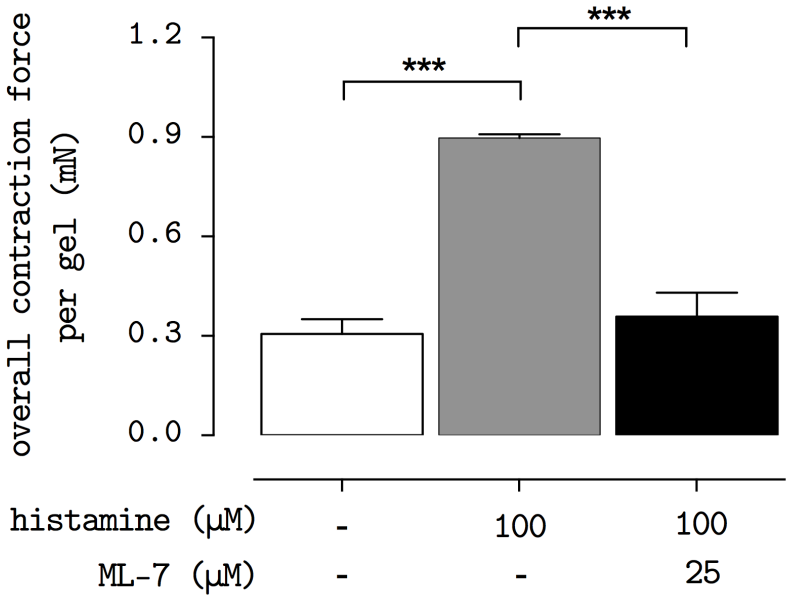

(b)

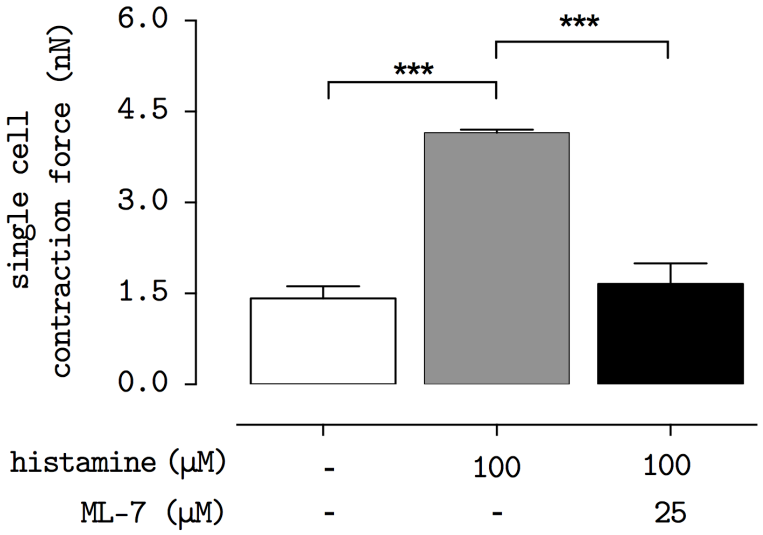

Figure 4.5: HAoAF were embedded into collagen gels at different density of 0.216×10^6(cells gel^{-1}). (a) Overall contraction force and (b) Single cell contraction force per gel with/without Histamine and ML-7. Data denote mean ± s.e.m from 3 independent measurements, P-value was calculated using One-Way ANOVA with Bonferroni Post-Hoc test. $^{***}P < 0.005$.

the seeding densities of fibroblasts. As a result, the cell densities within the gels can be assumed to have no significant influence on the single cell contraction force measurements.

4.5 Discussion

This chapter describes a novel method to assess cellular contraction force *in vitro* using a collagen gel-based sensing technique to demonstrate cell contraction force changes in fibroblasts treated with the agonist histamine, which increases intracellular calcium to elicit contraction, and attenuated by the MLCK inhibitor ML-7. It is worth highlighting that conventional collagen gel contraction assays have been mainly based on the observation of the change of cell-embedded collagen gel area [173], although a few studies have included measurement of the gel thickness [88]. However, the Young's modulus of the gel should be regarded as one of the key parameters required to estimate the cell contraction force, as described mathematically by the equation (4.9). The result (Figure 4.3 & 4.5) demonstrates the significant increase in cell contraction force after histamine treatment, despite the Young's modulus of collagen gel decreasing. Since the treatment conditions or state of cell differentiation may alter the gel elastic modulus, careful characterisation of the gel elasticity before and after the culturing period are critical to accurately determine the cell contraction forces.

A significant increase in single cell contraction force by histamine treatment has been demonstrated using this novel technique by combining nano-indentation with mathematical modelling of collagen gel contraction. As reported in the literature [66], histamine can elicit an extensive contraction of cells as measured using CGCA. However, adding ML-7, an MLCK inhibitor, to the collagen gel can significantly attenuate the cellular contraction elicited by histamine, confirming that the

(a)

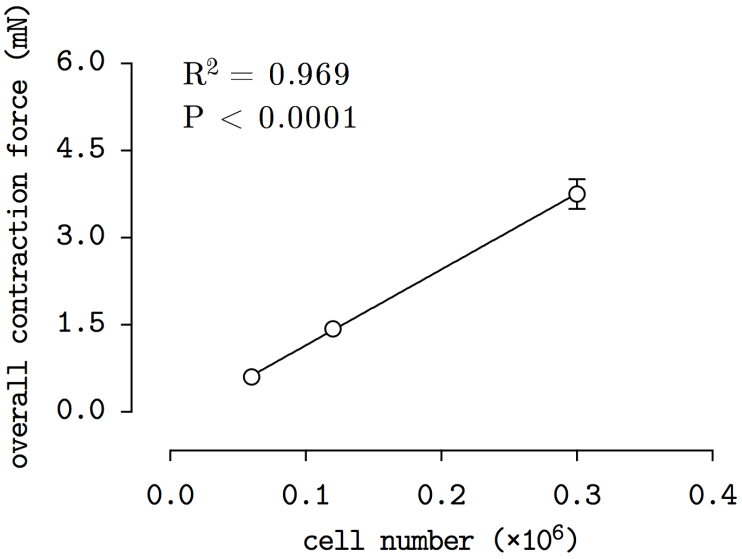

(b)

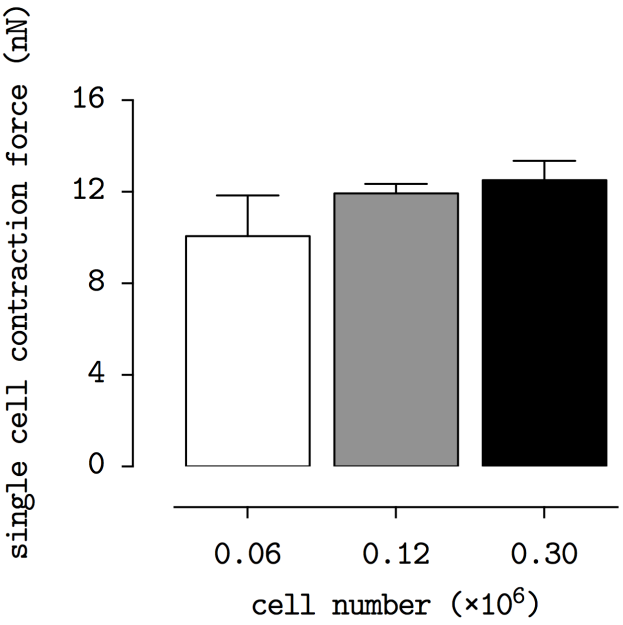

Figure 4.6: Cellular contraction force at different cell densities. (a) Overall contraction force of HAoAF at three different cell densities, *i.e.*, 0.06, 0.12 and 0.3×10^6(cells gel^{-1}). (b) Single cell contraction force of the three cell densities. Data denote mean $\pm$ s.e.m from 4 independent measurements, P-value and R^2-value in (a) were calculated based on the linear regression model.

fibroblast contraction was mediated via MLC phosphorylation [109]. Overall, the order of magnitude of cell contraction forces measured using this novel technique was in the same order to those values determined by other methods, *e.g.*, CFM [19, 48].

As shown in Figure 4.6, single cell contraction force was demonstrated to be cell-density independent. As the histamine treated collagen gels were only allowed to contract for 5 hours before the measurement, the cell proliferation during this period was negligible, and cell numbers can be reasonably assumed to remain constant throughout the measurements. Single cell contraction force can be therefore calculated by overall contraction force divided by known initial cell numbers. However, for longer-term measurement (more than 24 hours) in the cell-density contraction experiments, it was noticeable that cells were aligned on the bottom of the Petri dishes. This implies that there may be a potential cell-number loss and the collagen gel liquid content may be reduced [6]. Moreover, cell proliferation rate during long-term treatment could cause a significant increase in cell number within the gels. Assessment of total DNA content would be a possible way to verify whether the final cell numbers within the gels remain constant at the end of the assay.

Nevertheless, from the results shown in Figure 4.6b, single cell contraction force can be calculated by the initial cell seeding number as there was no significant force difference measured between the different cell densities. We have shown that 0.1×10^6 cell gel^{-1} is an ideal cell seeding density for the long-term contraction force measurement while a higher cell seeding density, *e.g.*, 0.3×10^6 cell gel^{-1} will be desirable for shorter periods of measurement (less than 24 hours). This is because with the same amount of cells embedded, contraction assays performed soon after seeding (less than 6 hours) will generate less overall contraction force than measurements taken after a longer period (24 hours) due to cell proliferation. Therefore increasing cell seeding density provides a greater overall contraction force and result in more accurate measurements of cell contraction force.

The novel technique reported in this study is applicable to assess forces generated by any cell type that can be cultured within a 3D collagen gel and responds to agonist stimulation leading to cell contraction. For example, assessment of forces elicited by vascular smooth muscle cells may indicate the likelihood of a treatment causing contractile responses that may lead to hypertension [166] while assessment of contraction forces in dermal fibroblasts may provide insights in wound healing potential of drugs, anti-wrinkling properties of therapeutic compounds or suitability of 3D gel matrices for tissue engineering of skin substitutes [2, 14, 54]. These are only a few potential applications where the novel technique to assess cellular and gel contraction forces may provide important information for future bioengineering and clinically relevant therapeutic strategies.

4.6 Summary

This chapter has demonstrated a novel technique to quantify cellular contraction force when cells are embedded in a three-dimensional collagen gel matrix. The histamine-induced contraction of fibroblasts through MLCK activation and MLC phosphorylation, determined in cells seeded in a collagen gel, are in agreement with observations previously reported in literature [48]. The alteration in the collagen gel elasticity before and after histamine treatment was measured. The measurements have confirmed that the mechanical property changes of the gel matrix should be taken into account to measure cell contraction forces accurately using gel contraction assays.

Chapter 5

Collagen matrix stiffness influences fibroblast contraction force

In the previous chapter, contraction force in human aortic adventitial fibroblasts seeded within a 3D collagen matrix was quantified by a novel force sensing technique. Furthermore, in this chapter, the quantitative correlation between the Young's modulus of the collagen matrix and the fibroblast contraction force has been studied by using the technique.

5.1 Introduction

The culture of cells within 3D matrices has been used for several decades [55]. The behaviours of cells in tissue-like matrices, such as migration, contraction and proliferation, exhibit an ideal model of their *in vivo* phenotype. Several materials have been

developed for the synthesis of cellular encapsulated hydrogels. Collagen, alginate, fibrin and agarose are extensively used as the natural polymer ingredients to construct engineered tissue equivalents [1]. Among these, collagen has been recognised as one of the major components in connective tissues, which forms stable fibrils and provides multiple cellular binding sites [7, 124]. Fibroblasts are the main cell type that influence remodelling and biosynthesis of collagen fibrils [55]. As the structure of collagen provides a mechanically stable framework, the contractile properties of fibroblasts seeded within a collagen matrix provides a good model for investigating tissue physiology and pathology.

Currently, one of the most prevailing techniques to obtain cellularised collagen gels is modified from the method of Bell *et al* [6]. Measuring the contraction of cells-embedded in 3D matrices is relatively straightforward using the conventional collagen gel contraction assay. When cells start to contract, the collagen matrix normally exhibits a noticeable reduction in size. However, previous studies using collagen gel-based assays to measure fibroblast contractility were limited to only examining the changes in overall gel radius and hence an accurate determination of cell contraction force was difficult to achieve. The concentrations of collagen used to form the gels reported in research studies are in different numbers. Therefore even a same degree of gel radius shrinkage does not provide an accurate representation of the same magnitude of contraction force, because the quantity of matrix stiffness needs to be considered in the determination of cellular contraction forces [2]. To date, there are very few reports demonstrating that the stiffness of collagen matrices can influence cellular contraction forces.

At the site of vascular diseases such as atherosclerosis, arterial injury leads to enhanced adventitial fibroblast contraction and changes in the extracellular matrix (ECM) contributing to vessel remodelling and restenosis [153]. Collagen fibrils form a tightly aligned structure due to the synthesis of connective tissues following vessel

injury and inflammation. Fibroblasts can produce a large amount of collagen protein to increase the overall tissue tensile strength that contributes to vascular stiffening and impaired function [53]. The presence of differentiated contractile myofibroblast has been associated with the increase of ECM stiffness and they mediate the production of force for wound contraction [118]. The interaction between fibroblasts and various ECM components has been investigated using a number of engineering tools. These methods include cell populated micropillar substrates [136] or Traction Force Microscopy (TFM) [17,33]. For both methods, cell contraction force is determined indirectly based on the relative displacement of substrate materials, such as the deflections of micropillars or the movements of fluorescence microbeads embedded polymer substrate. However, both of these methods do not provide an accurate assessment of cell behaviour as they only measure the contraction of fibroblasts on a two-dimensional surface while the actual physiological environment *in vivo* for cell contraction within the extracellular matrix is three-dimensional.

To overcome these challenges in the accurate measurements of cell contraction force, we have recently developed a novel nanoindentation device to measure the gel elasticity, and in combination with mathematical modelling, cell contraction force can be determined accurately based on the measured thickness and area of a disk-shaped cell-embedded collagen matrix [78]. In this chapter, we have applied the new technique to investigate the effect of collagen gel stiffness on cell contraction force in a quantitative manner.

5.2 Materials and methods

Confluent cultures of human aortic adventitial fibroblasts (HAoAF, PromoCell, Germany) were detached from flasks using trypsin/EDTA and cells were re-suspended in Dulbeccos Modified Eagles Medium (DMEM) containing 5% Fetal Calf Serum

(FCS). Cells were then mixed with culture medium containing collagen I on ice, to achieve a final density of 2.16×10^5 cells gel^{-1} in DMEM containing 2mM L-glutamine, 100 IU ml^{-1} penicillin, 100 μg ml^{-1} streptomycin, 5% FCS and different collagen concentrations of 1.5, 2.0 and 2.5 mg ml^{-1}. The collagen matrix with cell suspension was transferred into 35 mm Petri dishes (1.2 ml dish^{-1}) and incubated in a culture incubator (37 ℃, 5% CO_2) for 20 minutes to allow gel polymerisation before addition of a further 1.5 ml DMEM containing 5% FCS. After incubation overnight, the culture medium was replaced with fresh DMEM containing 5% FCS. Some dishes were then stimulated with the agonist histamine (100 μM) to elicit cell contraction. Collagen gels were then immediately dislodged from the dish using a sterile spatula with gel thickness and elasticity measurements conducted 5 hours later.

Histamine was employed in this study to elicit HAoAF contraction as it has been well characterised to act via G-protein coupled receptors. Upon activation, it triggers calcium release from the internal stores, leading to calmodulin-dependent myosin light chain (MLC) kinase activation resulting in MLC phosphorylation and subsequent actin-myosin crossbridge formation and cellular contractions [27, 40, 66]. I have demonstrated in the previous chapter that addition of histamine (100 μM) increased single HAoAF cell contraction force by two-fold and contractions were attenuated by treatment with ML-7, an inhibitor of MLC kinase [78]. Therefore, we used histamine (100 μM) in this study to elicit short-term contraction events in HAoAF.

A depth-sensing indentation device was used to measure the thickness and Young's modulus of the cell-embedded collagen gel. The first 30% of the curve was extracted to determine Young's modulus (E) by fitting a non-linear strain dependent elasticity model as shown in Figure 4.1b. The Young's modulus E of collagen gel was determined from the measured Force-Displacement (F-D) curve fitting with the

following non-linear mechanical equation [78], which was derived based on Hertz contact theory [60] in combination with non-linear strain dependent elasticity (see equation 4.4) [148].

5.3 Results

As illustrated in Figure 5.1a and Figure 5.1c, when fibroblast starts to contract, the contraction force will lead to gel radius shrinkage with a concomitant change in thickness of the disk-shaped gel. The thickness and radius of collagen gel were measured at the beginning and end of treatment to determine the overall fibroblast contraction force (see Equation 4.9). Ten random positions were measured to calculate average gel thickness (shown in Figure 5.1b). The depth sensing indentation device was used to measure displacement difference from the gel top surface to the Petri dish surface. The top view images of the disc-shaped collagen were captured and used to measure the gel radius before and after shrinkage by referencing the culture surface within the Petri dishes (illustrated as Figure 5.1c).

Figure 5.2a shows the results derived from measurement of Young's moduli of both the treated and untreated gels, demonstrating a dose-dependent increase with collagen concentrations. Interestingly, histamine treatment slightly reduces the Young's modulus of collagen gel compared with the untreated gels at the same collagen concentration. Figure 5.2b shows the overall contraction force of fibroblasts which was calculated based on the Equation 4.4 using the measured geometric parameters and Young's modulus of the gel. The result shows the contraction force decrease as the collagen concentration increases. It was evident that histamine treatments doubled overall contraction cell force in every concentration group. Figure 5.2c demonstrates that cell contraction force decreases monotonically as the gel concentration increases. Histamine treated gels exhibited a significant linear regression

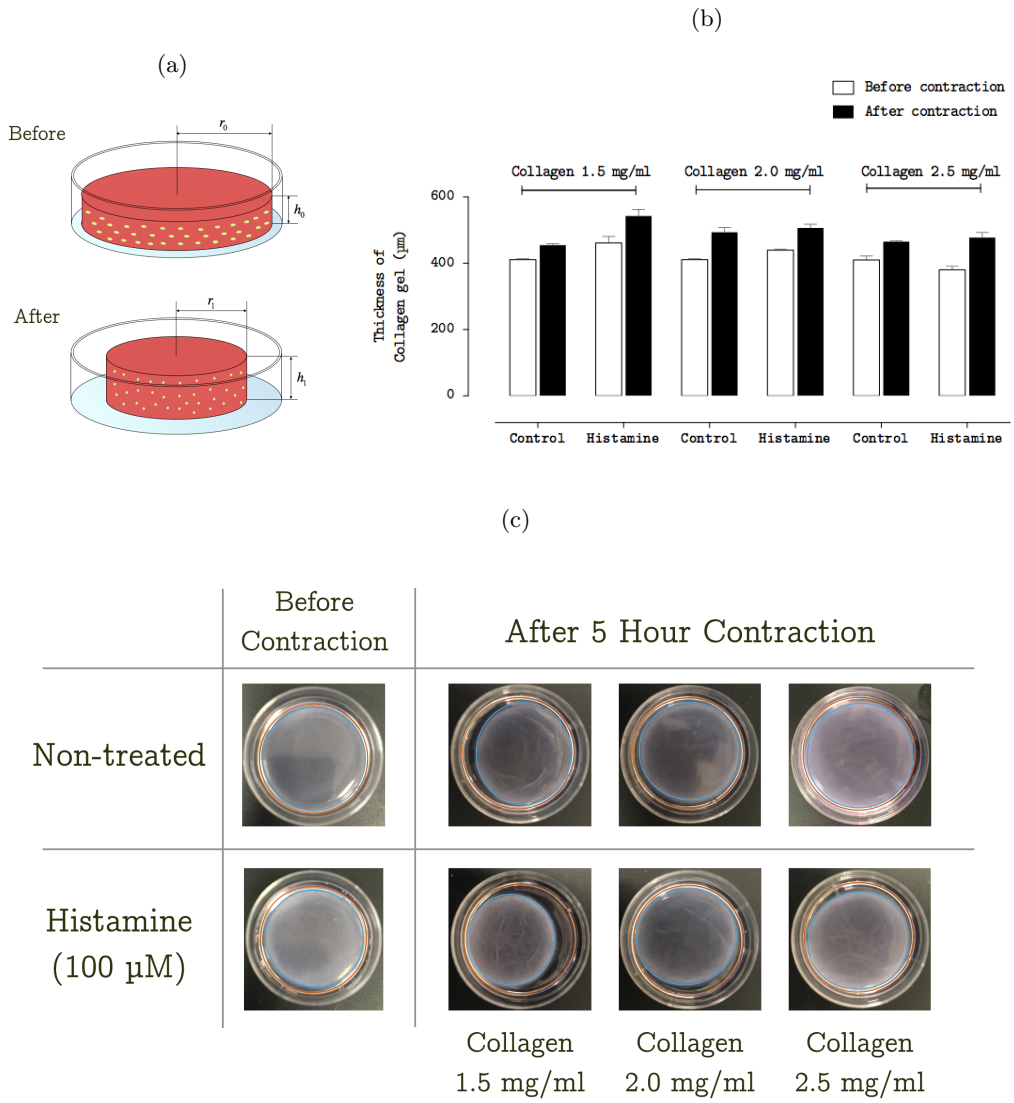

Figure 5.1: (*a*) Schematic of geometric parameters of collagen gel were measured before and after contraction for calculating contraction force. (*b*) Measured thickness of collagen gel in the absence and presence of agonist histamine with different collagen concentration (1.5, 2.0 and 2.5 mg ml^{-1}). (*c*) Top view images of typical HAoAF-embedded collagen gel before and after 5 hours histamine (100 μM) treatment. The areas circled with orange and blues lines denote the sizes of Petri dish (35 mm in diameter) and collagen gels respectively.

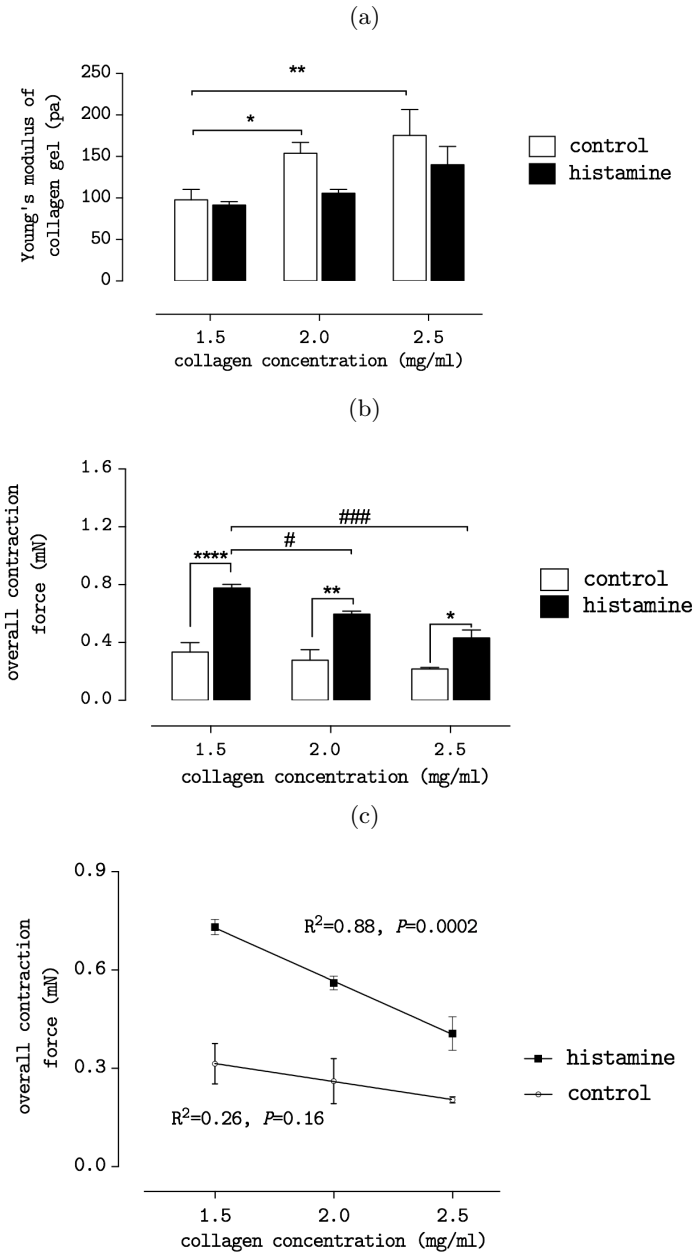

Figure 5.2: HAoAF were embedded into Type I collagen gels, formed at concentrations of 1.5, 2.0 and 2.5 mg ml^{-1}. (a) Young's modulus of each gel at different collagen concentration. (b) Overall contraction force per gel in the absence or presence of histamine treatments (100 μM, 5 hours). (c) Linear regression fitting of overall cell contraction force. Data denote mean ± s.e.m from three independent measurements ($N = 3$). P-Value was calculated using one-way ANOVA with Bonferroni post hoc test. $^{****}P < 0.0005$; $^{**}P < 0.05$; $^{*}P < 0.5$; $^{\#\#\#\#}P < 0.005$; $^{\#}P < 0.5$.

model in the overall contraction force against collagen concentration ($P = 0.0002$) compared with untreated cells ($P = 0.16$).

5.4 Discussion

In this chapter, adventitial fibroblast contraction forces were measured based on cell-populated collagen gels to investigate the effect of gel stiffness on overall contraction force generated by the fibroblasts. The Young's modulus (or stiffness) of collagen gel, as calculated by the non-linear strain dependent mechanical model [80, 148], demonstrates a clear increase as the gel collagen concentration increases. The increase in the gel Young's modulus regulated fibroblast contraction force as the cell contractility was significantly reduced in the stiffer matrices. Moreover, the addition of the agonist histamine elicited significant fibroblast contraction forces. In all collagen concentration groups, the histamine treated fibroblasts exhibited a two-fold increase in their contraction forces (Figure 5.2b) despite the decrease in Young's modulus of the collagen gels (Figure 5.2a). This proves the Young's modulus of gel matrices should be considered as a key parameter to properly assess cellular contraction forces using gel-based assays.

The results clearly demonstrate that the mechanical properties of collagen matrices influence the contractile responses of fibroblasts. Cells in stiffer (higher Young's modulus) materials exhibit a significant reduction in their contractility measured by our novel method, which is comparable to the results obtained by using other techniques, such as CFM [83]. For histamine-induced cell contraction assay, we showed a more significant decrease of overall contraction force as the matrix stiffness increases. With the activation of myosin light chain phosphorylation mediated by the agonist histamine, cell contractility increases, however, fibroblast contraction force will also be affected by the interaction between the cells and the

collagen matrix. The detailed mechanisms of how the cells translate the sensing of substrate stiffness into the downstream signals for regulating contraction requires further biomechanical studies.

In the blood vessel wall, inflammatory disease processes increase ECM collagen content thereby causing vascular dysfunction due to enhanced stiffness which impacts on the contractility of resident fibroblasts. In the earlier reports, a loss of mass has been shown in fibroblast collagen gel assays during cell contraction process [6]. This finding also implies that there were a potential loss in cell numbers in the collagen-gel-based contraction assay for long-term ($>$ 48 hours) measurements. Hence, a certain degree of inaccuracy is likely generated in the determination of fibroblast contraction force using previous techniques (*e.g.* culture force monitor (CFM) [32, 86], because the mass and cell loss may cause alterations in the mechanical properties of the collagen matrix. However, since the treatment time in our current study is only 5 hours, there was likely to be no significant loss of cells or gel mass.

5.5 Summary

In a 3D collagen matrix, the cells exhibit different levels of contractility depending on the collagen gel stiffness. Agonist treatment on fibroblast also have affected the collagen matrix stiffness. The finding confirms that the mechanical properties of the collagen matrix should be considered in the cellular contraction events. Overall, the study has shown the importance of matrix stiffness on cell contraction forces in the design of collagen-based biomaterials for clinical applications.

Chapter 6

Atomic force microscopy for cell-to-cell adhesion

In the previous three chapters, the novel biomechanical tester was introduced, and it was successfully applied to measure cellular contraction force and probe hydrogel elasticity effect. However, for cell-to-cell adhesion measurement, the bio-mechanical tester is not the best candidate as higher force resolution is required. So in this chapter, we have further used AFM force spectroscopy to examine cell-to-cell adhesion force. An established model cell line for human epithelial cells of the proximal tubule (HK2) was used to demonstrate that Ketamine (0.1 - 1 mg mL^{-1}) evokes the loss of adhesion force examined by AFM.

6.1 Backgrounds

Atomic Force Microscopy (AFM) technology has been widely applied in biomedical researches since its discovery in the 1980s [11]. Due to the high precision, it has been used to characterise many micro and nanobiological materials. In the tra-

ditional way, AFM's cantilever serves as a probe to indent the cell and to obtain Force-Displacement curves which can be used to determine the local mechanical properties of the sample (background information introduced in chapter 2.3). The measurement of cell-to-cell adhesion force is challenging in cell biology studies as it demands high precision and easy manipulation. Many disciplines have been interested in the measurement of cell-to-cell adhesion, including cell migration, wound healing, and regenerative medicine. Most recent studies regarding cell adhesion are limited to the availability of instruments such as fluorescence microscopy or flow chambers. These techniques deal with the adhesion of populated cells in response to the chemical or mechanical stimulus. Very few methods can provide a quantitative solution to the measurement of single cell-to-cell adhesion force.

In this chapter, we present a new protocol to investigate cell-to-cell adhesion force by using AFM-single cell force spectroscopy (AFM-SCFS). In traditional AFM-SCFS, AFM cantilever with different shapes of indenter approaches and then retracts to generate a Force-Displacement curve. Due to the heterogeneity of biological samples, the approaching part of the curve shows as non-linear because various compartments of the sample are probed, *e.g.* membrane, organelle and cytosol. The retraction curve shows even irregular as the protein cleavage, adhesion force drop between cantilever and cell may occur constantly. All of these are caused by the diverse mechanical properties of the biological sample. It is very difficult to systematically analyse all the mechanical events during one indentation curve. However, our novel cell-to-cell adhesion study has simplified the analysis procedure, and the whole experiment is easily repeatable. One free-floating cell is attached the AFM tipless cantilever. Force spectroscopy is performed similarly to AFM-SCFS as it shows approaching and retraction curve. The retraction curve is analysed to provide the energy required to pull two cells apart. This *in vitro* method provides an insight to quantify cell-to-cell adhesion by using high precision force spectroscopy.

6.2 Experimental method

6.2.1 AFM set-up

AFM force spectroscopy provides a feasible solution for long pulling length measurement. Figure 6.1a shows a schematic of AFM head which the key part of AFM force spectroscopy. The AFM head consists of a glass block, three adjustable holding foots, and a locked chamber where contains a laser beam and a photodetector. Prior to any experiment, the cantilever requires being mounted on the glass block with a spring clip. It is suggested that the glass block and cantilever should be sterilised (with 2% Hellmanex® solution, 5-10 minutes) and desiccated before mounting. The contact surface between cantilever and glass block should not be connected. It needs to be handled carefully with a tweezer or mounting tools as any dust, scratches or fingerprints will affect the measuring accuracy. After the installation of the cantilever to the glass block, the entire block will be placed upside down into the AFM head. In Figure 6.1a, the cantilever shows with 10° incline which not only ensures that the laser beam could have angles to reflect the photodetector but also prevents the glass block from touching the samples underneath. During the experiment, the transparent glass block allows the lights from the condenser to be transmitted to the inverted camera.

Figure 6.1b shows the entire set-up of the AFM system. The configuration is assembled Cell-hesion® 200 (JPK Instrument, Berlin, Germany) with Eclipse TE 300 inverted microscope (Nikon, USA) on an anti-variation table (TMC 63-530, USA). In order to maintain the ideal physiological environment, the cells are placed on a temperature controlling plate (Bio-Cell™, JPK, Berlin, Germany). The inverted microscope is fitted with a CCD camera (DFK 31AF01 Firewire, The Imaging Source, Germany). All components are controlled and monitored by JPK Cell-hesion® 200 software. The microscope is set between 20× to 40× magnification lens

(a)

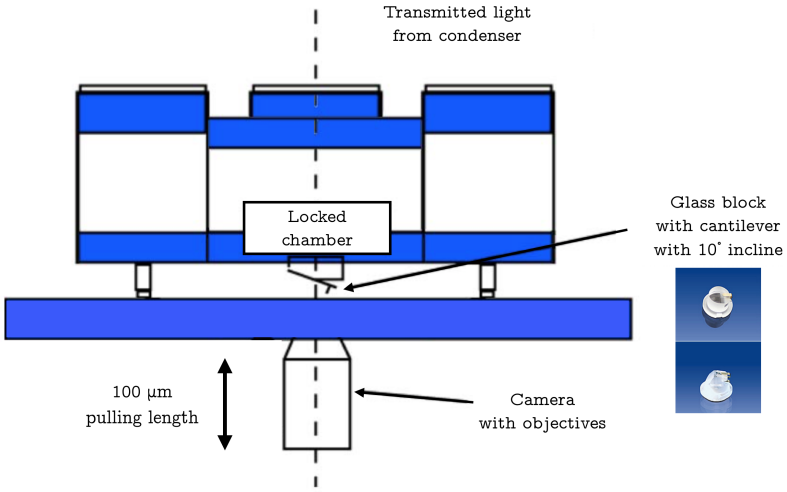

(b)

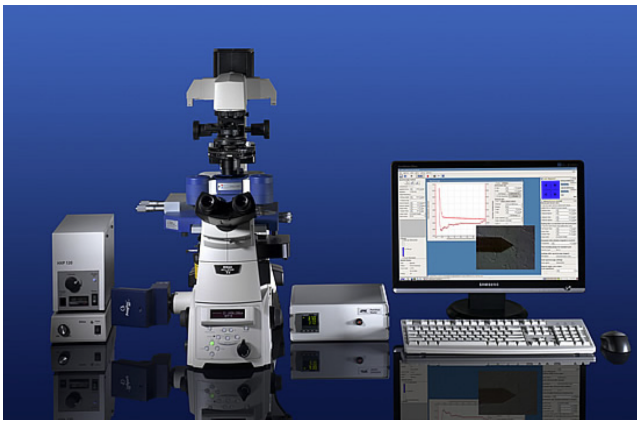

Figure 6.1: (*a*) Schematic of an AFM head which has 100 µm pulling length to perform cell-to-cell adhesion experiments. The cantilever is mounted on the glass block using a spring clip. 10-degree incline ensures the laser beam can be transmitted to the photodiode. The glass block is then transferred and mounted in the locked chamber along with the head. The head has three supporting foots which can adjust the level of horizontal. (*b*) Image of AFM head with the microscope. The system is placed on the anti-vibration table. Images are adapted from JPK instrument with permission.

and the temperature is set to 37 ℃. The noise and vibration are well controlled. Room temperature is within 15 ± 0.5 ℃ during experiment and all cables are firmly attached to the ground.

Another important function of AFM head before the experiment is to align the laser pathway. As cantilever beam is fitted manually, each installation would have a slight deviation before every experiment. The laser is required to align to the centre of the photodiode. The focused laser beam is irradiated on the back of cantilever and then transmitted to a quadric-sected photodiode. The first step is to align the laser beam with the cantilever. It can be observed by CCD camera. The best spot to place the laser dot is at the centre of the triangular head of the cantilever. Secondly, on the software, the laser beam is shown as a red dot on a simulated photodiode. It should be manually adjusted to the centre by using the two screws on the head (one for horizontal adjustment and the other is for vertical). It is suggested that the alignment of laser pathway should be performed in the liquid medium as a small draught may occur compared with the dry surface. When the laser is set to the centre of the photodiode, the maximum sum value is reached and the laser pathway is aligned well. In some experiments, due to the pre-functionalisation of the cantilever, some chemical or biological proteins may leave residues on the cantilever. It is necessary to find a clean spot for deflection alignment. If there is not red spot shown on the photodiode, the cantilever should be cleaned and redone the process.

6.2.2 AFM calibration

The purpose of calibration is to correlate the small deflections of AFM cantilever beam with applied forces. The basic principle is based on Hooke's law, which the cantilever can be regarded as a flexible beam with a spring constant, k. The force

(F) is linearly proportional to the deflection (x) of the cantilever as following:

$$F = kx \tag{6.1}$$

There are two steps to calibrate an AFM cantilever. The initial reading from AFM system is the voltage difference which represents the cantilever's vertical deflection on the photodiode. It is necessary to firstly determine the sensitivity of cantilever from the photodiode detection. Then, cantilever's deflection can be converted to the displacement x (nm). After calibrate the spring constant, the deflection will be further converted into force F (nN).

As each AFM cantilever has difference due to the manufacturing process, it is necessary to calibrate a newly replaced cantilever every time before performing experiments. The sensitivity calibration is to generate a voltage-displacement curve on the system. The cantilever is placed and programmed to indent a stiff surface (*e.g.* Petri dish or glass plate). With a given displacement, the voltage difference can be observed and the linear part is captured to represent the sensitivity of the system. The ideal range for the system sensitivity is approximately 50 - 60 nm Volt^{-1}.

Most AFM cantilever manufacturers have provided a range value of spring constant. It is necessary to calibrate the actual value of spring constant. In the study, commercial AFM provides software to calibrate the spring constant which is using the method called equipartition theorem or thermal noise method described in [69]. The method is essentially at a given temperature the amplitude of cantilever fluctuation at specific direction only depends on the spring constant. Simply speaking, the spring constant (k) can be express as [69]:

$$k = \frac{k_B T}{P} \tag{6.2}$$

where k_B is the Boltzmann's constant, T is temperature and P is the area of the power spectrum of the thermal fluctuations.

6.3 AFM force spectroscopy for cell-to-cell adhesion

The traditional purpose of AFM force spectroscopy is to measure the Young's moduli of the sample. The system generates a Force-Displacement curve which is applied to fit with mechanical models. Further application of AFM force spectroscopy is discovered to investigate the cell-to-cell adhesion force.

A suspended/isolated cell attached the cantilever was brought into contact with a cluster of cells on the surface and then retracted it. During the procedure, the system recorded the Force-Displacement curve. Hence, the detachment energy of the cell and substrate cell cluster can be calculated.

The very first step was to functionalise the tipless cantilever so that the cantilever can attach a cell. The functionalisation was normally performed the day before the experiment. Suitable binding protein should be selected [161]. In this study, the most widely used adhesion molecules, poly-l-lysine and fibronectin were chosen to coat the cantilever as the protein suits with HK2 cells. Firstly, poly-l-lysine was a polyvalent cation that charges the surface positively so that it can easily grab negatively charged cells and proteins. After sterilisation of the cantilever in UV light for 10 minutes, the cantilever was immersed in the poly-l-lysine (25 μg ml^{-1} in PBS) for 30 minutes at room temperature. Secondly, fibronectin was widely used for cell-cell adhesion and matrix assembly [5]. It was brought as the second layer

of coating to contact with the floating cells' plasma membrane. The poly-l-lysine treated cantilever was then placed in fibronectin solution (20 μg ml^{-1} in PBS) in 37 ℃ for 2 hours. After the entire functionalisation was finished, the cantilever was stored in 4 ℃ refrigerator in PBS solution overnight. Normally, multiple cantilevers can be functionalised simultaneously and used within 3 days.

Secondly, a free suspended cell was required in advanced to the grabbing process. Traditionally, cells were trypsinised to detach from the culturing plates. However, this enzymatic digestion method results in the specific adhesive protein on the cell membrane was temporarily cleavage. In most cases, these proteins were involved in the cell adhesion process. Hence, a more gentle method was used to detach the cells by using the sterile cell scraper. It was manufactured to impose the minimum damage to the cells. The cells were scraped from the T-25/T-75 culturing flask and suspended in CO_2-free medium.

Then, the free-floating cells were transported into the Petri dish which contains same passage of cells grown underneath. The functionalised cantilever was firstly calibrated in the dish. An area where no substrate cells reside was picked. By shaking the Petri dish, the floating cells were manipulated to approach the cantilever. With the aid of the CCD-linked microscope, the cantilever performs an indentation curve against the free floating cell until a set force (1 - 2 nN) was reached. Then, after 5 seconds holding times on the maximum set force, the unloading curve was then performed, and the free floating cell was attached to the cantilever. As the cell may be squished or flattened, it should allow 5 - 10 minutes for cells to recover. Figure 6.2a shows a cell was attached a functionalised AFM cantilever.

An AFM force spectroscopy for cell-to-cell adhesion experiment was performed by the cell-attached cantilever and cell cluster. The software was programmed to indent the substrate cells at a speed of 5 μm sec^{-1} until the maximum

(a)

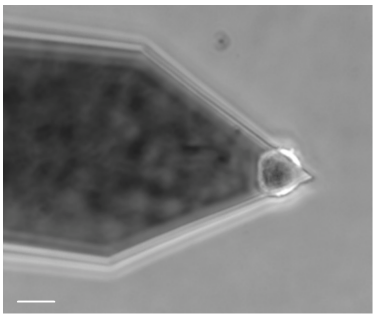

(b)

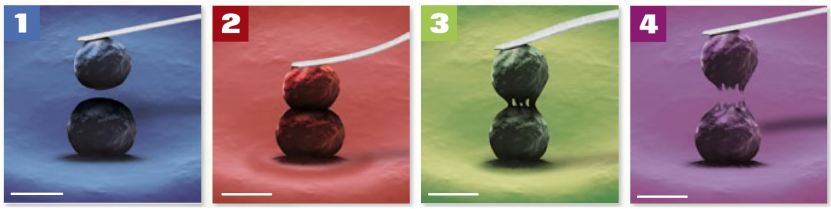

(c)

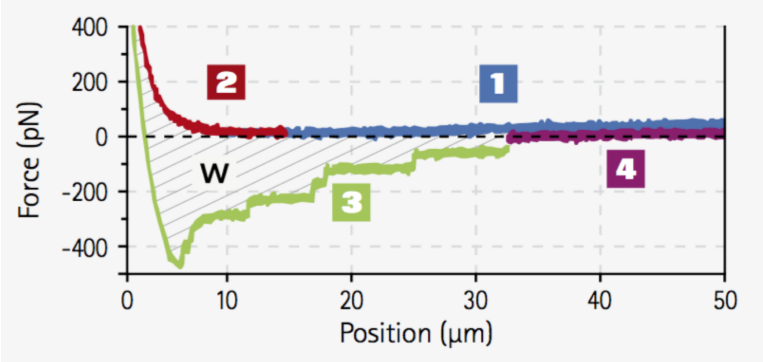

Figure 6.2: (*a*) One single cell attached to the cantilever. (*b*) Schematic of cell-to-cell adhesion assay. (*c*) Typical Force-Displacement curve between two adherent cells. Scale bar, 20 µm.

force (1 nN) was reached. Then two cells remained in contact for 10 seconds. Then cantilever was retracted as a constant speed of 5 μm sec^{-1} until the force was returned to zero. The procedure was repeated three times with the same cell with 30 seconds intervals for both substrate and cell attached cantilever to recover. Figure 6.2b shows the procedure of AFM force spectroscopy applied to measure cell-to-cell adhesion.

A Force-Displacement curve was generated as Figure 6.2c illustrated. The numbers captioned on the curve represents different phases of contact in Figure 6.2b. In phase 1, the cantilever with a cell was approaching the substrate cell. There was no force existing, and the piezo-actuator remains the constant speed. Then in phase 2, two cells were brought into contact, and positive forces are generated until maximum force is reached. Phase 3 was the retraction process where two cells were gradually isolated, and some protein unbinding process was taken place until two cells have been fully separated (*i.e.* phase 4). Two important pieces of information which have mechanical importance can be further interpreted in this Force-Displacement curve. First is the maximum unbinding force which is the lowest force in phase 3. Second is the work of adhesion or detachment energy, which is calculated by the grey shaded area in the diagram.

6.4 Ketamine reduces functional tethering between cells of the Proximal Tubule (HK2)

Ketamine is a tranquilliser that has been widely used as a NMDA receptor antagonist in the treatment of human bipolar disorders [164]. However, in 2006 the UK government made Ketamine a class C drug. Possessing mild hallucinogenic properties, Ketamine has rapidly replaced heroin and methamphetamine as the recreational drug of choice [163]. Cheap to buy and easily accessible, Ketamine has several street

names including 'Special K', 'Vitamin K' and 'LA Coke'. In 2008, the British Crime Survey revealed that Ketamine was the fastest growing 'party drug' among 16- to 24-year-old, and it has since been dubbed as the 'new ecstasy' [113]. In the UK, Ketamine affects an estimated 125,000 users, with more young people using Ketamine in England and Wales than heroin and crack cocaine combined. As the number of users increases, serious side effects are beginning to emerge. These effects, including bladder shrinkage, fibrosis, incontinence and bleeding, can ultimately lead to complete destruction and subsequent removal of the bladder [154]. Patients present with multiple symptoms including incontinence, bleeding, over-active bladder and bladder shrinkage, as well as damage to both the kidneys and the ureter [143]. Despite the growing presentation of these complications, there is an acute lack of understanding of the mechanisms of Ketamine in the pathological responses, and thus there is an urgently need to investigate how this mild hallucinogenic drug scars bladder and renal tissue to impair organ function [23].

In both the bladder and kidney, early changes in protein expression/function often occur before overt fibrosis. These changes include a loss of epithelial integrity and dysregulated formation of the intercellular junction, involving, loss of epithelial E-cadherin, altered cell morphology, reorganisation of the cytoskeleton and de-novo expression of fibroblastic markers [171]. Cadherins have a central role in the formation of the multiprotein adherens junction, which links the cell-cell contact to the actin cytoskeleton and various other signalling molecules [112]. The extracellular domain of the cell adhesion protein E-cadherin mediates ligation with neighbouring cadherins on adjacent cells [82], whilst the cytoplasmic domain binds to β-catenin linking cadherin to the actin cytoskeleton via α-catenin. The functional interaction of cadherin with F-actin, via the catenins, not only serves to increase the adhesive strength of the junction but also acts as a signalling node for proteins that influence adhesiveness and initiate intracellular signalling. The loss of E-cadherin-mediated

cell-to-cell adhesion represents a pivotal step in the transition of renal tubule cells from an epithelial phenotype to one more commonly associated with fibrosis [62]. Down-regulation of E-cadherin precedes changes in cell morphology, reorganisation of cell architecture and the subsequent gain in expression of phenotypic markers associated with renal pathology [62, 63].

Ketamine induced a concentration-dependent change in cell morphology towards an elongated fibroblast-like phenotype (Figure 6.3a). Cells at 80% confluence were fixed with 4% paraformaldehyde (PFA). Following blocking, the nuclear stain 49, 6-diamidino-2-phenylindole, dihydrochloride (DAPI; 1 mM) was added for 3 minutes. Cells were then incubated with TRITC-conjugated phalloidin (Sigma, UK) diluted at 1:100 in PBS-Triton for 1 hour at 25uC. Fluorescence was visualised using an Axiovert 200 fluorescence microscope (Carl Zeiss, Welwyn Garden City, UK). These gross morphological changes were accompanied by re-organisation of the actin cytoskeleton from a diffuse transcellular network of F-actin filaments that spanned the cytosol into more dense peripheral stress fibres (Figure 6.3b).

Cytosolic proteins were prepared and separated by gel electrophoresis and electro-blotting onto Immobilon P membranes as described in literature [61]. For determination of protein localisation, proteins were harvested using the Qproteome cell compartment kit. Membranes were probed with specific polyclonal antibodies against anti-E-cadherin (1:2000), N-Cadherin (1:1000), Snail (1:1000), Slug (1:1000), (1:2000), p-Smad 2 (1:1000), p-Smad 3(1:1000) (all R&D systems) and β-catenin (1:1000) (Santa Cruz). Ketamine induced a concentration-dependent decrease in whole cell expression of E-cadherin by 28 ± 1% ($P < 0.01$), 52 ± 12% ($P < 0.001$) and 76 ± 3% ($P < 0.001$) as compared to control at 0.1, 0.5 and 1 mg ml^{-1} respectively (n=3, Figure 6.3c). N-cadherin expression levels decreased in response to Ketamine by to 31 ± 7%, 47 ± 3% ($P < 0.001$) and 75 ± 2% ($P < 0.001$) as compared to control at 0.1, 0.5 and 1 mg ml^{-1} (n=3, see Figure 6.3d). The

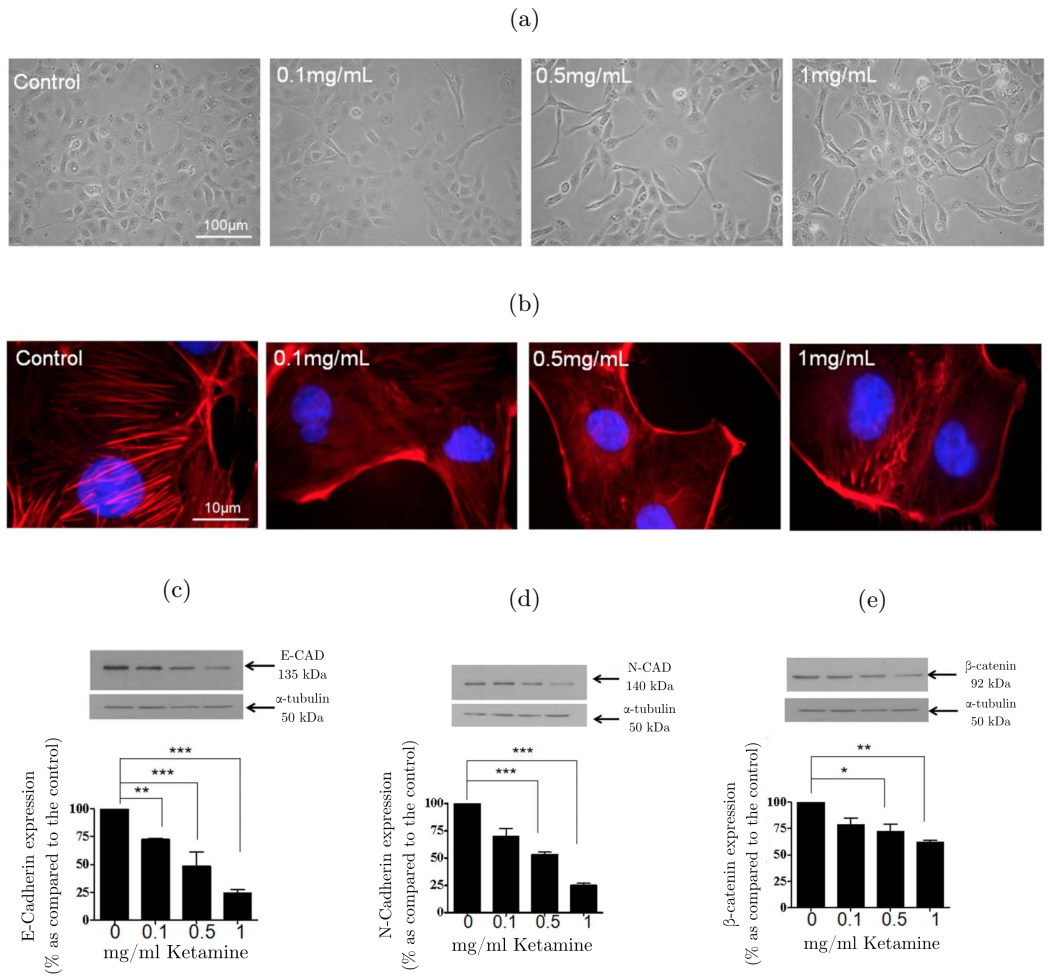

Figure 6.3: Ketamine evoked cell morphology and cytoskeletal reorganisation in HK2 Cells. HK2 cells were cultured in 5 mM glucose containing media for 48 hours prior to overnight serum starvation. Cells were stimulated for 24 hours with Ketamine (0.1 - 1 mg ml^{-1}) under serum-free conditions and morphological and phenotypic changes assessed. Phase contrast microscopy (panel (a)) and TRITC conjugated phalloidin (panel (b)) confirmed the dose dependent effects of Ketamine on cell morphology and cytoskeletal reorganisation respectively. Ketamine decreased expression of E-cadherin (panel (c)), N-cadherin (panel (d)) and β-catenin (panel (e)). P-value was calculated using One-Way ANOVA with Bonferroni Post-Hoc test. Key significances are shown, $^{*}P < 0.05$, $^{**}P < 0.01$, $^{***}P < 0.001$.

cytoplasmic domain of E-cadherin binds to β-catenin to link cell adhesion to the actin cytoskeleton Ketamine reduced whole cell expression of β-catenin by 28 ± 6%, 28 ± 7% ($P < 0.05$) and 39 ± 2% ($P < 0.01$) as compared to control at 0.1, 0.5 and 1 mg ml^{-1} (n=3, Figure 6.3e).

In the renal tubule, epithelial function depends on complex cell-to-cell interactions mediated through the adherens junction. In the current study, we presented data outlining early toxicological effects of Ketamine on proteins critical to the formation of the adherens junction complex in the kidney. Utilising the high-resolution AFM-SCFS, we assessed the functional consequence of cell-cell tethering in Ketamine-treated cells which exhibited a loss of cadherin expression. Our data provides compelling evidence that Ketamine reduces cell-to-cell adhesion in epithelial cells of the proximal tubule. Translated to the *in vivo* scenario, the subsequent loss of epithelial integrity, structure and function may contribute to the toxicological and potential fibrotic response to Ketamine in the kidney.

AFM-SCFS was used to measure cell-to-cell adhesion and the separation forces and energies required to uncouple cells (detailed introduced in Chapter 6.3). Prior to attachment, cells were cultured for 48 hours under identical conditions with/without Ketamine (0.1 - 1 mg ml^{-1}). A single HK2 cell was bound to a cantilever and subsequently brought into contact with an adherent cell within a cluster, using a fixed force. After 10 seconds, the cantilever was retracted (5 μm sec^{-1}) and force versus displacement measured until the cells were completely separated. Retraction Force-Displacement curves provide important information regarding the adhesion between two cells, *i.e.* the energy required to separate them (the grey area in Figure 6.4a - 6.4d) as well as maximum force of detachment (the red circle in Figure 6.4a - 6.4d).

The energy required to separate two cells is normally referred as 'detachment

energy' (Figure 6.4e) whilst the maximum force of detachment for complete separation is defined as the 'maximum unbinding force' (Figure 6.4f). The retraction measurements of control versus Ketamine (0.1 - 1 mg ml^{-1})-treated cells are shown in Figure 6.4e and 6.4f. In each case, data is recorded from multiple cells (>10) in 4 separate experiments at each concentration. Compared to control, Ketamine evokes a concentration-dependent decrease in the maximum unbinding force by 33 ± 6%, 41 ± 3%, and 58 ± 6% at 0.1 mg ml^{-1}, 0.5 mg ml^{-1} and 1 mg ml^{-1} receptively ($P < 0.001$), whilst the detachment energy decreased by 32 ± 8%, 63 ± 7%, and 86 ± 11% of control at 0.1 mg ml^{-1}, 0.5 mg ml^{-1} and 1 mg ml^{-1} receptively ($P < 0.001$).

6.5 Summary

In epithelial cells of the proximal tubule, disease-induced fibrosis commonly presents with cell atrophy, increased matrix deposition and tubulointerstitial scarring, all of which culminate in a loss of renal function [43, 81, 138]. The reciprocal loss of tubular epithelial cells and accumulation of interstitial fibroblasts promotes chronic fibrosis. Characteristic changes include morphological and phenotype alterations with the cytoskeletal reorganisation and the down-regulation of epithelial cell adhesion molecules, such as E-cadherin. The integrity of the adherens junction is vital to maintaining basic epithelial function, and the loss of E-cadherin-mediated cell adhesion represents a pivotal step in early phenotypic and morphological changes observed in tubular injury [43, 108].

AFM-SCFS has been successfully applied to determine how a loss in adherens junction proteins functionally affected cell-to-cell adhesion. The AFM-single-cell force spectroscopy used in this study has a displacement actuator of longer travelling distance (up to 100 μm) which provides an excellent capability for measur-

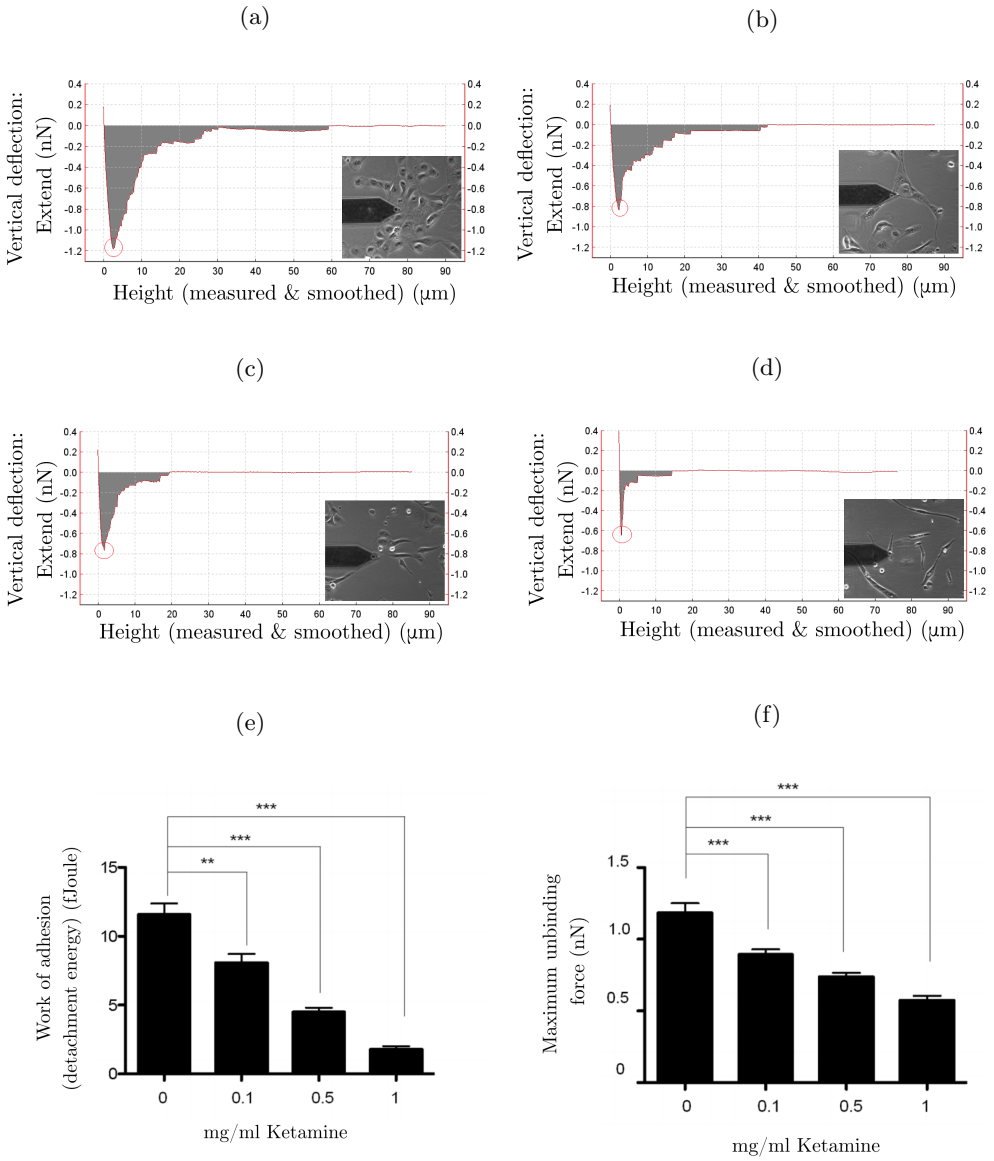

Figure 6.4: Ketamine reduces cell adhesion. AFM-cell-to-cell force spectroscopy was used to measure the detachment energy (fJoules) and maximum unbinding force (nN) required to uncouple two HK2 cells. The calculation of energy required to separate the cells was to integrate grey area in panel (a) control cells, panel (b) (0.1 mg ml^{-1} Ketamine treated cells), panel(c) (0.5 mg ml^{-1} Ketamine treated cells), panel (d) (1 mg ml^{-1} Ketamine treated cells) by JPK software, and maximum force of detachment (red circle) was measured. The former is known as the 'detachment energy' (panel (e)) and later is 'maximum unbinding force' (panel(f)). Ketamine decreased the maximum unbinding force and the work of adhesion in a dose dependent manner compared to control. Data is expressed as mean ± s.e.m of multiple cells from 4 separate experiments, where key significances are shown, $^{***}P < 0.001$, $^{**}P < 0.01$.

ing the complete Force-Displacement curve of cell detachment and is essential for studying large cells such as those as found in renal tubule epithelia. Retraction Force-Displacement curves allow determining the force and energy required to uncouple cells. The former is normally referred to as 'adhesion force' and the latter the 'detachment energy', which can be calculated from the integration of the separation Force-Displacement curves, *i.e.* the grey area under the curve in Figure 6.4a - 6.4d. Retraction Force-Displacement curves confirmed that 1 mg ml^{-1} Ketamine reduced the maximum unbinding force required to begin separate them by 86%. The greater decrease in the detachment energy could be partly explained due to the increase in cell rigidity following Ketamine treatment, as demonstrated by rearrangement of the cytoskeleton into peripheral stress fibres. These data suggest that it is the loss of E-cadherin expression and dissolution of the catenin/cadherin complex, which drives the detachment of cells in response to Ketamine.

Chapter 7

Synopsis and future work

Cellular contraction force and cell-to-cell adhesion force can be accurately measured using a novel biomechanical tester and AFM-SCFS, respectively. The measurement procedures and system set-up along with the development of mathematical models have been described in the thesis. This chapter concludes the remarks of this project and lists the advantages and limitations of the techniques for future recommendations.

7.1 Research highlight

The depth-sensing indentation device which is originally designed to investigate the mechanical properties of soft biological samples has been successfully applied to measure the contraction force of fibroblast. A non-linear strain dependent elasticity model combined with the indentation testing results has been successfully applied to evaluate Young's moduli of the collagen matrix. Furthermore, cell contraction force is estimated in a three-dimensional collagen gel matrix at high accuracy. Due to the features of measurement procedure which allows for the elasticity of collagen matrix

to be examined precisely, collagen matrix effects on influencing cell contraction force have been discovered.

The adhesive properties of soft biological cells (HK2) under the specific biochemical treatment have also been investigated quantitatively by using AFM-SCFS. The various states of cell-to-cell adhesion process have been demonstrated. The loss of E-cadherin expression caused by the mild hallucinogenic drug Ketamine has been presented. After the AFM-SCFS validation by a novel cell-to-cell adhesion experiment, a loss of adhesive energy induced by Ketamine is also clearly proved and stated. The results further confirmed that the cell-to-cell adhesion process is mediated by the interactions of E-cadherin and cytoskeleton at adherent junctions.

In the view of cell biomechanics, the cell entity and its micro-environment seek to establish a stable structure and functions. Contraction and adhesion forces are vital in many biological processes (introduced in Chapter 1). From a sub-cellular point of view, cells regulate themselves via signalling channels and cytoskeleton network which directs and adjusts motions. In the scale of cellular matrix level, cells are capable of mechano-sensing, translating and adapting to the mechanically or chemically stimulated micro-environment. The cell continuously converts the outside energy and responds to the external environment by changing its structure and forces. For example, cell adhesion forces are endlessly changing directed by the focal adhesion signalling channels during each state of migration. Cell migration requires contraction forces intermittently so that cell can move forward. Therefore, accurate determination of mechanical forces plays a critical role in understanding many biophysical and biochemical process.

Mechanical force generated by the cells can be regarded as a biomarker or diagnosis signal because it has significance in distinguishing treated and non-treated cells. The common understanding of a cell's phenotype is presented by the expression

of protein, morphology and cellular behaviour. However, physical forces can be regarded as an important parameter of a cell's characteristics. Under the controlled environment, systematically altering the protein expression, such as E-cadherin or actin-myosin cross-bridge, causes the cell to generate different amounts of forces. Subsequently, gene expression and force generation should be closely monitored especially in the cellular motional behaviours.

7.2 System limitations

The novel biomechanical tester has its advantage in the determination of Young's modulus of biomaterials, such as the hydrogel [78]. It provides an economic, feasible and quick solution to *in vitro* mechanical examination of samples. The contact time and approaching/retraction speed are easily and well controlled. The resolution is suitable for testing biomaterials such as collagen gel. However, it has limitations in its application for single cell mechanics because the tip of the indenter is not easily modified and fabricated. The system is also not easily replicable as each component is from different manufacturers and the assembly of the system requires great effort in development and programming.

Although AFM-SCFS has provided a new solution to measure cell-to-cell adhesion, it still has its limitation, *e.g.* it is time-consuming in measurements. Each functionalised cantilever can be only used for attaching one or two free-floating cell. In addition, many unexpected scenarios may occur in the process of cantilever grabbing a free-floating cell. For example, unwanted adherent particles may clutter in-between the cantilever and attached cell which can be observed under the microscopy. Alternatively, the attaching point of free cell and cantilever is not ideal as in many cases the cell is not fully inside the cantilever coverage.

All these unexpected attachment results in changing a new cantilever and restarting the attaching process. Cells gradually lose their viability and more unwanted secretions may be generated by the cells during the preparation. Any movement of the machine or change of condition would have led to the loss of cell adhesion.

Both techniques share the same limitation of testing samples *in vitro*. Although the system has a temperature compensation system, the CO_2 condition is different from the real physiological conditions. The solution to mitigate the limitation is to keep the untested samples in the incubator and to test the prepared sample in a stable and sterile environment during a limited experimental time, which is normally less than 2 hours.

7.3 Possible applications and recommendations

The biomechanical tester is designed in combination with the advanced fluorescence microscope and CCD camera. The future application of the device can be used to examine the mechanotransduction of cells. The addition of chemical or mechanical signals would activate intracellular signalling cascade which would ultimately change the cell behaviours. The device can be used as mechanical input to the cells, for example, a constant or intermittent pressure to mimic blood vessel compression or to generate force onto osteoblast to stimulate cell growth.

The biomechanical testing results can be used as a biomarker for diagnosis of disease. A comprehensive examination is needed in a more well-controlled environment. Biochemical factors should be examined separately by using western blot or microarray analysis for example. This will contribute to the advancement in the design of biomaterial and diagnostics.

The collagen gel-based contraction examination can be further improved by

applying a more sophisticated mathematical model which is not limited to the static one. For example, the time lapse video can be used to record the entire gel contraction process. Some micro-beads can be used as a marker to track the gel contraction in a 3D way. Optical coherent tomography can also be used as an imaging tool to enhance the accuracy of testing by scanning the collagen gel matrix continually. Growth factor-induced contraction event can be further analysed by the current technique.

In addition to the modification in the cell contraction assay, cell-to-cell adhesion assay also needs further improvement. Due to the accuracy of AFM-SCFS, focal adhesion effect can be examined thoroughly at a different stage of cell locomotion. Quantifying the distribution of mechanical force between different sub-cellular components, such as protein-protein and cell-protein, could be the next advancement in cellular biophysics.

Appendix A

This appendix contains a list of publications from the author related with this thesis, supplemental figures and tables that supporting the context.

IOP Publishing Biomed. Phys. Eng. Express 2 (2016) 047002 doi:10.1088/2057-1976/2/4/047002

Biomedical Physics & Engineering Express

NOTE

Collagen matrix stiffness influences fibroblast contraction force

Tianrong Jin[1], **Li Li**[2], **Richard CM Siow**[2,3] **and Kuo-Kang Liu**[1,3]

[1] School of Engineering, University of Warwick, Coventry, UK
[2] Cardiovascular Division, Faculty of Life Sciences and Medicine, King's College London, London, UK
[3] Authors contributed equally to this study.

E-mail: I.K-K.Liu@warwick.ac.uk

RECEIVED
20 January 2016

REVISED
18 May 2016

ACCEPTED FOR PUBLICATION
7 June 2016

PUBLISHED
27 July 2016

Keywords: cell mechanics, tissue engineering & regenerative medicine, extracellular matrix, hydrogel, nanoindentation, mechanical properties

Abstract

Cell-embedded hydrogel has been widely used as engineered tissue equivalents in biomedical applications. In this study, contraction force in human aortic adventitial fibroblasts seeded within a 3D collagen matrix was quantified by a novel force sensing technique. We demonstrate that contraction forces in cells treated with histamine are regulated by the gel stiffness in a linear manner. These findings provide novel insights into the design of collagen-based biomaterials for tissue engineering and clinical applications.

1. Introduction

The culture of cells within 3D matrices has been used for several decades [1]. The behaviours of cells in tissue-like matrices, such as migration, contraction and proliferation, exhibit an ideal model of their *in vivo* phenotype. Several materials have been developed for the synthesis of cellular encapsulated hydrogels. Collagen, alginate, fibrin and agarose are extensively used as the natural polymer ingredients to construct engineered tissue equivalents [2]. Among these, collagen has been recognised as one of the major components in connective tissues, which forms stable fibrils and provides multiple cellular binding sites [3, 4]. Fibroblasts are the main cell type that influence remodelling and biosynthesis of collagen fibrils [1]. As the structure of collagen provides a mechanically stable framework, the contractile properties of fibroblasts seeded within a collagen matrix provides a good model for investigating tissue physiology and pathology.

Currently, one of the most prevailing techniques to obtain cellularised collagen gels is modified from the method of Bell *et al* [5]. Measuring the contraction of cells embedded in 3D matrices is relatively straight forward using the conventional collagen gel contraction assay. When cells start to contract, the collagen matrix normally exhibits a noticeable reduction in size. However, previous studies using collagen gel-based assays to measure fibroblast contractility were limited to only examining the changes in overall gel radius and hence an accurate determination of cell contraction force was difficult to achieve. The concentrations of collagen used to form the gels reported in research studies are very different. Therefore even a same degree of gel radius shrinkage does not provide an accurate representation of the same magnitude of contraction force, because the quantity of matrix stiffness needs to be considered in the determination of cellular contraction forces [6]. To date, there are very few reports demonstrating that the stiffness of collagen matrices can influence cellular contraction forces.

At the site of vascular diseases such as atherosclerosis, arterial injury leads to enhanced adventitial fibroblast contraction and changes in the extra cellular matrix (ECM) contributing to vessel remodelling and restenosis [7]. Collagen fibrils form a tightly aligned structure due to the synthesis of connective tissues following vessel injury and inflammation. Fibroblasts can produce a large amount of collagen protein to increase the overall tissue tensile strength that contributes to vascular stiffening and impaired function [8]. The presence of differentiated contractile myofibroblast has been associated with the increase of ECM stiffness and they mediate the production of force for wound contraction [9]. The interaction between fibroblasts and various ECM components has been investigated using a number of engineering tools. These methods include cell populated micropillar substrates [10] or traction force microscopy [11, 12]. For both methods, cell contraction force is determined indirectly based on the relative displacement of substrate materials, such as the deflections

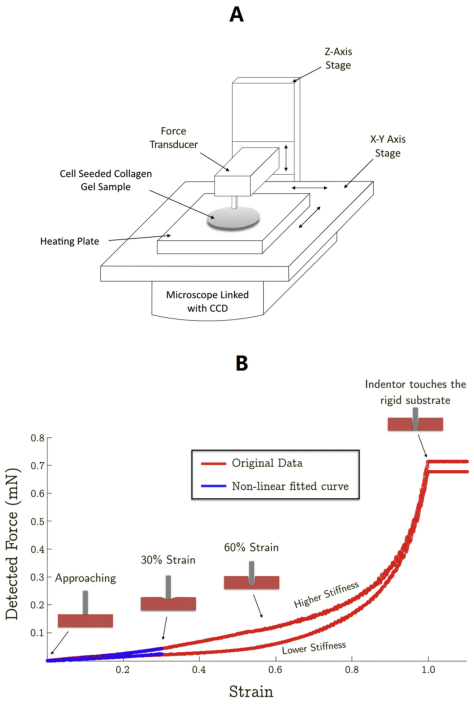

Figure 1. (A) The schematic setup of bio-nano-indentation tester. (B) Typical loading force–displacement curves of collagen gels with higher and lower stiffness indented by a flat punch.

of micropillars or the movements of fluorescence microbeads embedded polymer substrate. However, both of these methods do not provide an accurate assessment of cell behaviour as they only measure the contraction of fibroblasts on a two-dimensional surface while the actual physiological environment *in vivo* for cell contraction within the extracellular matrix is three-dimensional.

To overcome these challenges in the accurate measurements of cell contraction force, we have recently developed a novel nano-indentation device to measure the gel elasticity, and in combination with mathematical modelling, cell contraction force can be determined accurately based on the measured thickness and area of a disk-shaped cell-embedded collagen matrix [13]. In this study, we have applied the new technique to investigate the effect of collagen gel stiffness on cell contraction force in a quantitative manner.

2. Materials and method

Confluent cultures of human aortic adventitial fibroblasts (HAoAF, PromoCell, Germany) were detached from flasks using trypsin/EDTA and cells were re-suspended in Dulbecco's modified Eagle's medium (DMEM) containing 5% fetal calf serum (FCS). Cells were then mixed with culture medium containing collagen I on ice, to achieve a final density of 2.16×10^5 cells gel^{-1} in DMEM containing 2 mM L-glutamine, 100 IU ml^{-1} penicillin, 100 μg ml^{-1} streptomycin, 5% FCS and different collagen concentrations of 1.5, 2.0 and 2.5 mg ml^{-1}. The collagen matrix cell suspension was transferred into 35 mm Petri dishes (1.2 ml dish^{-1}) and incubated in a culture incubator (37 °C, 5% CO_2) for 20 min to allow gel polymerisation before addition of a further 1.5 ml DMEM containing 5% FCS. After incubation overnight, the culture medium was replaced with fresh DMEM containing 5% FCS. Some dishes were then stimulated with the agonist histamine (100 μM) to elicit cell contraction. Collagen gels were then immediately dislodged from the dish using a sterile spatula with gel thickness and elasticity measurements conducted 5 h later.

Histamine was employed in this study to elicit HAoAF contraction as it has been well characterised to act via G-protein coupled receptors. Upon activation, it

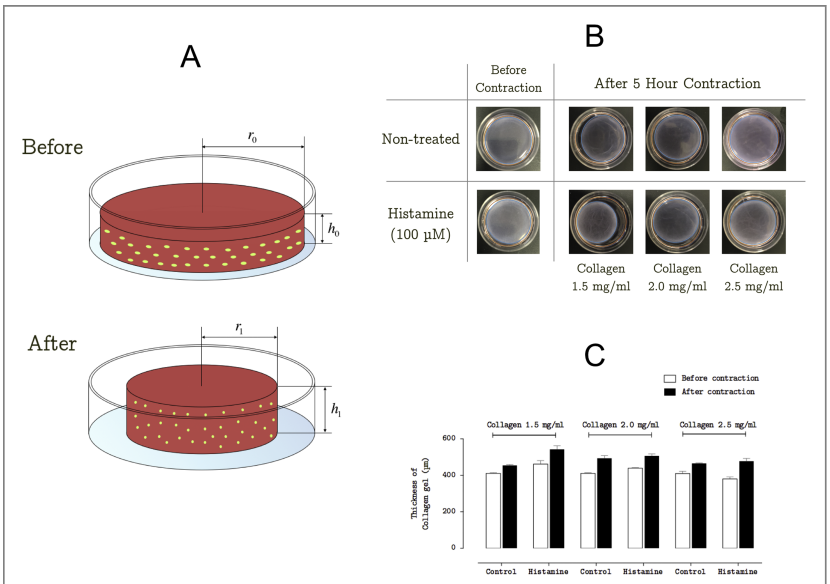

Figure 2. (A) Schematic of geometric parameters of collagen gel were measured before and after contraction for calculating contraction force. (B) Top view images of typical HAoAF-embedded collagen gel before and after 5 h with/without histamine (100 μM) treatment. The areas circled with orange and blues lines denote the sizes of Petri dish (35 mm in diameter) and collagen gels respectively. (C) Measured thickness of collagen gel in the absence and presence of agonist histamine with different collagen concentration (1.5, 2.0 and 2.5 mg ml^{-1}).

triggers calcium release from the internal stores, leading to calmodulin-dependent myosin light chain (MLC) kinase activation resulting in MLC phosphorylation and subsequent actin-myosin crossbridge formation and cellular contractions [14–16]. We demonstrated in our previous study that addition of histamine (100 μM) increased single HAoAF cell contraction force by two-fold and contractions were attenuated by treatment with ML-7, an inhibitor of MLC kinase [13]. Therefore, we used histamine (100 μM) in this study to elicit short-term contraction events in HAoAF.

A depth-sensing indentation device (figure 1(A)) was used to measure the thickness and Young's modulus of the cell-embedded collagen gel. The system has ultimate force and displacement resolutions of 10 nN and 100 nm, respectively. The gel indentation was performed at a controlled speed of 40 μm s^{-1} to generate force–displacement curve. The first 30% of the curve was extracted to determine Young's modulus (E) by fitting a nonlinear strain dependent elasticity model as shown in figure 1(B). The Young's modulus E_0 of collagen gel was determined from the measured force–displacement (F–D) curve fitting with the following nonlinear mechanical equation [13], which was derived based on Hertz contact theory [17] in combination with nonlinear strain dependent elasticity [18]

$$F = E_0 \cdot \frac{2rh}{(1-\nu^2)} \cdot \frac{\bar{\epsilon} - \bar{\epsilon}^2 + \frac{\bar{\epsilon}^3}{3}}{(1-\bar{\epsilon})^2}, \quad (1)$$

where E_0 and υ are Young's modulus and Poisson's ratio of collagen gel, respectively, F is the indentation force sensed by the force transducer, r is the radius of indenter, and $\bar{\epsilon}$ is applied strain which can be calculated as the ratio of the indentation displacement D normalised by the gel thickness h, i.e., $\bar{\epsilon} = D/h$. The values of υ are in the range of 0.42–0.48, which were calculated based on the measured radii and thicknesses of the collagen gel discs before and after contraction. At equilibrium status, the cell contraction force (F^*) is balanced by the elastic restoration force of the deformed or shrunk gel and can be expressed by the following equation:

$$F^* = \pi(h_0 + h_1)(r_0 - r_1)E_0 \cdot \frac{1 - \varepsilon^* + \frac{\varepsilon^{*2}}{3}}{(1-\varepsilon^*)^2}, \quad (2)$$

where h and r with subscript 0 and 1 represent the thickness and radius of collagen gel at beginning and end of contraction, and ε^* is the overall strain generated due to gel shrinkage, i.e., $\varepsilon^* = (r_0 - r_1)/r_0$ (see figure 2).

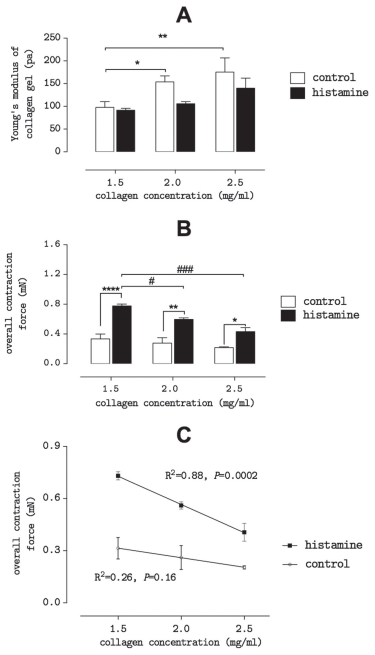

Figure 3. HAoAF were embedded into Type I collagen gels, formed at concentrations of 1.5, 2.0 and 2.5 mg ml^{-1}. (A) Young's modulus of each gel at different collagen concentration. (B) Overall contraction force per gel in the absence or presence of histamine treatments (100 μM, 5 h). (C) Linear regression fitting of overall cell contraction force. Data denote mean ± s.e.m from three independent measurements ($N = 3$). P-value was calculated using one-way ANOVA with Bonferroni post hoc testt. $^{****}P < 0.0005$; $^{**}P < 0.05$; $^{*}P < 0.5$; $\#\#\#P < 0.005$; $\#P < 0.5$.

3. Results

As illustrated in figure 2, when fibroblast starts to contract, the contraction force will lead to gel radius shrinkage with a concomitant change in thickness of the disk-shaped gel. The thickness and radius of collagen gel were measured at the beginning and end of treatment to determine the overall fibroblast contraction force (see equation (2)). Ten random positions were measured to calculate average gel thickness (shown in figure 2(C)). The depth sensing indentation device was used to measure displacement difference from the gel top surface to the Petri dish surface. The top view images of the disc-shaped collagen were captured and used to measure the gel radius before and after shrinkage by referencing the culture surface within the Petri dishes (illustrated as figure 2(B)).

Figure 3(A) shows the results derived from measurement of Young's moduli of both the treated and untreated gels, demonstrating a dose-dependent increase with collagen concentrations. Interestingly, histamine treatment slightly reduces the Young's modulus of collagen gel compared with the untreated gels at the same collagen concentration. Figure 3(B) shows the overall contraction force of fibroblasts which was calculated based on the equation (2) using the measured geometric parameters and Young's modulus of the gel. The result shows the contraction force decrease as the collagen concentration increases. It was evident that histamine treatments doubled overall contraction cell force in every concentration group. Figure 3(C) demonstrates that cell contraction force decreases monotonically as the gel concentration increases. Histamine treated gels exhibited a significant linear regression model in the overall contraction force against collagen concentration ($P = 0.0002$) compared with untreated cells ($P = 0.16$).

4. Discussion

In this study, adventitial fibroblast contraction forces were measured based on cell-populated collagen gels to investigate the effect of gel stiffness on overall contraction force generated by the fibroblasts. The Young's modulus (or stiffness) of collagen gel, as calculated by the nonlinear strain dependent mechanical model [18, 19], demonstrates a clear increase as the gel collagen concentration increases. The increase in the gel Young's modulus regulated fibroblast contraction force as the cell contractility was significantly reduced in the stiffer matrices. Moreover, the addition of the agonist histamine elicited significant fibroblast contraction forces. In all collagen concentration groups, the histamine treated fibroblasts exhibited a two-fold increase in their contraction forces (figure 3(B)) despite the decrease in Young's modulus of the collagen gels (figure 3(A)). This proves the Young's modulus of gel matrices should be considered as a key parameter to properly assess cellular contraction forces using gel-based assays.

The results clearly demonstrate that the mechanical properties of collagen matrices influence the contractile responses of fibroblasts. Cells in stiffer (higher Young's modulus) materials exhibit a significant reduction in their contractility measured by our novel method, which is comparable to the results obtained by using other techniques, such as CFM [20]. For histamine-induced cell contraction assay, we showed a more significant decrease of overall contraction force as the matrix stiffness increases. With the activation of MLC phosphorylation mediated by the agonist histamine, cell contractility increases, however, fibroblast contraction force will also be affected by the interaction between the cells and the collagen matrix. The detailed mechanisms of how the cells translate the sensing of substrate stiffness into the downstream signals for regulating contraction

requires further biomechanical studies. In the blood vessel wall, inflammatory disease processes would increase ECM collagen content thereby causing vascular dysfunction due to enhanced stiffness which impacts on the contractility of resident fibroblasts.

In the earlier reports, a loss of mass has been shown in fibroblast collagen gel assays during cell contraction process [5]. This finding also implies that there were a potential loss in cell numbers in the collagen-gel-based contraction assay for long-term (>48 h) measurements. Hence, a certain degree of inaccuracy is likely in the determination of fibroblast contraction force using previous techniques (e.g. culture force monitor (CFM) [21, 22]), because the mass and cell loss may cause alterations in the mechanical properties of the collagen matrix. However, since the treatment time in our current study is only 5 h, there was likely to be no significant loss of cells or gel mass.

5. Conclusion

We have demonstrated that in a 3D collagen matrix, the cells exhibit different levels of contractility depending on the collagen concentration and gel stiffness. The finding confirms that the mechanical properties of the collagen matrix should be considered in the cellular contraction events induced by physiological changes (e.g. effect of agonist treatments). Different cell types may have varying degrees of response depending on the mechanism of their sensing of the substrate stiffness. Overall, the study has shown the importance of matrix stiffness on cell contraction forces in the design of collagen-based biomaterials for clinical applications.

Acknowledgments

This work was supported by a grant from Leverhulme Trust (PRG-2012-738) awarded to K-KL and a grant from the British Heart Foundation (FS/09/037/27827) awarded to RCMS.

References

[1] Grinnell F and Petroll W M 2010 Cell motility and mechanics in three-dimensional collagen matrices *Annu. Rev. Cell Dev. Biol.* **26** 335–61
[2] Ahearne M 2014 Introduction to cell-hydrogel mechanosensing *Interface Focus* **4** 20130038
[3] Orgel J P R O, Miller A, Irving T C, Fischetti R F, Hammersley A P and Wess T J 2001 The in situ supermolecular structure of Type I collagen *Structure* **9** 1061–9
[4] Bella J, Eaton M, Brodsky B and Berman H M 1994 Crystal and molecular structure of a collagen-like peptide at 1.9 A resolution *Science* **266** 75–81
[5] Bell E, Ivarsson B and Merrill C 1979 Production of a tissue-like structure by contraction of collagen lattices by human fibroblasts of different proliferative potential *in vitro Proc. Natl Acad. Sci. USA* **76** 1274–8
[6] Ahearne M, Wilson S L, Liu K-K, Rauz S, El Haj A J and Yang Y 2010 Influence of cell and collagen concentration on the cell–matrix mechanical relationship in a corneal stroma wound healing model *Exp. Eye Res.* **91** 584–91
[7] Travis J A, Hughes M G, Wong J M, Wagner W D and Geary R L 2001 Hyaluronan enhances contraction of collagen by smooth muscle cells and adventitial fibroblasts: role of CD44 and implications for constrictive remodeling *Circ. Res.* **88** 77–83
[8] Grinnell F 1994 Fibroblasts, myofibroblasts, and wound contraction *J. Cell Biol.* **124** 401–4
[9] Mutsaers S E, Bishop J E, McGrouther G and Laurent G J 1997 Mechanisms of tissue repair: from wound healing to fibrosis *Int. J. Biochem. Cell Biol.* **29** 5–17
[10] Schoen I, Hu W, Klotzsch E and Vogel V 2010 Probing cellular traction forces by micropillar arrays: contribution of substrate warping to pillar deflection *Nano Lett.* **10** 1823–30
[11] Butler J P, Tolić-Nørrelykke I M, Fabry B and Fredberg J J 2002 Traction fields, moments, and strain energy that cells exert on their surroundings *Am. J. Physiol.-Cell Physiol.* **282** C595–605
[12] Dembo M and Wang Y-L 1999 Stresses at the cell-to-substrate interface during locomotion of fibroblasts *Biophys. J.* **76** 2307–16
[13] Jin T, Li L, Siow R C M and Liu K-K 2015 A novel collagen gel-based measurement technique for quantitation of cell contraction force *J. R. Soc. Interface* **12** 20141365
[14] Ehrlich H P, Rockwell W B, Cornwell T L and Rajaratnam J B 1991 Demonstration of a direct role for myosin light chain kinase in fibroblast-populated collagen lattice contraction *J. Cell. Physiol.* **146** 1–7
[15] Dallon J C and Ehrlich H P 2008 A review of fibroblast-populated collagen lattices *Wound Repair Regeneration: Official Publ. Wound Healing Soc. Eur. Tissue Repair Soc.* **16** 472–9
[16] Horie M *et al* 2014 Histamine induces human lung fibroblast-mediated collagen gel contraction via histamine H1 receptor *Exp. Lung Res.* **40** 222–36
[17] Heinrich H 1881 Über die Berührung fester elastischer Körper *J. reine Angew. Math.* **92**
[18] Tatara Y 1991 On compression of rubber elastic sphere over a large range of displacements: 1. Theoretical study *J. Eng. Mater. Technol.* **113** 285–91
[19] Johnson K L 1987 *Contact Mechanics* (Cambridge: Cambridge University Press)
[20] Karamichos D, Brown R A and Mudera V 2007 Collagen stiffness regulates cellular contraction and matrix remodeling gene expression *J. Biomed. Mater. Res.* A **83** 887–94
[21] Delvoye P, Wiliquet P, Levêque J-L, Nusgens B V and Lapière C M 1991 Measurement of mechanical forces generated by skin fibroblasts embedded in a three-dimensional collagen gel *J. Investigative Dermatology* **97** 898–902
[22] Kolodney M S and Wysolmerski R B 1992 Isometric contraction by fibroblasts and endothelial cells in tissue culture: a quantitative study *J. Cell Biol.* **117** 73–82

INTERFACE

rsif.royalsocietypublishing.org

Research

Cite this article: Jin T, Li L, Siow RCM, Liu K-K. 2015 A novel collagen gel-based measurement technique for quantitation of cell contraction force. *J. R. Soc. Interface* **12**: 20141365.
http://dx.doi.org/10.1098/rsif.2014.1365

Received: 12 December 2014
Accepted: 17 March 2015

Subject Areas:
bioengineering, biomaterials, biomechanics

Keywords:
collagen gel, human aortic adventitial fibroblast, histamine, cell contraction force, nano-indentation, elasticity

Author for correspondence:
Kuo-Kang Liu
e-mail: i.k.liu@warwick.ac.uk

†These authors contributed equally to this study.

THE ROYAL SOCIETY
PUBLISHING

A novel collagen gel-based measurement technique for quantitation of cell contraction force

Tianrong Jin[1], Li Li[2], Richard C. M. Siow[2,†] and Kuo-Kang Liu[1,†]

[1]School of Engineering, University of Warwick, Coventry CV4 7AL, UK
[2]Cardiovascular Division, British Heart Foundation Centre of Research Excellence, Faculty of Life Sciences and Medicine, King's College London, London SE1 9NH, UK

TJ, 0000-0002-3146-4268; K-KL, 0000-0003-1871-9876

Cell contraction force plays an important role in wound healing, inflammation, angiogenesis and metastasis. This study describes a novel method to quantify single cell contraction force *in vitro* using human aortic adventitial fibroblasts embedded in a collagen gel. The technique is based on a depth sensing nano-indentation tester to measure the thickness and elasticity of collagen gels containing stimulated fibroblasts and a microscopy imaging system to estimate the gel area. In parallel, a simple theoretical model has been developed to calculate cell contraction force based on the measured parameters. Histamine (100 μM) was used to stimulate fibroblast contraction while the myosin light chain kinase inhibitor ML-7 (25 μM) was used to inhibit cell contraction. The collagen matrix used in the model provides a physiological environment for fibroblast contraction studies. Measurement of changes in collagen gel elasticity and thickness arising from histamine treatments provides a novel convenient technique to measure cell contraction force within a collagen matrix. This study demonstrates that histamine can elicit a significant increase in contraction force of fibroblasts embedded in collagen, while the Young's modulus of the gel decreases due to the gel degradation.

1. Introduction

The collagen contraction assay was firstly reported by Bell *et al*. [1] and has been described as fibroblast-populated collagen lattice (FPCL). The mechanism for fibroblast contraction is mediated by the control of myosin light chain (MLC) phosphorylation status through the action of MLC kinase (MLCK) [2]. As reviewed by Dallon & Ehrlich [3], raised intracellular calcium levels leads to calmodulin-dependent MLCK activation, which results in MLC phosphorylation and actin–myosin crossbridge formation and filament sliding.

Human aortic adventitial fibroblasts (HAoAF) are resident in the adventitia of the aorta and they have been employed in experimental models of arterial remodelling and restenosis [4]. Histamine is an agonist that elicits increases in intracellular calcium and is released by basophils and mast cells during inflammatory responses. It acts on cells via a family of G protein-coupled histamine receptors, histamine receptor H1–H4. Several studies have shown that human fibroblasts express H1 receptor and can be activated via histamine binding, resulting in phospholipase C activation and production of inositol triphosphates (IP_3) and diaglycerol (DAG) [5,6]. The increase of IP_3 causes calcium release from the internal stores and consequently triggers fibroblast contraction via activation of MLCK [7].

Several approaches have been developed to measure cell contraction forces *in vitro*; among these, collagen gel contraction assay (CGCA) and traction force microscopy (TFM) are the most common techniques. For the both methods, cell contraction forces are measured indirectly based on measurement of deformation of the matrix surrounding the cells, such as a cell-embedded collagen gel or cell-seeded polymer substrate. However, the CGCA technique is used for the measurement of forces in populations of cells, while TFM is more suited for the measurement of forces in single cells.

When CGCA is used for assessing contraction forces, cells are embedded within the collagen matrix, which provides cells with a physiological environment. Collagen is a key component of the extracellular matrix that facilitates cell migration and contraction [8]. Cell-embedded collagen gels are easily constructed and the measurement of their contraction is straightforward. Conventional techniques used to measure collagen gel contraction rely on imaging only the gel area from a top view. The estimation of contraction is often expressed by the area changes of the gels between the beginning and end of the treatment or cell contraction period [9,10]. To improve the measurement of cell contraction kinetics for time-dependent changes, time-lapse-video-based imaging techniques have been developed to record changes in gel areas continuously while the cells contract [11]. Although the versatility of the CGCA method facilitates general use, it does not provide quantification of cellular contraction forces, since the mechanical properties of the collagen matrix will dictate the measurement accuracy of the cellular contraction forces. The elasticity of the disc-shaped collagen gel can be influenced by the cell treatments and the same amount of gel radius shrinkage may result from very different cellular contraction forces. Moreover, in the normal physiological environment, cells do not merely contract in a two-dimensional manner, therefore, measuring the radius of the gel disc only from the top view will not provide an accurate assessment of the magnitude of cellular contraction.

Alternatively, TFM was developed to measure single cell contraction forces by observing the underlying elastic polymer substrate (e.g. polyacrylamide gel) embedded with multiple fluorescence microbeads [12–14]. A number of mathematical models have been developed to facilitate the estimation of contraction force based on the relative motion of the beads. However, the stiffness of the gel substrate can be altered by cell differentiation and biochemical treatments during the measurement and this may affect the accuracy of the force measurement. More importantly, it is more technically challenging to obtain results using the TFM method and measurements do not provide a true physiological model because the assessment of cellular contraction based on a two-dimensional surface, instead of a three-dimensional gel matrix.

To improve the accuracy of CGCA force measurements, a culture force monitor (CFM) system was developed by attaching strain gauges at the edges of a cell-embedded collagen gel to directly assess cell contraction [15–20]. Cellular contraction force can be measured continuously without influence of the elastic variation of collagen gel. Single cell contraction force can thus be approximately estimated by the measured force divided by the total number of the embedded cells. However, the measurement was only limited to a random uniaxial stress as the strain gauges could only measure the contraction in single directions.

Having taken into account the variation in elasticity of the collagen matrix, we re-designed the collagen gel-based assay technique to quantify cell contraction forces with a significantly higher degree of accuracy. The method essentially correlates the relationship between gel deformation and embedded cell contraction force. The elastic modulus and thickness of each collagen gel were routinely quantified by a bespoke nano-indentation tester and the data were used as input parameters for a simple mathematical model that correlates cell contraction force with gel properties, including radius, thickness and elasticity, which varied throughout the different treatments. The single cell contraction force can also be determined providing that the total cell number embedded in the gels are known. In this study, we have also applied the new gel-based sensing technique to investigate the contraction force of HAoAF treated with the agonist histamine or following co-treatment with ML-7, a well-established inhibitor of MLCK, to attenuate fibroblast contraction.

2. Material and methods

2.1. Cell culture

Cryopreserved HAoAF were purchased from PromoCell GmbH at passage 2. Cells were cultured at 37°C in a 95% air/5% CO_2 atmosphere using phenol red-free Dulbecco's modified Eagle's medium (DMEM) supplemented with fetal calf serum (FCS, 10%), penicillin (100 IU m l^{-1}), streptomycin (100 µg ml^{-1}) and L-glutamine (2 mM). Cells at passage 7–9 were used in all experiments.

2.2. Collagen gel contraction assay

2.2.1. Collagen gel assay

Confluent HAoAF cultures were detached from flasks using trypsin/EDTA and cell number determined using a haemocytometer. After centrifugation, cells were re-suspended in DMEM containing 10% FCS at densities of between 0.5×10^6 and 2.5×10^6 cells ml^{-1} and mixed with culture medium containing collagen I on ice at a ratio of 1 : 9, resulting in the final DMEM containing 1.76 mg ml^{-1} collagen I, 2 mM L-glutamine, 100 IU ml^{-1} penicillin, 100 µg ml^{-1} streptomycin and 5% FCS. The cell suspension was transferred into 35 mm Petri dishes (1.2 ml $dish^{-1}$, achieving cell densities between 0.06×10^6 and 0.3×10^6 cells gel^{-1}) and incubated in a cell culture incubator for 20 min to polymerize the gel before addition of a further 1.5 ml DMEM containing 5% FCS. After incubation for 16 h, the culture medium was replaced with fresh DMEM containing 5% FCS and collagen gels were dislodged from the edge of the dish using a sterile spatula. Gel thickness and elasticity measurements were conducted 48 h later. In experiments to address the effects of histamine on cell contraction, fibroblasts were re-suspended in DMEM containing 10% FCS at a density of 1.8×10^6 cells ml^{-1} (achieving a cell density of 0.216×10^6 cells gel^{-1}) and incubated for 16 h before treatment of cells in the presence or absence of the MLCK inhibitor ML-7 (25 µM) for 30 min. Some dishes were then stimulated with the agonist histamine (100 µM) to elicit cell contraction. Collagen gels were then immediately dislodged from the dish using a sterile spatula with gel thickness and elasticity measurements conducted 5 h later.

2.2.2. Experimental measurements

A depth-sensing nano-indentation tester was developed to quantitatively measure the thickness and Young's modulus of the cell-embedded collagen gel, which were used as input parameters to estimate contraction force (§2.3.2). As shown in the figure 1, the system is mainly comprised of a force transducer (406A, Aurora Scientific Inc.) attached with a cylindrical flat punch or indenter (*ca* 1 mm in diameter), *Z*-axis step motor linear stage (UTS 100CC with ESP301 Motion Controller, Newport), *XY*-axis stage (ProScan III, Prior Scientific) and a temperature control heating plate (Temp. Control, iBidi). All components are mounted on an inverted microscope (TE2000-S, Nikon) and controlled by Labview software (National Instrument). The system has ultimate force and displacement resolutions of 10 nN and 100 nm, respectively. The force transducer senses the force via the cylindrical indenter. The mechanical properties of collagen gels were measured by the system described. Nano-indentation of collagen gel was performed at a controlled indentation speed of 40 µm s^{-1}. Force and displacement were recorded simultaneously during the loading/unloading indentation cycles.

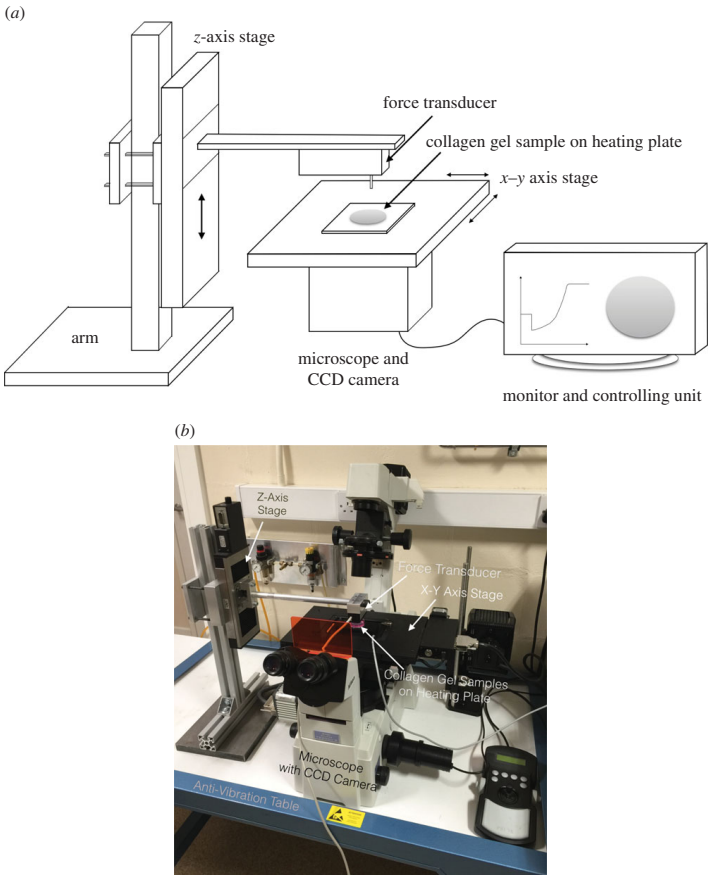

Figure 1. (*a*) Schematic of the depth-sensing nano-indentation system for force–displacement measurement. (*b*) Image of nano-indentation system. (Online version in colour.)

When the thickness and elasticity were measured, collagen gel was plated in the 35 mm Petri dishes with no culturing medium on the heating plate at 37°C. The whole system was placed on an anti-vibration table (Wentworth Laboratories Ltd). Ten random positions were picked and measured to generate 10 different force–displacement (F–D) curves for analysis. The thickness of the gel was measured based on the displacement difference between the gel's top surface and the Petri dish surface, while the gel's elasticity was measured based on the analysis of the indentation F–D curves (§2.3.1).

In parallel, a computerized CCD-enhanced camera (ORCA-ER, Hamamatsu) has been used to measure the radius of the disc-shaped hydrogel, from the vertical top view, and the radius change before and after cell contraction can be determined by referencing the culturing area of the Petri dishes. The measurement accuracy of the radius was up to 1 µm.

2.3. Theoretical analysis

2.3.1. Young's modulus of collagen gel

Young's modulus of collagen gel is modelled by employing nonlinear strain-dependent elasticity [21]:

$$E = E_0 \frac{1 - \bar{\epsilon} + (\bar{\epsilon}^2/3)}{(1 - \bar{\epsilon})^2}. \tag{2.1}$$

where E_0 is Young's modulus at strain $\bar{\epsilon} = 0$. To estimate Young's modulus, it is necessary to find a suitable connection between the F–D curve and the modulus. When a cylindrical punch indenting a flat elastic substrate (collagen gel), a linear relationship derived from Hertz contact theory can be expressed as [22]:

$$E^* = \frac{F}{2rD}, \tag{2.2}$$

where E^* is the reduced modulus of collagen gel, r is the radius of the cylindrical indenter, D is the displacement or depth of the indenter into the collagen gel surface and F is the force measured by the force transducer. For two elastic bodies in contact, the reduced modulus can be also described as follows according to Hertz contact theory [23]:

$$E^* = \left[\frac{1 - \nu^2}{E} + \frac{1 - \nu_i^2}{E_i}\right]^{-1}, \tag{2.3}$$

where ν is the Poisson's ratio and E is Young's modulus of the indented collagen gel. The subscript i refers to the properties of the cylindrical indenter. Hydrogel can normally be considered as an incompressible material, i.e. $\nu = 1/2$, and the indenter is regarded as perfectly rigid, i.e. $E_i = \infty$, and thus equation (2.3) can be simplified as follows:

$$E^* = \frac{4E}{3}. \tag{2.4}$$

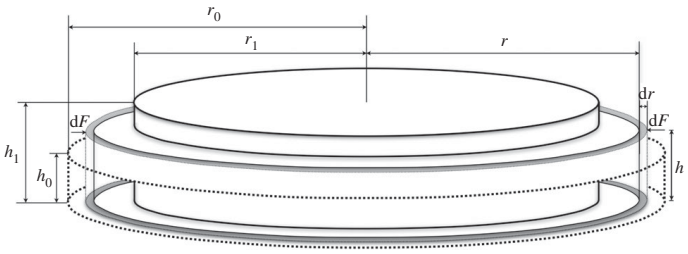

Figure 2. Schematic of theoretical model for collagen gel before and after contraction.

Combining (2.1), (2.2) and (2.4), the following equation can be derived:

$$F(\bar{\epsilon}) = E_0 \cdot \frac{8rD}{3} \cdot \frac{\bar{\epsilon} - \bar{\epsilon}^2 + (\bar{\epsilon}^3/3)}{(1-\bar{\epsilon})^2}. \tag{2.5}$$

For the strain $\bar{\epsilon}$ can be approximately calculated as the ratio of the displacement of the indenter to the measured thickness of the collagen gel, H, i.e. $\bar{\epsilon} = D/H$. Hence, by using nonlinear least square regression to fit $F(\bar{\epsilon})$ with D based on equation (2.5), Young's modulus E_0 of the collagen gel can be estimated from each measured F–D curve.

2.3.2. Contraction force

A simple theoretical model has been developed to estimate cell contraction force based on the force balance between cell contraction and gel deformation. Figure 2 shows the thickness (h_0 and h_1) and radius (r_0 and r_1) of a disc-shape collagen gel at the beginning and end of contraction. Young's modulus E_0 of the collagen gel is described by the linear elastic mechanics as:

$$E_0 = \frac{\mathrm{d}\sigma}{\mathrm{d}\varepsilon}, \tag{2.6}$$

where dσ and dε represent stress and strain, respectively, generated by cell contraction to the gel. During the entire contraction process, the contraction force acts perpendicularly on the circumference surface which area can be expressed as $2\pi r \cdot h$. Hence the stress dσ can be calculated by radial contraction force dF per unit area as the equation:

$$\mathrm{d}\sigma = \frac{\mathrm{d}F}{2\pi r \cdot h}, \tag{2.7}$$

where r and h are the immediate radius and thickness of collagen gel. Correspondingly, the strain dε can be expressed as the deformation of collagen gel in the radial direction.

$$\mathrm{d}\varepsilon = \frac{\mathrm{d}r}{r}. \tag{2.8}$$

Hence, combing equations (2.6), (2.7) and (2.8), Young's modulus E_0 can be expressed as:

$$E_0 = \frac{\mathrm{d}\sigma}{\mathrm{d}\varepsilon} = \frac{\mathrm{d}F}{2\pi h \cdot \mathrm{d}r}. \tag{2.9}$$

Here, the average thickness can be expressed as $h = (h_0 + h_1)/2$ if the gel thickness change is approximately linear during the contraction process. After rearranging equation (2.9) with integration, the final overall contraction force therefore can be presented as:

$$F = \int_{r_1}^{r_0} \mathrm{d}F = \int_{r_1}^{r_0} \pi E_0 (h_0 + h_1)\mathrm{d}r = \pi E_0 (h_0 + h_1)(r_0 - r_1). \tag{2.10}$$

The model simply correlates the overall cell contraction force F with the measured material parameters, including Young's modulus, thickness and radius of collagen gel. The single cell contraction force is approximately calculated as the overall contraction force divided by the counted cell numbers.

3. Result

3.1. Young's modulus of collagen gel

Typical indentation curves and their corresponding nonlinear fitting curves are represented in figure 3*a*. The first 25% of the indentation depth to the gel thickness (i.e. strain up to 0.25) is selected to estimate Young's modulus of the collagen based on the minimum least square fitting of equation (2.5) with the experimental force–strain data. Figure 3*b* shows Young's modulus for HAoAF-embedded collagen gels for controlled gels and treated gels at a cell density of 0.216×10^6 cells gel^{-1}. After treatment with histamine, Young's modulus of the collagen gels was decreased by 41.2% compared with the untreated gels, while treatment with ML-7 shows the inhibitory effect of decreasing elasticity (*ca* 59.3%).

3.2. HAoAF contraction force after histamine and ML-7 treatment

The images shown in figure 4*b*,*c* demonstrate the shrinkage of the HAoAF-embedded collagen gels treated by histamine with/without ML-7 compared with the untreated gel (figure 4*a*). The shaken gel sizes/radii can be calculated by counting the pixels of the gel images referencing the culturing area of the Petri dishes. By substituting the measured radius, Young's modulus and thickness of collagen gels into equation (2.10), HAoAF contraction force can then be estimated. Figure 5 shows that when cells were treated with histamine (100 µM), there was a nearly threefold increase in contraction force from 0.3 ± 0.04 to 0.89 ± 0.02 mN of overall contraction force. In the meantime, the contraction forces of single cells were calculated by the overall contraction force divided with the total number of cells embedded in the collagen gel. The single cell contraction force correspondingly increased from 1.41 ± 0.4 nN to 4.15 ± 0.5 nN when histamine was added. The MLCK inhibitor ML-7 (25 µM) attenuated the increase in contraction force by 60%.

3.3. Cell-density effect on contraction force

In the study, a constant volume of collagen gel was embedded with different cell densities to examine whether cell density could potentially have an influence on single cell contraction force. As shown in figure 6, the gel

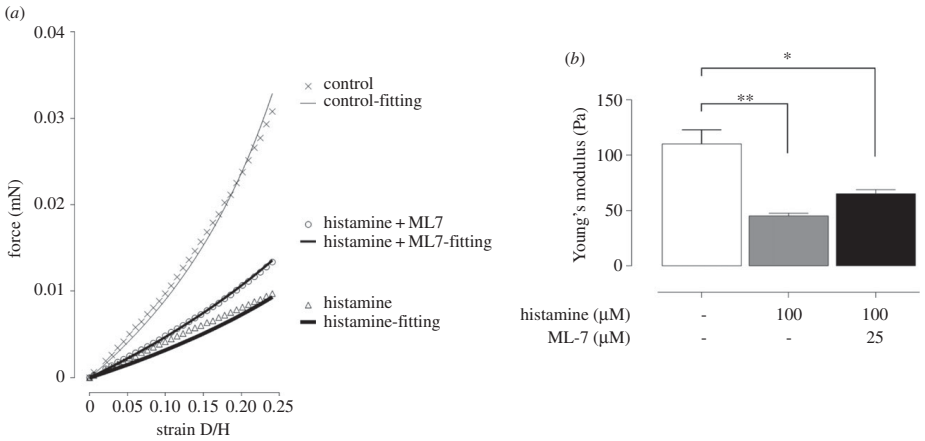

Figure 3. (*a*) Typical Young's modulus fitting of collagen gel contraction measurement from force–strain curve. (*b*) Data denote mean ± s.e.m. of Young's modulus of collagen gel with/without histamine and ML-7. *P*-value was calculated using one-way ANOVA with Bonferroni *post hoc* test. $^{**}p < 0.05$; $^{*}p < 0.5$.

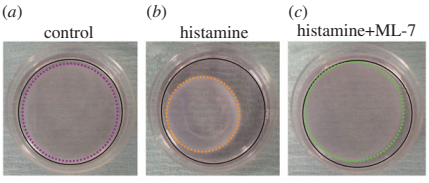

Figure 4. Photographs of the typical HAoAF-embedded collagen gel after treatments. (*a*) Controlled collagen gel, (*b*) agonist histamine (100 μM) stimulated collagen gel, (*c*) histamine stimulated collagen gel with the presence of MLCK inhibitor ML-7 (25 μM). The areas circled with black solid lines in (*a–c*) represent the culturing areas of 35 mm Petri dishes. The areas circled with coloured dash lines in (*a–c*) denote the sizes of collagen gels, which were calculated by referencing the culturing area of Petri dishes. (Online version in colour.)

contraction forces determined for three different cell densities, i.e. 0.06, 0.12 and 0.3×10^6 (cells gel^{-1}), have been measured after 48 h. The result shows that the overall contraction force calculated as determined by linear regression increases in a linear manner with the seeding densities of fibroblasts. As a result, the cell densities within the gels can be assumed to have no significant influence on the single cell contraction force measurements.

4. Discussion

This study describes a novel method to assess cellular contraction force *in vitro* using a collagen gel-based sensing technique to demonstrate cell contraction force changes in fibroblasts treated with the agonist histamine, which increases intracellular calcium to elicit contraction, and attenuated by the MLCK inhibitor ML-7. It is worth highlighting that conventional collagen gel contraction assays have been mainly based on the observation of the change of cell-embedded collagen gel area [24], although a few studies have included measurement of the gel thickness [25]. However, Young's modulus of the gel should be regarded as one of the key parameters required to estimate the cell contraction force, as described mathematically by equation (2.10). The result (figures 3 and 5) demonstrates the significant increase in cell contraction force after histamine treatment, despite Young's modulus of collagen gel decreasing. Since the treatment conditions or state of cell differentiation may alter the gel elastic modulus, careful characterization of the gel elasticity before and after the culturing period are critical to accurately determine the cell contraction forces.

A significant increase in single cell contraction force by histamine treatment has been demonstrated using this novel technique by combining nano-indentation with mathematical modelling of collagen gel contraction. As reported in the literature [7], histamine can elicit an extensive contraction of cells as measured using CGCA. However, adding ML-7, a MLCK inhibitor, to the collagen gel can significantly attenuate the cellular contraction elicited by histamine, confirming that the fibroblast contraction was mediated via MLC phosphorylation [26]. Overall, the order of magnitude of cell contraction forces measured using this novel technique was comparable with those values determined by other methods, e.g. CFM [20,27].

As shown in figure 6, the single cell contraction force was demonstrated to be cell-density independent. As the histamine-treated collagen gels were only allowed to contract for 5 h before the measurement, the cell proliferation during this period was negligible and cell numbers can be reasonably assumed to remain constant throughout the measurements. The single cell contraction force can therefore be calculated by dividing the overall contraction force by the known initial number of cells. However, for longer term measurement (more than 24 h) in the cell-density contraction experiments, it was noticeable that cells were aligned on the bottom of the Petri dishes. This implies that there may be a potential cell number loss and the collagen gel liquid content may be reduced [1]. Moreover, the cell proliferation rate during long-term treatment could cause a significant increase in cell number within the gels. Assessment of total DNA

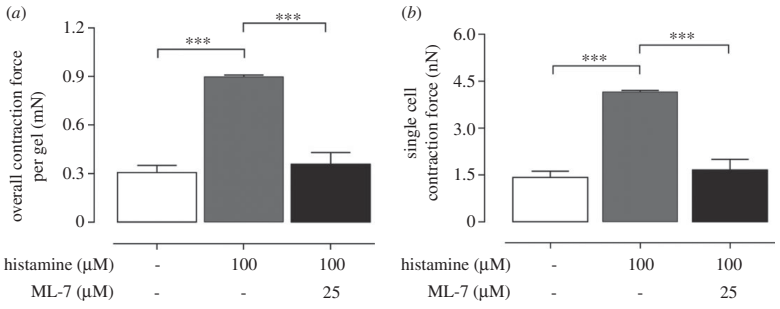

Figure 5. HAoAF were embedded into collagen gels at a density of 0.216×10^6 (cells gel^{-1}). (*a*) Overall contraction force and (*b*) single cell contraction force per gel with/without histamine and ML-7. Data denote mean $\pm$ s.e.m. from three independent measurements, *p*-value was calculated using one-way ANOVA with Bonferroni *post hoc* test. ***$p < 0.005$.

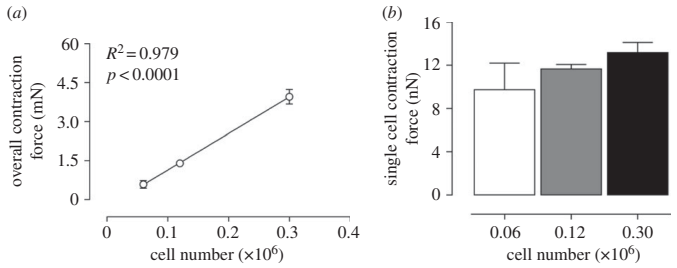

Figure 6. Cellular contraction force at different cell densities. (*a*) Overall contraction force of HAoAF at three different cell densities, i.e. 0.06, 0.12 and 0.3×10^6 (cells gel^{-1}). (*b*) Single cell contraction force of the three cell densities. Data denote mean $\pm$ s.e.m. from four independent measurements, *p*-value and R^2-value in (*a*) were calculated based on the linear regression model.

content would be a possible way to verify that the final number of cells within the gels remained constant until the end of assay.

Nevertheless, from the results shown in figure 6*b*, the single cell contraction force can be calculated by the initial cell seeding number as there was no significant force difference measured between the different cell densities. We have shown that 0.1×10^6 cell gel^{-1} is an ideal cell seeding density for the long-term contraction force measurement while a higher cell seeding density, e.g. 0.3×10^6 cell gel^{-1} will be desirable for shorter periods of measurement (less than 24 h). This is because with same amount of cells embedded, contraction assays performed soon after seeding (less than 6 h) will generate less overall contraction force than measurements taken after a longer period (24 h) due to cell proliferation. Therefore, increasing cell seeding density would provide a greater overall contraction force and result in more accurate measurements of cell contraction force.

The novel technique reported in this study is applicable to assess forces generated by any cell type that can be cultured within a three-dimensional collagen gel and responds to agonist stimulation leading to cell contraction. For example, assessment of forces elicited by vascular smooth muscle cells may indicate the likelihood of a treatment causing contractile responses that may lead to hypertension [28] while assessment of contraction forces in dermal fibroblasts may provide insights into the wound healing potential of drugs, anti-wrinkling properties of therapeutic compounds or suitability of three-dimensional gel matrices for tissue-engineering of skin substitutes [29–31]. These are only a few potential applications where the novel technique to assess cellular and gel contraction forces may provide important information for future bioengineering and clinically relevant therapeutic strategies.

5. Conclusion

This study has demonstrated a novel technique to quantify cellular contraction force when cells are embedded in a three-dimensional collagen gel matrix. The histamine-induced contraction of fibroblasts through MLCK activation and MLC phosphorylation, determined in cells seeded in a collagen gel, are in agreement with observations previously reported [27]. Moreover, the alteration in the collagen gel elasticity before and after histamine treatment was measured. The nonlinear theoretical fittings of collagen gel elasticity are in agreement with the experimental data. The measurements have confirmed that the mechanical property changes of the gel matrix should be taken into account to accurately measure cell contraction forces using gel contraction assays.

Acknowledgement. This work was supported by a grant from Leverhulme Trust (PRG-2012-738) awarded to K.-K.L. and a grant from the British Heart Foundation (FS/09/037/27827) awarded to R.C.M.S. We would also like to thank Prof. Giovanni E. Mann and Dr Ron Jacob, Cardiovascular Division, King's College London, for their insightful suggestions and technical support.

References

1. Bell E, Ivarsson B, Merrill C. 1979 Production of a tissue-like structure by contraction of collagen lattices by human fibroblasts of different proliferative potential *in vitro*. *Proc. Natl Acad. Sci. USA* **76**, 1274–1278. (doi:10.1073/pnas.76.3.1274)
2. Ehrlich HP, Rockwell WB, Cornwell TL, Rajaratnam JB. 1991 Demonstration of a direct role for myosin light chain kinase in fibroblast-populated collagen lattice contraction. *J. Cell. Physiol.* **146**, 1–7. (doi:10.1002/jcp.1041460102)
3. Dallon JC, Ehrlich HP. 2008 A review of fibroblast-populated collagen lattices. *Wound Repair Regen.* **16**, 472–479. (doi:10.1111/j.1524-475X.2008.00392.x)
4. Travis JA, Hughes MG, Wong JM, Wagner WD, Geary RL. 2001 Hyaluronan enhances contraction of collagen by smooth muscle cells and adventitial fibroblasts: role of CD44 and implications for constrictive remodeling. *Circ. Res.* **88**, 77–83. (doi:10.1161/01.RES.88.1.77)
5. Liang W, McDonald P, McManus B, van Breemen C, Wang X. 2003 Histamine-induced Ca^{2+} signaling in human valvular myofibroblasts. *J. Mol. Cell. Cardiol.* **35**, 379–388. (doi:10.1016/S0022-2828(03)00010-5)
6. Johnson CL, Johnson CG, Bazan E, Garver D, Gruenstein E, Ahluwalia M. 1990 Histamine receptors in human fibroblasts: inositol phosphates, Ca^{2+}, and cell growth. *Am. J. Physiol.* **258**, C533–C543.
7. Horie M *et al*. 2014 Histamine induces human lung fibroblast-mediated collagen gel contraction via histamine H1 receptor. *Exp. Lung Res.* **40**, 222–236. (doi:10.3109/01902148.2014.900155)
8. Ahearne M. 2014 Introduction to cell–hydrogel mechanosensing. *Interface Focus* **4**, 20130038. (doi:10.1098/rsfs.2013.0038)
9. Jeng JH, Lan WH, Wang JS, Chan CP, Ho YS, Lee PH *et al*. 2006 Signaling mechanism of thrombin-induced gingival fibroblast-populated collagen gel contraction. *Br. J. Pharmacol.* **147**, 188–198. (doi:10.1038/sj.bjp.0706462)
10. Yanase M *et al*. 2003 Functional diversity between Rho-kinase- and MLCK-mediated cytoskeletal actions in a myofibroblast-like hepatic stellate cell line. *Biochem. Biophys. Res. Commun.* **305**, 223–228. (doi:10.1016/S0006-291X(03)00726-5)
11. Nakamura Y, Hirano S, Suzuki K, Seki K, Sagara T, Nishida T. 2002 Signaling mechanism of TGF-β1-induced collagen contraction mediated by bovine trabecular meshwork cells. *Invest. Ophthalmol. Vis. Sci.* **43**, 3465–3472.
12. Dembo M, Wang Y-L. 1999 Stresses at the cell-to-substrate interface during locomotion of fibroblasts. *Biophys. J.* **76**, 2307–2316. (doi:10.1016/S0006-3495(99)77386-8)
13. Butler JP, Tolić-Nørrelykke IM, Fabry B, Fredberg JJ. 2002 Traction fields, moments, and strain energy that cells exert on their surroundings. *Am. J. Physiol.-Cell Physiol.* **282**, C595–C605. (doi:10.1152/ajpcell.00270.2001)
14. Yang Z, Lin J-S, Chen J, Wang JH. 2006 Determining substrate displacement and cell traction fields—a new approach. *J. Theor. Biol.* **242**, 607–616. (doi:10.1016/j.jtbi.2006.05.005)
15. Delvoye P, Wiliquet P, Levêque J-L, Nusgens BV, Lapière CM. 1991 Measurement of mechanical forces generated by skin fibroblasts embedded in a three-dimensional collagen gel. *J. Invest. Dermatol.* **97**, 898–902. (doi:10.1111/1523-1747.ep12491651)
16. Kolodney MS, Wysolmerski RB. 1992 Isometric contraction by fibroblasts and endothelial cells in tissue culture: a quantitative study. *J. Cell Biol.* **117**, 73–82. (doi:10.1083/jcb.117.1.73)
17. Eastwood M, McGrouther DA, Brown RA. 1994 A culture force monitor for measurement of contraction forces generated in human dermal fibroblast cultures: evidence for cell–matrix mechanical signalling. *Biochim. Biophys. Acta* **1201**, 186–192. (doi:10.1016/0304-4165(94)90040-X)
18. Eastwood M, Porter R, Khan U, McGrouther G, Brown R. 1996 Quantitative analysis of collagen gel contractile forces generated by dermal fibroblasts and the relationship to cell morphology. *J. Cell. Physiol.* **166**, 33–42. (doi:10.1002/(SICI)1097-4652(199601)166:1<33::AID-JCP4>3.0.CO;2-H)
19. Freyman T, Yannas I, Pek Y, Yokoo R, Gibson L. 2001 Micromechanics of fibroblast contraction of a collagen–GAG matrix. *Exp. Cell Res.* **269**, 140–153. (doi:10.1006/excr.2001.5302)
20. Campbell BH, Clark WW, Wang JH. 2003 A multi-station culture force monitor system to study cellular contractility. *J. Biomech.* **36**, 137–140. (doi:10.1016/S0021-9290(02)00325-1)
21. Tatara Y. 1991 On compression of rubber elastic sphere over a large range of displacements—part 1: theoretical study. *J. Eng. Mater. Technol.* **113**, 285–291. (doi:10.1115/1.2903407)
22. Johnson KL. 1987 *Contact mechanics*. Cambridge, UK: Cambridge University Press.
23. Heinrich H. 1881 Über die Berührung fester elastischer Körper. *J. Die Reine Angew. Math.* **92**, 156–171.
24. Zhu Y *et al*. 2001 Contraction of fibroblast-containing collagen gels: initial collagen concentration regulates the degree of contraction and cell survival. *In Vitro Cell. Dev. Biol.* **37**, 10–16. (doi:10.1290/1071-2690(2001)037<0010:COFCCG>2.0.CO;2)
25. Kurosaka H, Kurosaka D, Kato K, Mashima Y, Tanaka Y. 1998 Transforming growth factor-beta 1 promotes contraction of collagen gel by bovine corneal fibroblasts through differentiation of myofibroblasts. *Invest. Ophthalmol. Vis. Sci.* **39**, 699–704.
26. Matsumoto H *et al*. 2007 Comparison of gel contraction mediated by airway smooth muscle cells from patients with and without asthma. *Thorax* **62**, 848–854. (doi:10.1136/thx.2006.070474)
27. Fujimura T, Hotta M, Kitahara T, Takema Y. 2011 Loss of contraction force in dermal fibroblasts with aging due to decreases in myosin light chain phosphorylation enzymes. *Archiv. Pharmacol. Res.* **34**, 1015–1022. (doi:10.1007/s12272-011-0619-9)
28. Wynne BM, Chiao CW, Webb RC. 2009 Vascular smooth muscle cell signaling mechanisms for contraction to angiotensin II and endothelin-1. *J. Am. Soc. Hypertens.* **3**, 84–95. (doi:10.1016/j.jash.2008.09.002)
29. Brown RA, Sethi KK, Gwanmesia I, Raemdonck D, Eastwood M, Mudera V. 2002 Enhanced fibroblast contraction of 3D collagen lattices and integrin expression by TGF-β1 and -β3: mechanoregulatory growth factors? *Exp. Cell Res.* **274**, 310–322. (doi:10.1006/excr.2002.5471)
30. Grinnell F. 2003 Fibroblast biology in three-dimensional collagen matrices. *Trends Cell Biol.* **13**, 264–269. (doi:10.1016/S0962-8924(03)00057-6)
31. Ahearne M, Wilson SL, Liu K-K, Rauz S, El Haj AJ, Yang Y. 2010 Influence of cell and collagen concentration on the cell–matrix mechanical relationship in a corneal stroma wound healing model. *Exp. Eye Res.* **91**, 584–591. (doi:10.1016/j.exer.2010.07.013)

OPEN ACCESS Freely available online

PLOS ONE

'Special K' and a Loss of Cell-To-Cell Adhesion in Proximal Tubule-Derived Epithelial Cells: Modulation of the Adherens Junction Complex by Ketamine

Claire E. Hills[1]*, Tianrong Jin[2], Eleftherios Siamantouras[2], Issac K-K Liu[2], Kieran P. Jefferson[3], Paul E. Squires[1]

1 School of Life Sciences, University of Warwick, Coventry, United Kingdom, **2** School of Engineering, University of Warwick, Coventry, United Kingdom, **3** University Hospital of Coventry and Warwickshire, Coventry, United Kingdom

Abstract

Ketamine, a mild hallucinogenic class C drug, is the fastest growing 'party drug' used by 16–24 year olds in the UK. As the recreational use of Ketamine increases we are beginning to see the signs of major renal and bladder complications. To date however, we know nothing of a role for Ketamine in modulating both structure and function of the human renal proximal tubule. In the current study we have used an established model cell line for human epithelial cells of the proximal tubule (HK2) to demonstrate that Ketamine evokes early changes in expression of proteins central to the adherens junction complex. Furthermore we use AFM single-cell force spectroscopy to assess if these changes functionally uncouple cells of the proximal tubule ahead of any overt loss in epithelial cell function. Our data suggests that Ketamine (24–48 hrs) produces gross changes in cell morphology and cytoskeletal architecture towards a fibrotic phenotype. These physical changes matched the concentration-dependent (0.1–1 mg/mL) cytotoxic effect of Ketamine and reflect a loss in expression of the key adherens junction proteins epithelial (E)- and neural (N)-cadherin and β-catenin. Down-regulation of protein expression does not involve the pro-fibrotic cytokine TGFβ, nor is it regulated by the usual increase in expression of Slug or Snail, the transcriptional regulators for E-cadherin. However, the loss in E-cadherin can be partially rescued pharmacologically by blocking p38 MAPK using SB203580. These data provide compelling evidence that Ketamine alters epithelial cell-to-cell adhesion and cell-coupling in the proximal kidney via a non-classical pro-fibrotic mechanism and the data provides the first indication that this illicit substance can have major implications on renal function. Understanding Ketamine-induced renal pathology may identify targets for future therapeutic intervention.

Citation: Hills CE, Jin T, Siamantouras E, Liu IK-K, Jefferson KP, et al. (2013) *'Special K'* and a Loss of Cell-To-Cell Adhesion in Proximal Tubule-Derived Epithelial Cells: Modulation of the Adherens Junction Complex by Ketamine. PLoS ONE 8(8): e71819. doi:10.1371/journal.pone.0071819

Editor: Steen Henning Hansen, Children's Hospital Boston, United States of America

Received April 4, 2013; **Accepted** July 3, 2013; **Published** August 29, 2013

Funding: This work was supported by the generous support of The Teresa Rosenbaum Golden Charitable Trust (Rosetree Trust). AFM-SCFS was made possible by the support of an equipment grant from Diabetes UK (BDA: 12/0004546). The funders had no role in study design, data collection and analysis, decision to publish, or preparation of the manuscript.

Competing Interests: The authors have declared that no competing interests exist.

* E-mail: C.Hills@warwick.ac.uk

Introduction

Ketamine is a tranquilliser that has also found use as an NMDA receptor antagonist in the treatment of human bipolar disorders [1]. However, in 2006 the UK government made Ketamine a class C drug. Possessing mild hallucinogenic properties, Ketamine is rapidly replacing heroin and methamphetamine as the recreational drug of choice [2]. Cheap to buy and easily accessible, Ketamine has several street names including "Special K", "vitamin K" and "LA Coke". In 2008, the British Crime Survey revealed that Ketamine was the fastest growing "party drug" among 16–24 year olds and it has since been dubbed the "new ecstasy" [3]. In the UK, Ketamine boasts an estimated 125,000 users, with more young people using Ketamine in England and Wales than heroin and crack cocaine combined. As the number of users rise, serious side effects are beginning to emerge. First documented in 2007, Ketamine has been shown to injure the bladder, causing ulcers (wounds) and fibrosis (stiffening of the bladder walls and shrinkage) [4]. Patients present with multiple symptoms including incontinence, bleeding, overactive bladder and bladder shrinkage, as well as damage to both the kidneys and the ureter [5]. Despite the growing presentation of these complications, there is an acute lack of understanding for the mechanisms that underlie the pathophysiological of Ketamine, and we urgently need to investigate how this mild hallucinogenic drug scars bladder and renal tissue to impair function [6].

In adults, wound repair is commonly associated with the accumulation of scar tissue (fibrosis or sclerosis). Its effects are variable and often impaired by disease or other pathophysiological insult (e.g. diabetes/drug abuse) [7]. Fibrosis involves excess accumulation of extracellular matrix (ECM), primarily composed of collagen. As normal tissue is replaced with scar tissue, a number of phenotypic and morphological changes occur and the fibrosis ultimately results in loss of function [8]. Regardless of etiology, patients subsequently exhibit a progressive decline in organ function, a largely irreversible process that, in the case of Ketamine abuse, can lead to removal of the bladder and potential end stage renal disease. In both the bladder and kidney, early changes in protein expression/function often occur before overt

fibrosis. These changes include a loss of epithelial integrity and dysregulated formation of the intercellular junction, involving, loss of epithelial E-cadherin, altered cell morphology, re-organisation of the cytoskeleton and *de-novo* expression of fibroblastic markers [9]. Cadherins have a central role in the formation of the multi-protein adherens junction, which links cell-cell contact to the actin cytoskeleton and various other signalling molecules [10]. The extracellular domain of the cell adhesion protein E-cadherin mediates ligation with neighbouring cadherins on adjacent cells [11], whilst the cytoplasmic domain binds to β-catenin linking cadherin to the actin cytoskeleton via α-catenin. The functional interaction of cadherin with F-actin, via the catenins, not only serves to increase adhesive strength of the junction but also acts as a signalling 'node' for proteins that influence adhesiveness &/or initiate intracellular signalling. The loss of E-cadherin mediated cell-to-cell adhesion represents a pivotal step in the transition of renal tubule cells from an epithelial phenotype to one more commonly associated with fibrosis [12]. Down-regulation of E-cadherin precedes changes in cell morphology, reorganisation of cell architecture and the subsequent gain in expression of phenotypic markers associated with renal pathology [12–13].

In the renal tubule, epithelial function depends on complex cell-cell interactions mediated through the adherens junction. In the current study we present data outlining early toxicological effects of Ketamine on proteins critical to formation of the adherens junction complex in the kidney. Using pharmacological manipulation, we examine potential cellular mechanisms orchestrating these changes and utilise high resolution AFM-single-cell force spectroscopy to assess the functional consequence of cell-cell tethering in Ketamine-treated cells exhibiting a loss in cadherin expression. Our data provide compelling evidence that Ketamine reduces cell-cell adhesion in epithelial cells of the proximal tubule. Translated to the *in vivo* scenario, the subsequent loss of epithelial integrity, structure and function may in part contribute to the toxicological and potential fibrotic response to Ketamine in the kidney.

Methods

Supplies for tissue culture were purchased from Invitrogen (Paisley, UK). Immobilon P membrane was from Millipore, Watford, UK and ECL from Amersham Biosciences, Buckinghamshire, UK. A Qproteome kit was obtained from Qiagen (Sussex, UK). Antibodies were obtained from Santa Cruz (CA, USA) and R&D systems (Abingdon, UK). Ketamine, TRITC-Phalloidin and Fibronectin, were obtained from Sigma (Poole, UK), as were all other general chemicals. Anti-TGF-β1 ELISA was obtained from R&D systems.

Model Cell Line

HK2 cells were obtained from the ATCC Bio-resource Centre (LGC Standards. Middlesex, UK). Cells (passages 18–30) were maintained in DMEM/Hams F12 (DMEM/F12) medium, supplemented with 10% fetal calf serum (FCS), glutamine (2 mM), and EGF (5 ng/ml) and cultured at 37°C in a humidified atmosphere of 5% CO_2. Prior to treatment, cells were transferred to DMEM/F12 low glucose (5 mM) for 48 hr as described previously [14]. Cells were serum starved overnight before applying either Ketamine (0–1 mg/mL) in the presence/absence of signalling inhibitors Wortmannin (2 μM), PD98059 (10 μM), and SB203580 (1 μM) for 24 hr. Cells were pre-incubated for 30 minutes with their corresponding inhibitors prior to Ketamine application. For assessment of Smad activity HK2 cells were incubated for 0–10 minutes with Ketamine (1 mg/mL).

MTT Assay

The 3-(4,5-Dimethylthiazol-2-yl)-2,5-diphenyltetrazolium bromide (MTT) assay is widely used for cytotoxicity assessments of pharmacological and chemical agents. Viable cells transport MTT into their mitochondria, the compound is then reduced to formazin (purple in color), and the latter is quantified colorometrically. The amount of color formed corresponds to the number of viable cells. HK2 cells were cultured in 96-well plates (5×10^3 cells/well) in 5 mM glucose containing media for 48 hrs prior to an overnight period of serum starvation. Cells were stimulated for 24 and 48 hrs with Ketamine (0.1–1 mg) and proliferation analyzed using the MTT colorimetric assay (Roche) according to manufacturers instructions. The values were presented as a percentage of the MTT uptake that was observed as compared to control cells.

Lactate Dehydrogenase Assay

Cell death or cytotoxicity is classically evaluated by the quantification of plasma membrane damage. Lactate dehydrogenase (LDH) is a stable enzyme, present in all cell types, and rapidly released into the cell culture medium upon damage of the plasma membrane. Therefore, LDH is a common marker used to determine cytotoxicity. HK2 cells were cultured in 96-well plates (5×10^3 cells/well) in 5 mM glucose containing media for 48 hrs prior to an overnight period of serum starvation. Cells were stimulated for 24 and 48 hrs with Ketamine (0.1–1 mg) and Lactate dehydrogenase levels assayed using the LDH-cytoxicity assay kit II (Abcam) according to manufacturers instructions. The values were presented as a percentage of the LDH release that was observed as compared to control cells.

Crystal Violet Assay

This is a simple assay useful for obtaining quantitative information about the relative density of cells adhering to multi-well cluster dishes. Crystal Violet stains DNA and upon solubilization, the amount of dye taken up by the monolayer can be quantitated in a plate reader. HK2 cells were cultured in 96-well plates (5×10^3 cells/well) in 5 mM glucose containing media for 48 hrs prior to an overnight period of serum starvation. Cells were stimulated for 24 and 48 hrs with Ketamine (0.1–1 mg) and cell density determined with crystal violet staining. Briefly, media was removed and cells were fixed for 10 mins with PFA. Following a brief wash with PBS, cells were incubated for 10 mins at room temperature in a 1% Crystal Violet solution. After this time interval, all traces of dye were removed with distilled water and the stain solubilized with 1% SDS. The values were presented as a percentage of cells staining in Ketamine treated cells as compared to control cells.

Quantification of TGF-β1

HK2 cells were cultured in 5 mM glucose containing media for 48 hrs prior to an overnight period of serum starvation. Cells were stimulated for 24 hrs with Ketamine (0.1–1 mg) under serum-free conditions and total TGF-β1 was measured by specific enzyme-linked immunosorbent assay (ELISA) of cell culture supernatant collected from growth-arrested HK2 cells. Active TGF-β1 is measured directly and latent TGF-β1 can be measured indirectly following acid activation of samples. This assay has <1% cross-reactivity for TGF-β2 and TGF-β3. TGF-β1 concentration was normalized to mg/ml of protein. Data were obtained as picograms of TGF-β1 per milliliter per mg of protein and are expressed as a percent as compared to control.

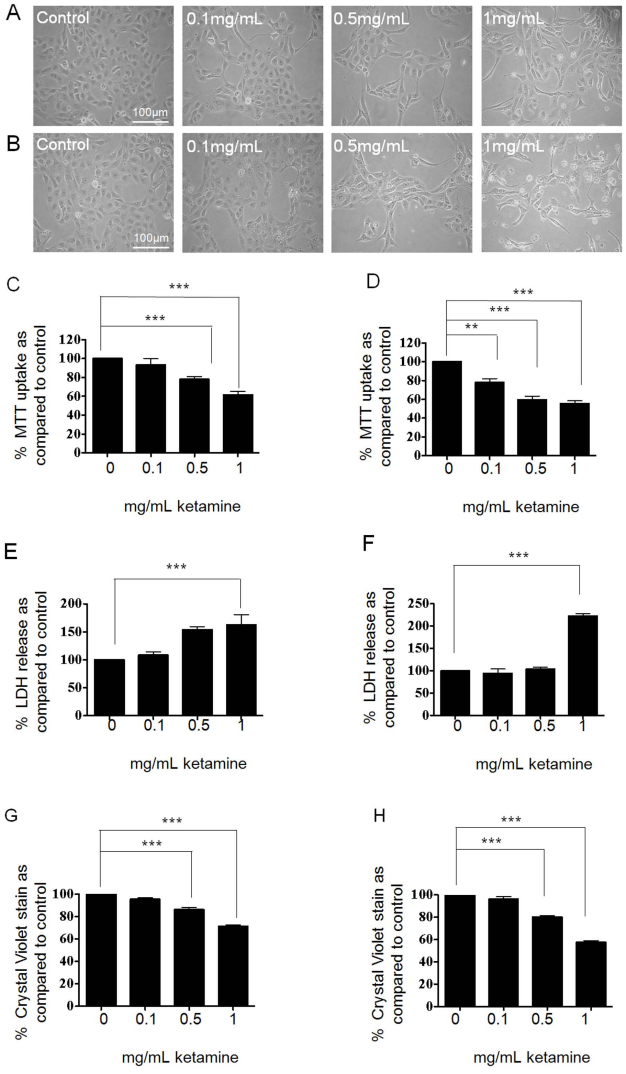

Figure 1. Impact of Ketamine on HK2 cell viability, as assessed by phase contrast microscopy, MTT uptake, Crystal Violet staining and LDH release. HK2 cells were cultured in 5 mM glucose containing media for 48 hrs prior to an overnight serum starvation. Cells were stimulated for 24–48 hrs with Ketamine (0.1–1 mg/mL) under serum-free conditions and morphological changes assessed (Panels A and B respectively). Ketamine evoked a concentration dependent change in cell morphology from a typical proximal tubular epithelial "cobblestone" appearance to an elongated fibroblast appearance. Cell viability was assessed by MTT uptake at 24 and 48 hrs (panels C and D respectively). Incubation with Ketamine at 0.5 and 1 mg/mL caused a significant decrease in viable cells as measured by MTT uptake. Cell membrane damage was assessed via LDH release at 24 and 48 hrs (panels E and F respectively). At both 24 and 48 hrs, Ketamine (1 mg/mL) caused a significant increase in LDH release. Finally cell density was determined by the Crystal violet assay. Ketamine evoked a reduction in cell density at 24 and 48 hrs (panels G and H respectively). The values obtained are expressed as a % of control (C). Results are representative of 3 separate experiments. Key significances are shown where $^{**}P<0.01$ and $^{***}P<0.001$.
doi:10.1371/journal.pone.0071819.g001

Immunoblotting

Cytosolic proteins were prepared and separated by gel electrophoresis and electro-blotting onto Immobilon P membranes as described previously [15]. For determination of protein localization, proteins were harvested using the Qproteome cell compartment kit. Membranes were probed with specific polyclonal antibodies against anti-E-cadherin (1:2000), N-Cadherin (1:1000), Snail (1:1000), Slug (1:1000), (1:2000), p-Smad 2 (1:1000), p-Smad 3(1:1000) (all R&D systems) and beta-catenin (1:1000) (Santa Cruz).

Immunocytochemistry

Cells at 80% confluence were fixed with 4% paraformaldehyde (PFA). Following blocking, the nuclear stain 4′, 6-diamidino-2-phenylindole, dihydrochloride (DAPI; 1 mM) was added for 3 mins. Cells were then incubated with TRITC-conjugated phalloidin (Sigma) diluted at 1:100 in PBS-Triton for 1 hr at 25°C. Fluorescence was visualized using an Axiovert 200 fluorescence microscope (Carl Zeiss, Welwyn Garden City, UK).

Single Cell Force Spectroscopy

Atomic Force Microscopy (AFM) Single-Cell Force Spectroscopy (CellHesion® module, JKP Instruments Germany) was used to measure cell-cell adhesion and the separation forces required to uncouple cells cultured in Ketamine as compared to control untreated cells. A single HK2 cell was bound to a cantilever using fibronectin (20 μg/ml) and poly-l-lysine (25 μg/ml) and subsequently brought into contact with an adherent cell (in a cluster of coupled cells) using a known force (1 nN). The two cells remained in contact for a defined period of time (10 sec) whilst bonding formed. The cantilever was then retracted at a constant speed (5 μm/sec) and force (nN) versus displacement (deflection of the cantilever) measured by the position of a laser beam reflected from the cantilever, until the cells were completely separated (pulling length 90 μm). Each cell-cell recording was repeated in triplicate with a 30 sec pause interval between successive measurements. Retraction recordings from multiple cells (approx. 40) in separate experiments (n = 4) were made and the maximum unbinding force (nN) and the detachment energy (fJoules) calculated.

Analysis

Autoradiographs were quantified by densitometry using TotalLab 2003 (NonLinear Dynamics, Durham, NC USA). Where data was quantified, the non-stimulated, low glucose control condition was normalized to 100% and data from all other experimental conditions compared to this. Statistical analysis of data was performed using a one-way ANOVA test with a Tukey's multiple comparison post-test. AFM data was analysed via *t*-test. Data are expressed as mean ± SEM, where 'n' denotes the number of experiments. A probability (P) <0.05 was taken to signify statistical significance.

Results

The Effect of Ketamine on Cell Viability and Cytoxicity

Cells were cultured in 5 mM glucose for 48 hrs prior to being serum starved overnight. Cells were either unstimulated (control) or stimulated for 24–48 hrs with Ketamine (0.1–1 mg/mL) under serum-free conditions. Phase contrast microscopy revealed that control HK2-cells exhibited a typical cobblestone morphology, characteristic of proximal tubular epithelial cells (Fig. 1, A and B). Exposure to increasing concentrations of Ketamine (0.1, 0.5 and 1 mg/mL) for 24 or 48 hrs evoked a concentration-dependent change in morphology towards an elongated fibrous phenotype. Furthermore, cells treated for 48 hrs at the highest concentration (1 mg/mL), appeared to exhibit cytosolic granulation and a reduction in cell number (Fig. 1B).

Cells stimulated for 24 and 48 hrs with Ketamine (0.1–1 mg/mL) under serum-free conditions were assessed for cell viability by MTT uptake (uptake directly correlates with the number of viable cells). At 24 hrs, incubation with Ketamine at 0.5 and 1 mg/mL significantly decreased viability by 22±4% and 39±5% respectively as compared to control (Fig. 1C, $P<0.001$, n = 3). At 48 hrs, Ketamine decreased cell viability by 22±4% ($P<0.01$), 41±3% ($P<0.001$) and 45±3% ($P<0.001$) as compared to control over the same range of concentrations (Fig. 1D, n = 3).

As a complimentary strategy to assess cytotoxicity, we used the Lactate Dehyrdogenase assay as a marker of LDH release into cell supernatant of control versus Ketamine-treated cells. To assess membrane damage, cells were stimulated for 24 and 48 hrs with Ketamine (0.1–1 mg/mL) under serum-free conditions prior to measuring LDH release. Results are expressed as a % of LDH release as compared to control cells. At 24 hrs, Ketamine (1 mg/mL) increased LDH levels by 62% to 162±17% of that under control (100%) conditions (Fig. 1E, $P<0.001$, n = 3), At 48 hrs Ketamine (1 mg/mL) significantly increased LDH levels by 140% to 240±18% as compared to control (Fig. 1F; $P<0.001$, n = 3). Release of LDH into the media suggests cell membrane damage and a concentration-dependent cytotoxic effect of Ketamine.

To further confirm the toxic role of Ketamine, we measured the number of adherent cells using a crystal violet assay. Cells were fixed and stained with crystal violet (1% w/v) at 24 and 48 hrs. Quantification of dye uptake was significantly reduced by 14±2% ($P<0.001$) and 29±1% ($P<0.001$) at 0.5 and 1 mg/mL respectively as compared to control at 24 hrs (Fig. 1G), and by 20±1% ($P<0.001$) and 43±2% ($P<0.001$) at 48 hrs over the same range of concentrations (Fig. 1H, n = 3). Based on our observations from all three strategies, subsequent analysis determined the effects of Ketamine (0.1–1 mg/mL) on cell-to-cell adhesion and adherens junction proteins over the more acute 24 hr time window.

The Effect of Ketamine on Expression of Adherens Junction Proteins

The transition of tubular epithelial cells from a typical, cobblestone morphology to a fibrotic phenotype is commonly associated with reorganisation of cell architecture and alterations in the expression of epithelial proteins involved in adherens and tight junction formation [12–13]. HK2 cells were cultured in 5 mM glucose containing media for 48 hrs prior to overnight serum starvation. Cells were stimulated for 24 hrs with Ketamine (0.1–1 mg/mL) under serum-free conditions and morphological and phenotypic changes assessed. At 24 hrs, Ketamine induced a concentration-dependent change in cell morphology towards an elongated fibroblast-like phenotype (Fig. 2A). These gross morphological changes were accompanied by re-organisation of the actin cytoskeleton from a diffuse transcellular network of F-actin filaments that spanned the cytosol, into more dense peripheral stress fibres (Fig. 2B).

This architectural reorganisation intimates that Ketamine causes dysregulation of the adherens junction complex and has repercussions for the integrity of the epithelial sheet. To resolve these changes, we examined the effects of Ketamine on adherens junction proteins and their transcriptional regulators. Ketamine induced a concentration-dependent decrease in whole-cell expression of E-cadherin by 28±1% ($P<0.01$), 52±12% ($P<0.001$) and 76±3% ($P<0.001$) as compared to control at 0.1, 0.5 and 1 mg/mL respectively (n = 3, Fig. 2C). The loss in expression reflected a loss in E-cadherin from all cell compartments examined (Fig. 2Hi).

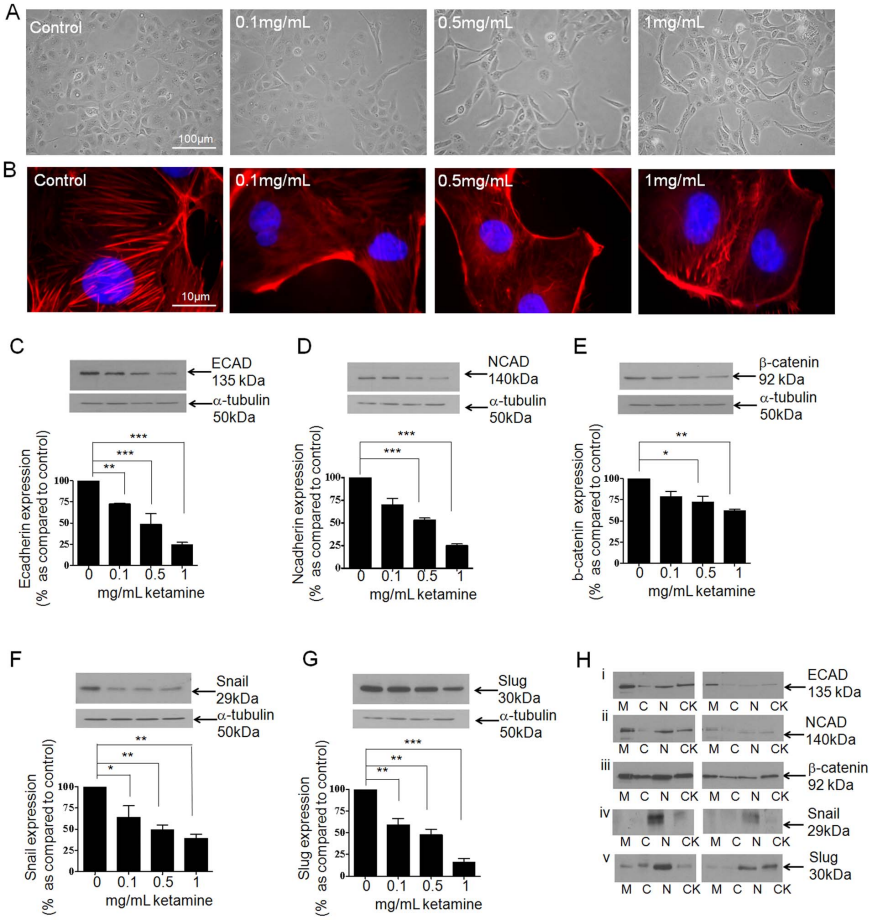

Figure 2. Ketamine evoked changes in AJ-protein expression in HK2-cells. To assess the effect of Ketamine on expression of key AJ proteins, HK2 cells were cultured in 5 mM glucose containing media for 48 hrs prior to overnight serum starvation. Cells were stimulated for 24 hrs with Ketamine (0.1–1 mg/mL) under serum-free conditions and morphological and phenotypic changes assessed. Phase contrast microscopy (panel A) and TRITC conjugated phalloidin (panel B) confirmed the dose dependent effects of Ketamine on cell morphology and cytoskeletal reorganization respectively. Whole cell expression of E-cadherin and its transcriptional co-repressor Snail were determined by western blotting. Ketamine decreased expression of E-cadherin (panel C) Snail (panel F) and Slug (panel G). Compartmental localisation of E-cadherin, Snail and Slug expression were determined for membrane (M), cytosol (C), nuclear (N) and cytoskeletal (CK) fractions +/− Ketamine (1 mg/mL). Ketamine altered the cellular localization of all three proteins, compared to control (panels Hi, Hiv and Hv respectively). Ketamine also down-regulated expression of N-cadherin (panel D) and β-catenin (panel E), with a loss in expression being apparent throughout the cell (panel Hii and Hiii respectively). Upper panels show representative blots for each protein and re-probed for α-tubulin as a loading control. Lower panels show mean (±SEM) densitometry data, normalised against the non-stimulated low glucose control (100%), from 3 or more separate experiments. Each lane in the representative blot corresponds to the associated bar in the graph. Key significances are shown, *$P<0.05$, *$P<0.01$, ***$P<0.001$.
doi:10.1371/journal.pone.0071819.g002

Previously implicated in the differentiation of epithelial cells into fibroblast, e.g. mesenchymal cells (epithelial-mesenchymal transitions), following down regulation of expression of the adhesion protein E-cadherin [16–18] we next examined the effect of Ketamine on whole cell and cell-compartment expression of the transcriptional repressors Snail (Fig. 2F) and Slug (Fig. 2G). Data suggests that Ketamine down-regulated whole cell expression of Snail by 36±13% ($P<0.05$), 51±6% ($P<0.01$) and 61±4%

($P<0.01$) as compared to control (100%) and of Slug by 41±7% ($P<0.01$), 53±6% ($P<0.01$) and 84±4% ($P<0.001$) of control at 0.1, 0.5 and 1 mg/mL respectively (n = 3). Cell compartment analysis highlighted a predominant loss in expression of both these transcription factors from the nucleus (Fig. 2Hiv and Fig. 2Hv, Snail and Slug respectively). Normally exhibiting a reciprocal relationship's with E-cadherin these data suggest a toxic, but non-lethal effect of Ketamine in cells of the proximal tubule.

The cytoplasmic domain of E-cadherin binds to β-catenin to link cell-adhesion to the actin cytoskeleton Ketamine reduced whole cell expression of β-catenin by 28±6%, 28±7% ($P<0.05$) and 39±2% ($P<0.01$) as compared to control at 0.1, 0.5 and 1 mg/mL (n = 3, Fig. 2E), an effect attributable to a loss in expression from all 4 cell compartments (Fig. 2Hiii). In the kidney, a loss in E-cadherin expression is often paralleled by a concomitant gain in the expression of neural (N)-cadherin, a mechanism commonly referred to as the cadherin switch [18–19]. However, in the current study, Ketamine was unable to induce this compensatory switch and Ketamine induced a concentration-dependent down-regulation in N-cadherin expression. N-cadherin expression levels decreased in response to Ketamine by to 31±7%, 47±3% ($P<0.001$) and 75±2% ($P<0.001$) as compared to control at 0.1, 0.5 and 1 mg/mL (n = 3, see Fig. 2D). Cell compartment analysis revealed that the loss in expression of N-cadherin was attributable to loss in expression at the membrane, nucleus and cytoskeleton fractions of the cell (Fig. 2Hii).

The Effects of Ketamine are TGF-β1 Independent

It is well established that TGF-β1 is a principal mediator of fibrotic changes in the kidney. TGF-β1 modulates the expression of several epithelial cell recognition and organizational proteins, whilst contributing to the reciprocal loss of tubular epithelial cells and accumulation of interstitial fibroblasts, changes associated with declining excretory function [20–21]. To determine if Ketamine mediated its effects through downstream TGF-β1, we examined whether Ketamine stimulated TGF-β1 secretion (Fig. 3A) &/or regulate expression of its downstream signalling intermediates Smad2 and Smad3 (Fig. 3B and C) [22]. Cells were cultured in 5 mM glucose containing media for 48 hrs prior to an overnight serum starvation. Cells were stimulated for 24 hrs with Ketamine (0.1–1 mg/mL) under serum-free conditions and ELISA was used to measured total TGF-β1 secretion from growth-arrested HK2 cells. Ketamine significantly decreased total TGF-β1 secretion from basal control conditions (20 pg/ml) by 69±11% at 0.5 and 83±6% at 1 mg/mL as compared to control ($P<0.01$; Fig. 3A). Differences in TGF-β1 were only detected following acidification of the samples, suggesting that TGF-β1 was produced in its latent form (data not shown). Smad activity was assessed via immunoblotting. HK2 cells were cultured in 5 mM glucose containing media for 48 hrs prior to overnight serum starvation. Cells were stimulated for 0–30 minutes with Ketamine (1 mg/mL) and expression levels of p-Smad2 and p-Smad3 examined. P-Smad2 expression levels decreased by 6±3%, 12±17%, 37±7%, and 68±4% ($P<0.01$), at 1, 5, 10 and 30 minutes respectively as compared to control (Fig. 3B, n = 3). P-Smad3 expression levels were also altered in response to Ketamine with levels decreasing 24±6%, 37±7% ($P<0.01$), and 79±5% ($P<0.001$), at 5, 10, and 30 minutes respectively as compared to control (Fig. 3C, n = 3). The decrease in TGF-β1 secretion with a concomitant reduction in the associated signalling intermediaries, i.e. Smad 2 and 3, and the inability of Ketamine to induce reciprocal up-regulation of Snail and N-cadherin to coincide with a loss in E-cadherin, suggest that the cytotoxic effects of Ketamine are independent of TGF-β1.

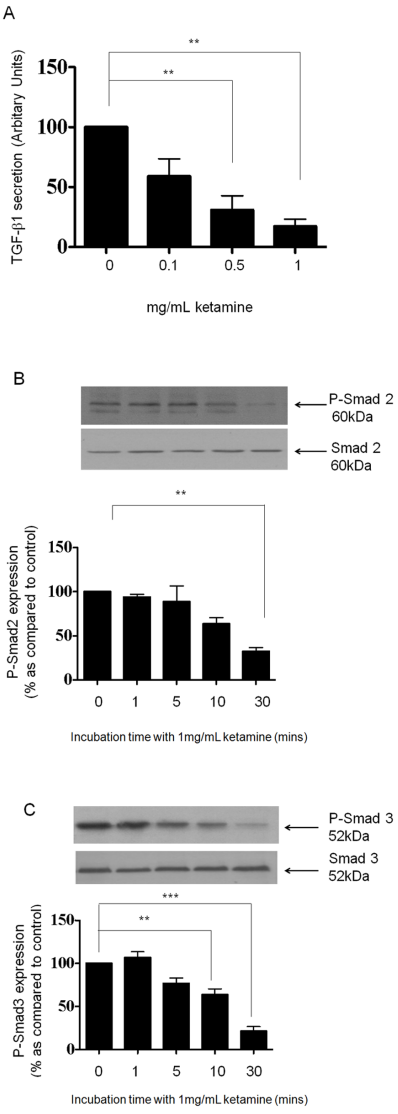

Figure 3. Ketamine inhibits TGF-β1 secretion and down-regulates P-Smad2 and P-Smad3 expression in HK2 cells. HK2 cells were cultured in 5 mM glucose containing media for 48 hrs prior to overnight serum starvation. Cells were stimulated for 24 hrs with Ketamine (0.1–1 mg/mL) under serum-free conditions. The supernatant was removed and TGF-β1 secretion quantified by ELISA and expressed as % TGF-β1 secretion as compared to control (panel A). Results are representative of 3 separate experiments. Key significances are shown

where **$P<0.01$ and ***$P<0.001$. Whole cell expression of p-Smad2 (panel B) and p-Smad3 (panel C) were determined by immuno-blotting. HK2 cells were cultured in 5 mM glucose containing media for 48 hrs prior to overnight serum starvation. Cells were stimulated for 0–30 minutes with Ketamine (1 mg/mL) under serum-free conditions. Upper panels show representative blots for each protein and re-probed for Total Smad as a loading control. Lower panels show mean (±SEM) densitometry data, normalised against the non-stimulated low glucose control (100%), from 3 or more separate experiments. Each lane in the representative blot corresponds to the associated bar in the graph. Key significances are shown, **$P<0.01$, *** $P<0.001$.
doi:10.1371/journal.pone.0071819.g003

Ketamine Stimulates Downstream MAPK Signalling in HK2 Cells

HK2 cells were cultured in 5 mM glucose containing media for 48 hrs prior to overnight serum starvation. Cells were stimulated for 0–30 minutes with Ketamine (1 mg/mL) and expression levels of p-P38 and p-P42/44 assessed by immunoblotting (Fig. 4). P-ERK expression levels increased by 166±11% ($P<0.01$), 222±27% ($P<0.01$) and 259±30% ($P<0.01$), at 1, 5 and 10 minutes respectively as compared to control (Fig. 4A, n = 3). p-P38 expression levels were also altered in response to Ketamine with levels increasing by 63±4% ($P<0.01$), and 98±25% ($P<0.001$), at 10 and 30 minutes respectively as compared to control (Fig. 4B, n = 3).

Signalling Cascades Regulating the Effects of Ketamine on the Adherens Junction Complex

Having confirmed that Ketamine does not depend on TGF-β dependent signalling and that it can evoke activation of MAPK signalling, we examined whether the morphological and phenotypic effects of Ketamine could be arrested or reversed by pharmacological intervention with downstream inhibitors of the MAPK pathway. Cells were cultured in 5 mM glucose containing media for 48 hrs prior to an overnight serum starvation. Cells were stimulated for 24 hrs with the highest, non-lethal concentration of Ketamine (1 mg/mL) in the presence or absence of wortmannin (2 μM), PD98059 (10 μM), and SB203580 (1 μM) under serum-free conditions. Phase contrast morphology confirmed that incubation with wortmannin, PD98059, or SB203580 partly reversed gross Ketamine induced changes in cell morphology (See Fig. 5A). Qualitatively, SB203580 treated cells most closely resembled the cobblestone appearance observed under control conditions, and suggest that p38 MAPK may partially mediate the Ketamine response. Restoration of a normal cellular architecture may reflect the partial reclamation of E-cadherin expression following SB203580 treatment (see Fig. 5C). Contradictory to this, TRITC-conjugated phalloidin, suggested that the pattern of filamentous F-actin staining seen in control cells, was partially restored following treatment with the ERK inhibitor PD98059 and not SB203580 (Fig. 5B).

In order to assess changes in protein expression following inhibition of candidate signaling pathways, cells were cultured in 5 mM glucose for 48 hrs prior to an overnight serum starvation. Cells were then stimulated for 24 hrs with Ketamine in the presence or absence of wortmannin (2 μM), PD98059 (10 μM), and SB203580 (1 μM) under serum-free conditions. Whole cell expression of candidate proteins was assessed. At 24 hrs, Ketamine (1 mg/mL) decreased E-cadherin expression by 48±7% of control (Fig. 5C $P<0.001$). This effect was compounded by co-incubation with the PI3-K inhibitor wortmannin, with expression decreasing a further 36% giving a 74±5% reduction in E-cadherin expression as compared to control. Whilst wortmannin exacerbated the effect of Ketamine, PD98059 failed to significantly alter the Ketamine-evoked loss in E-cadherin. Blocking p38 MAPK improved cadherin expression in response to Ketamine (n = 3; $P<0.01$), increasing expression by 15% to 63±2% of that under control conditions and suggesting a role for p38 MAPK in regulating the effects of Ketamine on E-cadherin mediated cell adhesion (Fig. 5C).

Contrary to the data above, wortmanin completely reversed the inhibitory effects of Ketamine on Snail expression ($P<0.01$) and actually increased expression levels by 11% as compared to that observed under control control conditions (111±14%, n = 3) (Fig. 5F). As a negative regulator of E-cadherin, an increase in Snail in response inhibition of PI3-K could account for the exacerbated reduction of E-cadherin expression observed in Fig. 5C. The transcriptional repressors Snail and Slug are both situated at the core of several signaling pathways proposed to mediate EMT and are central to the regulation of E-cadherin [12–

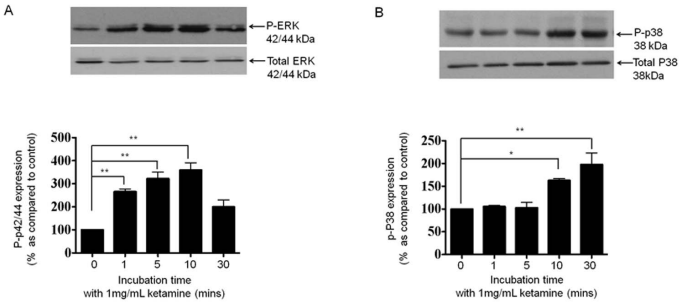

Figure 4. Ketamine stimulates phosphorylation of ERK and p38 MAPK. HK2 cells were cultured in 5 mM glucose containing media for 48 hrs prior to overnight serum starvation. Cells were stimulated with Ketamine (1 mg/mL) for 0–30 minutes under serum free conditions and expression of p-ERK and p-P38 assessed by immunoblotting. Upper panels show representative blots for each protein and re-probed for Total ERK and Total p38 respectively as a loading control. Lower panels show mean (±SEM) densitometry data, normalised against the non-stimulated low glucose control (100%), from 3 or more separate experiments. Each lane in the representative blot corresponds to the associated bar in the graph. Key significances are shown, **$P<0.01$, *** $P<0.001$.
doi:10.1371/journal.pone.0071819.g004

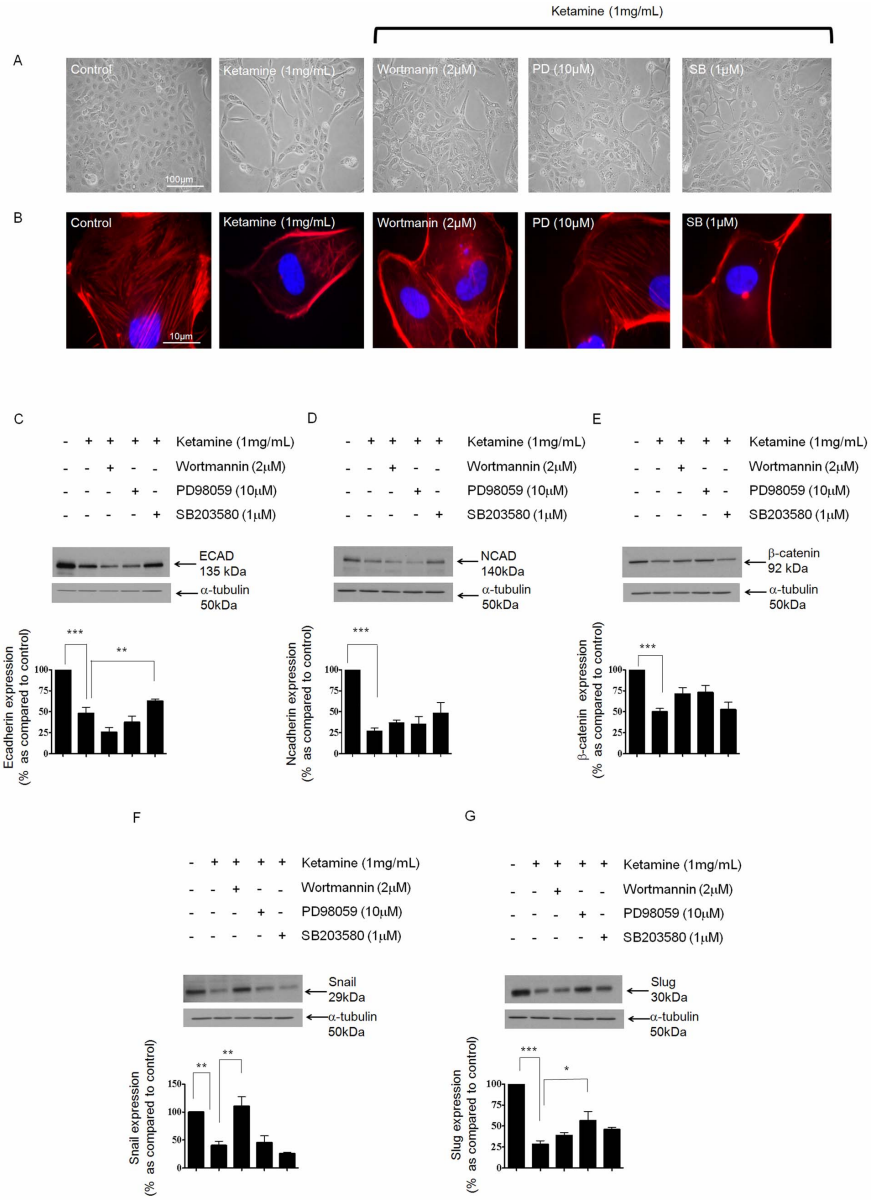

Figure 5. The role of PI3-K, ERK and p38 MAPK in mediating the Ketamine response. HK2 cells were cultured in 5 mM glucose containing media for 48 hrs prior to overnight serum starvation. Cells were stimulated with Ketamine (1 mg/mL) for 24 hrs in the presence or absence of Wortmannin (2 μM), PD98059 (10 μM), and SB203580 (1 μM) under serum-free conditions. Phase contrast microscopy (panel A) and TRITC

conjugated phalloidin (panel B) were used to confirm if blockade of PI3-K, ERK or p38 MAPK was able to negate Ketamine-induced changes in cell morphology and cytoskeletal reorganization. HK2 cells were cultured in 5 mM glucose containing media for 48 hrs prior to overnight serum starvation. Cells were stimulated with Ketamine (1 mg/mL) for 24 hrs in the presence or absence of Wortmannin (2 μM), PD98059 (10 μM), and SB203580 (1 μM) under serum-free conditions and the expression levels of E-cadherin (panel C), N-cadherin (panel D), β-catenin (panel E), Snail (panel F) and Slug (panel G) determined by immuno-blotting. Upper panels show representative blots for each protein and re-probed for α-tubulin as a loading control. Lower panels show mean (±SEM) densitometry data, normalised against the non-stimulated low glucose control (100%), from 3 or more separate experiments. Each lane in the representative blot corresponds to the associated bar in the graph. Key significances are shown, *$P<0.05$, * $P<0.01$, *** $P<0.001$.
doi:10.1371/journal.pone.0071819.g005

13]. As with Snail, Ketamine decreased Slug expression (Fig. 5G) by 72±4% as compared to control ($P<0.001$). Neither wortmannin nor SB203580 were able to significantly attenuate the inhibitory effect of Ketamine, however, inhibition of ERK regained the expression of Slug ($P<0.05$), and suggests potential involvement of ERK in regulating the effects of Ketamine over Slug expression (n = 3). In support of the data in Fig. 2, Ketamine evoked a down-regulation in both N-cadherin and β-catenin with expression levels decreasing by 73±3% and 50±4% respectively as compared to control ($P<0.001$; Fig. 5D and E). None of the inhibitors were able to negate the effects of Ketamine on these two proteins. It should be noted that treatment with inhibitors alone, did not significantly alter the expression of our five candidate proteins (see Figure S1).

Ketamine Reduces Functional Tethering between Cells of the Proximal Tubule

Atomic Force Microscopy (AFM) Single-Cell Force Spectroscopy was used to measure cell-to-cell adhesion and the separation forces and energies required to uncouple cells [23]. Prior to attachment, cells were cultured for 48 hrs under identical conditions +/− Ketamine (0.1–1 mg/mL). A single HK2 cell was bound to a cantilever and subsequently brought into contact with an adherent cell within a cluster, using a fixed force. After 10 sec, the cantilever was retracted (5 μm/sec) and force versus displacement measured until the cells were completely separated. Retraction force-displacement curves provide important information regarding the adhesion between two cells, such as the energy required to separate them (the grey area in Fig. 6A–D) and maximum force of detachment (the red circles in Fig. 6A–D). The energy required to separate two cells is normally referred to as "detachment energy" (Fig. 6E) whilst the maximum force of detachment for complete separation the "maximum unbinding force" (Fig. 6F). The retraction measurements of control versus Ketamine (0.1–1 mg/mL)-treated cells are shown in panels E & F. In each case, data is recorded from multiple cells (>10) in 4 separate experiments at each concentration. Compared to control (0 mg/mL), Ketamine evokes a concentration-dependent decrease in the maximum unbinding force by 33±6%, 41±3%, and 58±6% at 0.1 mg/mL, 0.5 mg/mL and 1 mg/mL respectively ($P<0.001$), whilst the detachment energy decreased by 32±8%, 63±7%, and 86±11% of control at 0.1 mg/mL, 0.5 mg/mL and 1 mg/mL respectively ($P<0.001$).

Discussion

In the UK, Ketamine is fast becoming the "party drug" of choice amongst 16–24 year olds. The Independent Scientific Committee on Drugs (ISCD) found that 68% of UK clubbers had taken the drug in 2009, whilst the British Crime Survey reported an increase in users from 85,000 in 2006/07 to 113,000 in 2008/09 [2]. Although effective as a mild hallucinogen at 60 mg to 100 mg, some users are reportedly taking 5 g to 10 g a day. Stimulated by public concern about the popularity and potential harms of Ketamine, our study coincides with a recent BBC report in which the UK Home Secretary Theresa May, asked the Advisory Council on the Misuse of Drugs (ACMD) to update their advice on the abuse of ketamine. As the number of users increases, serious side effects are beginning to emerge. These effects, including bladder shrinkage, fibrosis, incontinence and bleeding, can ultimately lead to complete destruction and subsequent removal of the bladder [4]. Whilst the effects of Ketamine on the bladder are established, recent evidence suggests that damage to other tissues is also on the increase, and patients regularly present with both bladder and renal complications [24]. The escalating problem highlights an urgent need to improve our understanding of how Ketamine mediates its effects on the entire urological system.

In epithelia cells of the proximal tubule, disease-induced fibrosis commonly presents with cell atrophy, increased matrix deposition and tubulointerstitial scarring, all of which culminate in a loss of renal function [25–27]. The reciprocal loss of tubular epithelial cells and accumulation of interstitial fibroblasts promotes chronic fibrosis. Characteristic changes include morphological and phenotypic alterations with cytoskeletal reorganization and the down-regulation of epithelial cell adhesion molecules, such as E-cadherin. The integrity of the adherens junction is vital to maintain basic epithelial function and the loss of E-cadherin mediated cell-adhesion represents a pivotal step in early phenotypic and morphological changes observed in tubular injury [25] [28].

Changes in adherens junction proteins are central to early morphological and phenotypic alterations that precede overt signs of tissue damage. The aim of the current study was to understand of how Ketamine altered cell adhesion and cell-coupling in epithelial cells of the proximal tubule. Assessing cell morphology confirmed that Ketamine produced a concentration-dependent change in cellular architecture towards an elongated fibrotic phenotype at 24 and 48 hrs. The reduction in both MTT uptake and crystal violet staining was consistent with reduced cell viability and concomitant to an increase of lactate dehydrogenase release, confirming cytotoxicity. We confirmed that Ketamine reduced membrane expression of E-cadherin and showed for the first time that the drug decreases functional tethering between cells of the proximal tubule, a potentially catastrophic event in cells whose primary function depends on formation of a tight epithelial sheet. Whilst our previous studies in the proximal tubule suggest that a pro-fibrotic loss of E-cadherin is paralleled by an up-regulation of transcriptional repressors Snail and Slug, the effects of Ketamine appear toxic and are not mediated via classic signalling pathways [17–18].

The actin cytoskeleton stabilizes both tight junctions and adherent junctions and alterations in actin dynamics disrupt E-cadherin-mediated adhesion [29–30]. TRITC-conjugated phalloidin revealed that Ketamine redistributed F-actin in to stress fibres at the cell periphery. This data was supported by a significant reduction in expression of E-cadherin at the cell membrane, a response that, unlike classic renal fibrosis, was not paralleled by up-regulation in expression of transcription factors Snail and Slug. Furthermore, the cadherin-switch associated with

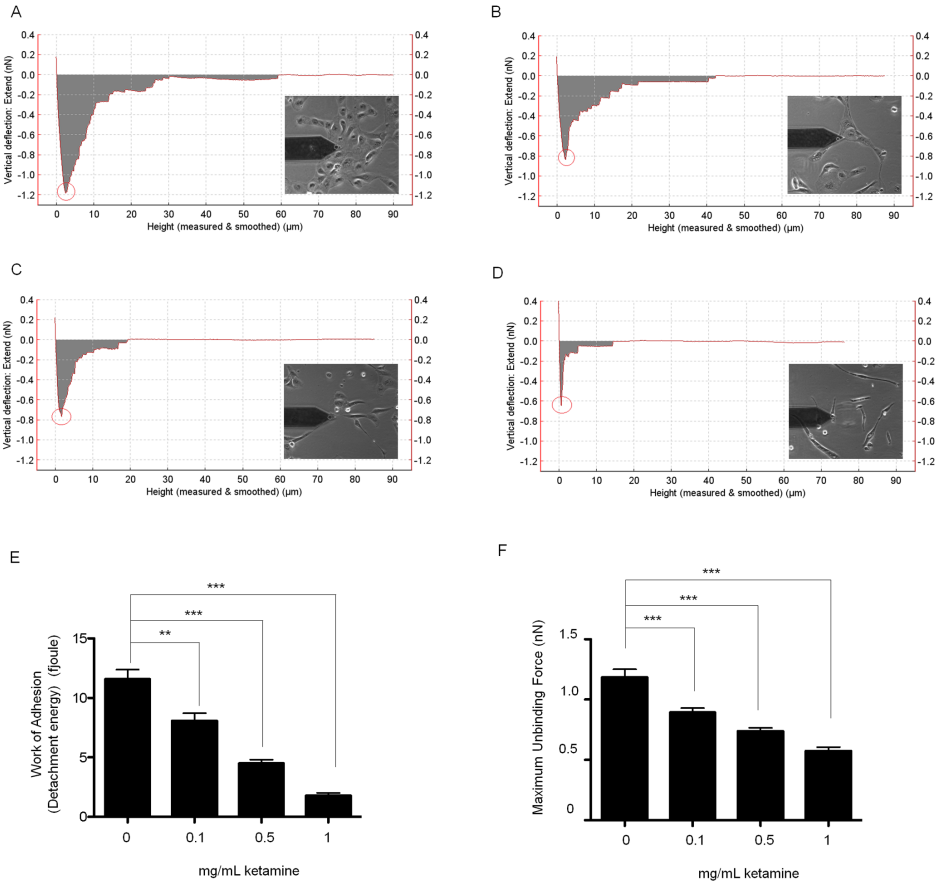

Figure 6. ***Ketamine reduces cell adhesion.*** AFM-single-cell force spectroscopy was used to measure the detachment energy (fJoules) and maximum unbinding force (nN) required to uncouple two HK2 cells. The energy required to separate the cells; grey area in panel A (control cells), panel B (0.1 mg/mL Ketamine treated cells), panel C (0.5 mg/mL Ketamine treated cells), and panel D (1 mg/mL Ketamine treated cells), and maximum force of detachment (red circle) was measured. The former is known as the "detachment energy" (panel E) and the later is "maximum unbinding force" (panel F). Ketamine decreased the maximum unbinding force and the work of adhesion in a dose dependent manner compared to control. Data is expressed as mean ± SEM. of multiple cells from 4 separate experiments, where key significances are shown, **** $P<0.0001$.
doi:10.1371/journal.pone.0071819.g006

EMT [18–19] and favouring the up-regulation of neural (N)-cadherin to replace the loss in E-cadherin, did not occur. These data suggest that the effects of Ketamine are cytotoxic, and not mediated through classic, canonical pathways usually associated with renal fibrosis.

TGF- β1 is a pro-fibrotic cytokine known to play an important role in the pathogenesis of disease-induced renal fibrosis, e.g. diabetic nephropathy [27]. Having previously shown that TGF-β1 instigates a loss in E-cadherin expression in HK2-cells, we investigated if Ketamine directly altered TGF- β1 secretion [18]. Ketamine (1 mg/mL) reduced TGF- β1 secretion to 80% of control. In renal fibrosis, TGF- β1 binds to a trans-membrane TBRII receptor and initiates several intracellular signalling cascades, including the small mothers against decapentaplegic (SMADs) and mitogen activated protein kinases (MAPK), such as extracellular regulated kinase (ERK), p38 and Jun Kinase [22]. The majority of TGF- β1 targeted genes regulated in fibrosis rely on Smad3-dependent transcriptional regulation (Brown *et al.* 2007). In the current study, Ketamine not only decreased TGF-β1 secretion but also down-regulated p-Smad2 and p-Smad3 expression at 24 hours. The failure of Ketamine to stimulate canonical TGF- β1 signalling suggests that an alternative

mechanism must mediate Ketamine-evoked effects. Co-incubation of Ketamine with inhibitors of PI3-K, p38 MAPK and ERK confirmed a partial role for all three in regulating our candidate proteins. There was a counter-intuitive relationship observed between E-cadherin and Snail in response to Ketamine treatment in the presence of the PI3-K inhibitor wortmannin. Blockade of PI3-K signalling further reduced the expression of E-cadherin, an effect most likely to reflect the dramatic up-regulation Snail under the same conditions. This suggests that Ketamine down-regulates Snail expression in a PI3-K dependent manner and that blockade of this pathway restores the reciprocal relationship between E-cadherin and its transcriptional repressor. Inhibition of p38MAPK partially restored E-cadherin expression to those of control, an effect that may, in part, be responsible for the restoration of cell morphology observed with SB203580. Co-incubation of Ketamine with wortmannin failed to negate the inhibitory effects of Ketamine on Slug, whilst the ERK inhibitor, PD98059, restored expression to approximately 50% of control, indicating a downstream involvement ERK in regulating Slug. Whilst it was evident that PI3-K and ERK have a role in regulating E-cadherin, Snail and Slug, elucidating the pathway controlling N-cadherin and β-catenin expression was not clear. Ketamine reduced the expression of both these proteins and the effect could not be restored by pharmacological inhibition.

To determine how a loss in adherens junction proteins functionally affected cell-cell adhesion, we used AFM-SCFS. The AFM-single-cell force spectroscopy used in this study has a displacement actuator of longer travelling distance (up to 100 μm) which provides an excellent capability for measuring the complete force-displacement curve of cell detachment and is essential when studying large cells such as those as found in renal tubule epithelia. Retraction force-displacement curves allow us to determine the force and energy required to uncouple cells. The former is normally referred to as "adhesion force" and the latter the "detachment energy", which can be calculated from the integration of the separation force-displacement curves, i.e. the grey area under the curve in Fig. 6A–D. Retraction force-displacement curves confirmed that 1 mg/mL Ketamine reduced the maximum unbinding force required to begin separation of two cells by 58%, whilst reducing the detachment energy required to completely separate them by 86%. The greater decrease in the detachment energy could be partly explained due to the increase in cell rigidity following Ketamine treatment, as demonstrated by re-arrangement of the cytoskeleton into peripheral stress fibres. These data suggest that it is the loss in E-cadherin expression and dissolution of the catenin/cadherin complex, which drives the detachment of cells in response to Ketamine.

In the current study, we report on Ketamine-evoked cytotoxic damage to epithelial cells of the proximal tubule. The acute effects of Ketamine are associated with early functional changes in the adherens junction complex. This loss in expression of proteins central to cell-adhesion, promotes functional disassociation of the epithelia, and is the most likely cause of early morphological and phenotypic alterations observed following Ketamine exposure. The reported changes may represent the initial basis for overt renal complications of Ketamine abuse. Whilst our studies provide novel and exciting data on the effects of this recreational drug in the proximal tubule, it is clear that this area of research demands fuller investigation. To reduce the confounding influence of the multifactorial molecular pathology that is likely to underlie Ketamine-induced renal damage within epithelia cells of the proximal tubule, we utilized the well-characterized human HK2 cell line as a minimalistic model. Despite HK2 cells having many advantages to primary tissue, the authors concede that responses are open to modification by the complexities of the *in vivo* situation. Despite this caveat, the current data provides a compelling foundation, identifying likely targets associated with early Ketamine damage, and as such, identifies future candidates for maintaining or restoring renal function in response to and from this toxic substance particularly given the catastrophic tissue damage reported for the bladder. Future work will need to extrapolate these data in to the primary scenario.

Supporting Information

Figure S1 The effect of Inhibitors alone on candidate protein expression in HK2 cells. HK2 cells were cultured in 5 mM glucose containing media for 48 hrs prior to overnight serum starvation. Cells were treated for 24 hrs with Wortmannin (2 μM), PD98059 (10 μM), and SB203580 (1 μM) under serum-free conditions and the expression levels of E-cadherin (panel A), N-cadherin (panel B), β-catenin (panel C), Snail (panel D) and Slug (panel E) determined by immuno-blotting. Upper panels show representative blots for each protein and re-probed for α-tubulin as a loading control. Lower panels show mean (±SEM) densitometry data, normalised against the non-stimulated low glucose control (100%), from 3 or more separate experiments. Each lane in the representative blot corresponds to the associated bar in the graph.
(TIFF)

Author Contributions

Conceived and designed the experiments: CEH PES. Performed the experiments: CEH TJ ES PES. Analyzed the data: CEH TJ PES. Contributed reagents/materials/analysis tools: CEH PES. Wrote the paper: CEH PES. Reviewed and edited the manuscript: IKKL KPJ.

References

1. Wright M (1982) Pharmacologic effects of ketamine and its use in veterinary medicine. J Am Vet Med Assoc. 180: 1462–71.
2. Wood D, Cottrell A, Baker SC, Southgate J, Harris M, et al. (2011) Recreational ketamine: from pleasure to pain. BJU Int. 107: 1881.
3. Morgan CJ, Muetzelfeldt L, Curran HV (2010) Consequences of chronic ketamine self-administration upon neurocognitive function and psychological wellbeing: a 1-year longitudinal study. Addiction. 105: 121–33.
4. Tsai TH, Cha TL, Lin CM, Tsao CW, Tang SH, et al. (2009) Ketamine-associated bladder dysfunction. Int J Urol. 16, 826–9.
5. Srirangam S, Mercer J (2012) Ketamine bladder syndrome: an important differential diagnosis when assessing a patient with persistent lower urinary tract symptoms. BMJ Case Rep. doi:pii: bcr2012006447. 10.1136/bcr-2012-006447.
6. Chu PS, Ma WK, Wong SC, Chu RW, Cheng CH, et al. (2008) The destruction of the lower urinary tract by ketamine abuse: a new syndrome? BJU Int 102: 1616–22.
7. Klingberg F, Hinz B, White ES (2013) The myofibroblast matrix: implications for tissue repair and fibrosis. J Pathol. 229: 298–309.
8. Guo S, DiPietro LA (2010) Factors Affecting Wound Healing. J Dent Res 89: 219–229.
9. Zeisberg M, Kalluri R (2004) The role of epithelial-to-mesenchymal transition in renal fibrosis. J Mol Med. 82: 175–181.
10. Moreno AP, Berthoud VM, Pérez-Palacios G, Pérez-Armendariz EM (2005) Biophysical evidence that connexin-36 forms functional gap junction channels between pancreatic mouse beta-cells. Am J Physiol Endocrinol Metab 288: E948–56.
11. Kanno Y, Sasaki Y, Shiba Y, Yoshida-Noro C, Takeichi M (1984) Monoclonal antibody ECCD-1 inhibits intercellular communication in teratocarcinoma PCC3 cells. Exp Cell Res. 152: 270–4.
12. Hills CE, Squires PE (2010) TGF-beta1-induced epithelial-to-mesenchymal transition and therapeutic intervention in diabetic nephropathy. Am J Nephrol 31: 68–74.

13. Hills CE, Squires PE (2011) The role of TGF-β and epithelial-to mesenchymal transition in diabetic nephropathy. Cytokine Growth Factor Rev. 22: 131–9.
14. Hills CE, Bland R, Wheelans DC, Bennett J, Ronco PM, et al. (2006) Glucose-evoked alterations in connexin43-mediated cell-to-cell communication in human collecting duct: a possible role in diabetic nephropathy. Am J Physiol Renal Physiol 291: F1045–51.
15. Hills CE, Bland R, Bennett J, Ronco PM, Squires PE (2009) TGF-beta1 mediates glucose-evoked up-regulation of connexin-43 cell-to-cell communication in HCD-cells. Cell Physiol Biochem 24: 177–86.
16. Hills CE, Al-Rasheed N, Al-Rasheed N, Willars GB, Brunskill NJ (2009) C-peptide reverses TGF-beta-1 induced changes in renal proximal tubular cells: implications for treatment of DN. Am J Physiol 296: F614–621.
17. Hills CE, Willars GB, Brunskill NJ (2010) Proinsulin C-peptide antagonizes the profibrotic effects of TGF-beta1 via up-regulation of retinoic acid and HGF-related signaling pathways. Mol Endocrinol 24: 822–31.
18. Hills CE, Siamantouras E, Smith SW, Cockwell P, Liu KK, et al. (2012) TGFβ modulates cell-to-cell communication in early epithelial-to-mesenchymal transition. Diabetologia. 55: 812–24.
19. Maeda M, Johnson K, Wheelock MJ (2005) Cadherin switching: essential for behavioural but not morphological changes during an epithelium-to-mesenchyme transition. Journal of cell Science 118: 873–887.
20. Eddy AA (1996) Molecular insights into renal interstitial fibrosis. J Am Soc Nephrol 12: 2495–2508.
21. Remuzzi G, Ruggenenti P, Benigni A (1997) Understanding the nature of renal disease progression. Kidney Int. 51: 2–15.
22. Brown KA, Pietenpol JA, Moses HL (2007) A tale of two proteins: differential roles and regulation of Smad2 and Smad3 in TGF-beta signaling. J Cell Biochem 101 9–33.
23. Hills CE, Younis MY, Bennett J, Siamantouras E, Liu K, et al. (2012) Calcium-sensing receptor activation increases cell-cell adhesion and β-cell function. Cell Physiol Biochem. 30: 575–86.
24. Selby NM (2008) Obstructive nephropathy and kidney injury associated with ketamine abuse. Clinical kidney journal. 5: 310–312.
25. Farris AB, Colvin RB (2012) Renal interstitial fibrosis: mechanisms and evaluation. Curr Opin Nephrol Hypertens 21: 289–300.
26. Kalluri R, Weinberg RA (2009) The basics of epithelial-mesenchymal transition. J Clin Invest. 119: 1420–1428.
27. Sharma K, Ziyadeh FN (1995) Hyperglycaemia and diabetic kidney disease. The case for transforming growth factor-beta as a key mediator. Diabetes 44: 1139–1146.
28. Masszi A, Fan L, Rosivall L, McCulloch CA, Rotstein OD, et al. (2004) Integrity of cell-cell contacts is a critical regulator of TGF-beta 1-induced epithelial-to-myofibroblast transition: role for beta-catenin. Am J Patho. 165: 1955–1967.
29. Angres B, Barth A, Nelson WJ (1996) Mechanism for transition from initial to stable cell-cell adhesion: kinetic analysis of E-cadherin-mediated adhesion using a quantitative adhesion assay. J Cell Biol 134: 549–57.
30. Ivanov AI (2008) Actin motors that drive formation and disassembly of epithelial apical junctions. Front Biosci. 13: 6662–81.

Culture of human aortic adventitial fibroblast (HAoAF)

Cryopreserved human aortic adventitial fibroblasts (HAoAF) were commercially obtained from PromoCell GmbH at passage 2 and subsequently defrosted and cultured in a T25 (25 cm^2) flask. Cells were cultured in phenol red-free Dulbecco's modified Eagles medium (DMEM, Sigma-Aldrich UK) containing 1000 mg L^{-1} glucose and supplemented with 10% fetal calf serum (FCS), L-glutamine (5 mM), penicillin (100 U ml^{-1}) and streptomycin (100 ug ml^{-1}). Cells were maintained in an atmosphere of air at 37 ℃ and 5% CO_2. Experiments were conducted with cells from passages 7-9. Once cells had reached confluence in the T25 flask, they were detached using trypsin/EDTA (0.1% trypsin and 0.02% EDTA) in sterile phosphate-buffered saline (PBS). The detachment of cells was checked using an inverted light microscope (Nikon, TMS). The trypsin/EDTA was inactivated using phenol red-free DMEM supplemented with 10% FCS (37 ℃). The cells were then resuspended and transferred to T75 (culture area 75 cm^2) flasks. Once confluence was reached, cells were further subcultured into T75 flasks or in 6-, 24- or 96-well plates for experiments. The media was replaced every 2 days until an 80%-95% confluent monolayer was observed.

Culture of HK2 cells

HK2 cells were purchased from the American Type Culture Collection (ATCC; Gaithersburg, MD 20878 USA). The cells at passages 18-30 were maintained in DMEM/Hams F12 (DMEM/F12, Sigma-Aldrich UK) medium, supplemented with 10% fetal calf serum (FCS), L-glutamine (2 mM), and epidermal growth factor (5 ng ml^{-1}). During culturing, the seeding and medium change procedure is same as the culture of HAoAF. Cells were then seeded onto 40 mm Petri dishes and cultured at 37 ℃ in a humidified atmosphere of 5% CO_2 in air for further experiments.

Cell counting

To seed the number of HAoAF for experiments (see Table A.1), cell density was determined using a Neubauer modified counting chamber (Figure A.1a). Confluent fibroblasts at passage 7-9 were trypsinised and resuspended in DMEM supplemented with 10% FCS. For counting, a random 20 µl of cell suspension was transferred onto two haemocytometer chambers (10 µl for each chamber). The total number of cells overlying on four 1 mm^2 areas of the haemocytometer (blue framed area in Figure A.1b) were counted using an inverted light microscope (4× objective magnification). The counting procedure are illustrated at Figure A.1c and A.1d. Get the number of cells in both chambers and record as N_a and N_b. The final concentration C of cells in original solution can be calculated as below equation:

$$C = \frac{(N_a + N_b)/2}{4} \times 10^4 \text{ (cells ml}^{-1}\text{)}$$

Table A.1: Number of HAoAF seeded for different multiple well plates.

Culture plate type	Seeding area (cm^2 $well^{-1}$)	Number of cells (ml^{-1} $well^{-1}$)
6-well plate	9.5	20×10^4
24-well plate	1.9	4×10^4
96-well plate	0.32	0.8×10^4

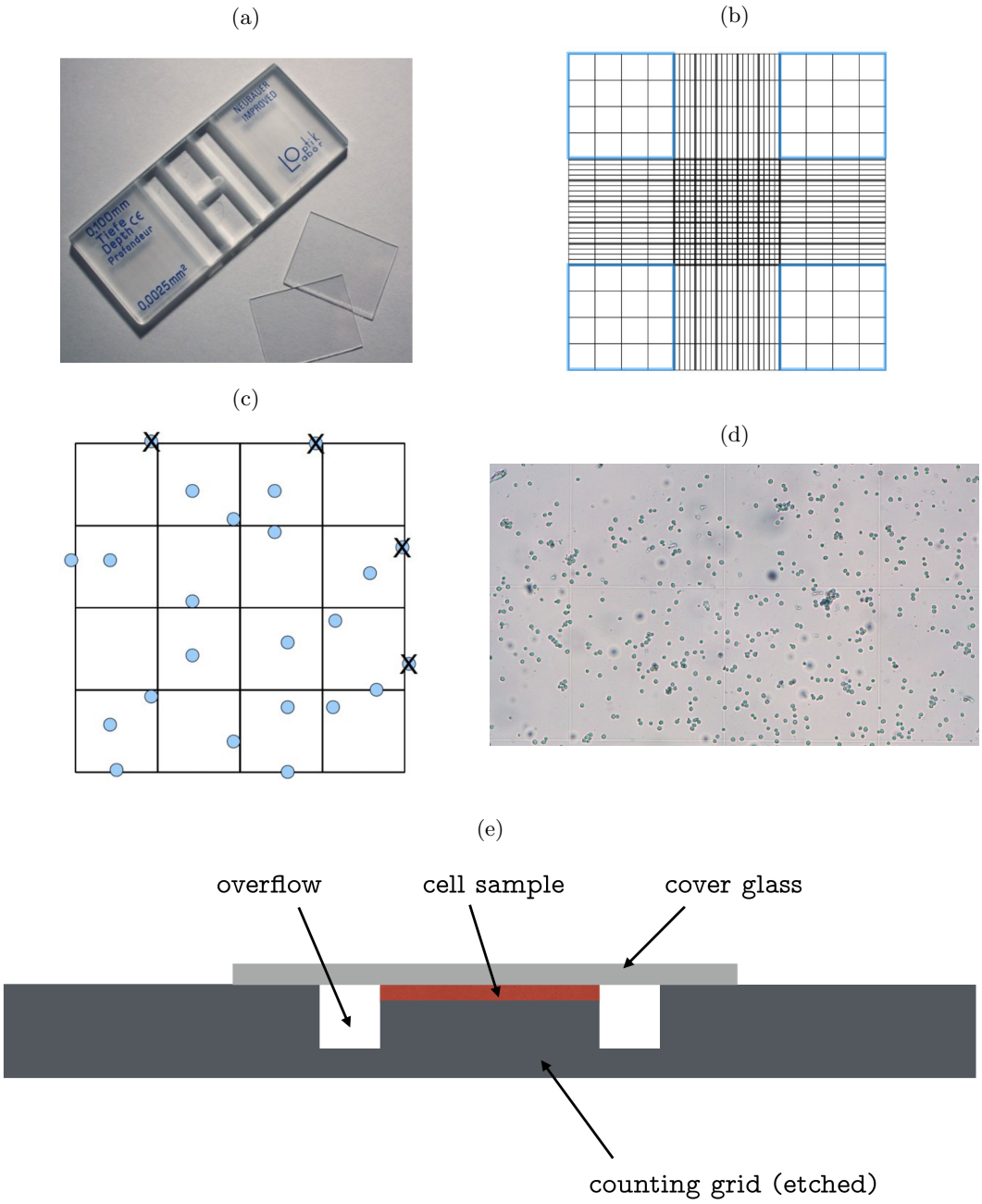

Figure A.1: Cell counting by using a haemocytometer (a) Exterior of Neubauer improved counting chamber. (b) Grid layout of the Neubauer improved hemocytometer. Blue line enclosed areas are mainly used for cell counting. (c) Magnification of one blue circled area in (b) with cells on. As cells have the same probability of dropping onto the edge of the counting area, cells on the top and right lines are not taken into calculation. (d) Real cells on the counting area. Grid is visible under microscope. (e) Side view of hemocytometer. Cell samples are placed on the red area.

Table A.2: Specification of force transducer 400A-407A series, Aurora Scientific Inc.

Specifications	**Model**					
	400A	**403A**	**404A**	**405A**	**406A**	**407A**
Full scale [± mN]	50	5	100	10	0.5	1000
Sensitivity [mN volt^{-1}]	5	0.5	10	1	0.05	100
Resolution [µN]	1	0.1	2	0.2	0.01	20
Step response time [ms]	0.3	1.0	0.3	1.0	5.0	0.1
Resonant frequency [Hz]	2000	600	2000	600	100	4000
Compliance [micron mN^{-1}]	0.1	1.0	0.1	1.0	10.0	0.01
Zero drift [µN degC^{-1}]	5	0.5	10	1	0.05	100
Gain drift [% degC^{-1}]	0.01	0.01	0.01	0.01	0.01	0.01
Hysteresis [%]	0.01	0.01	0.01	0.01	0.01	0.01
Maximum overload force [mN]	250	100	250	100	20	2500
Output tube length (L) [mm]	7.0	7.0	7.0	7.0	7.0	7.0
Output tube diameter (D) [mm]	1.0	1.0	1.0	1.0	1.0	1.0

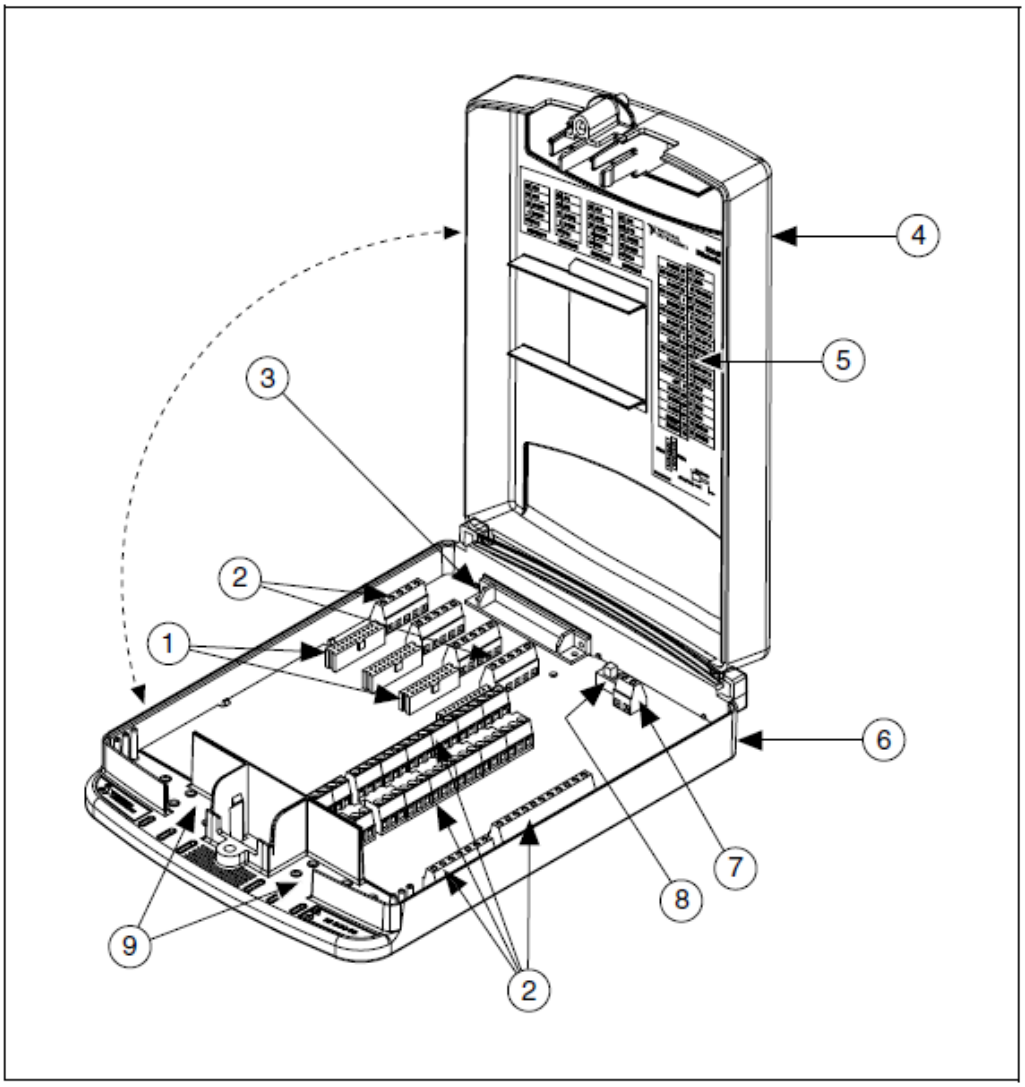

1	SCC Slots	6	Enclosure Base
2	Screw Terminals	7	External Power Screw Terminal
3	68-Pin I/O Connector	8	External Power Switch
4	Enclosure Cover	9	Strain Relief Wire Entry
5	Quick Reference Guide		

Figure A.2: SCC-68 parts locator diagram. The cable, in the project, is connected from NO.9 to the terminal NO.2 in the diagram.

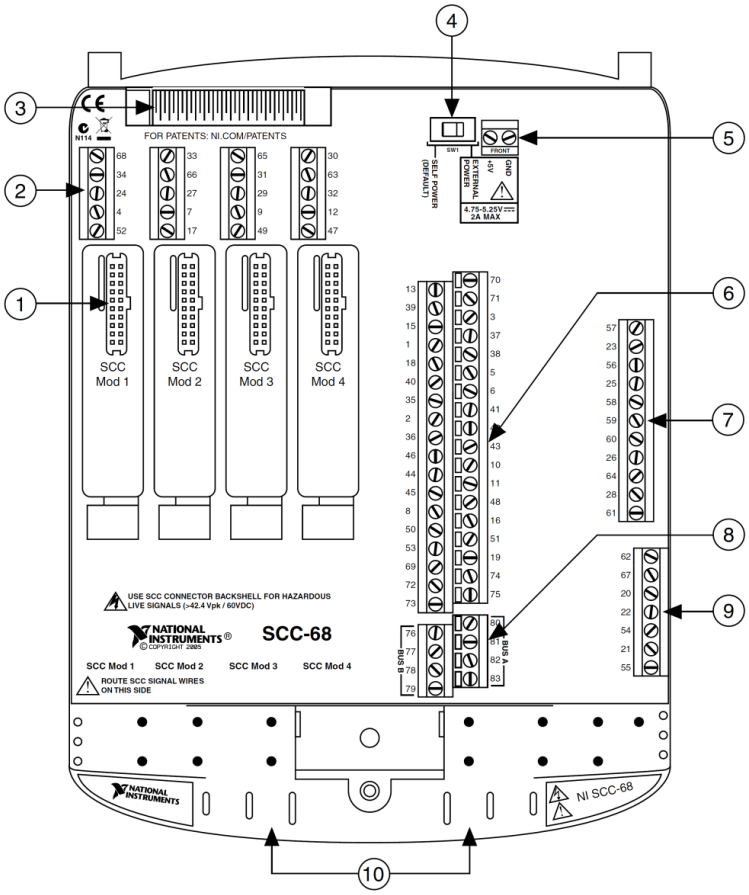

1	SCC Slots	6	DIO Screw Terminals
2	SCC Screw Terminals	7	AI Screw Terminals
3	68-Pin I/O Connector	8	Bus Screw Terminals
4	External Power Switch	9	AO Screw Terminals
5	External Power Screw Terminals	10	Strain-Relief Wire Entry

Figure A.3: SCC-68 parts locator diagram (top view).

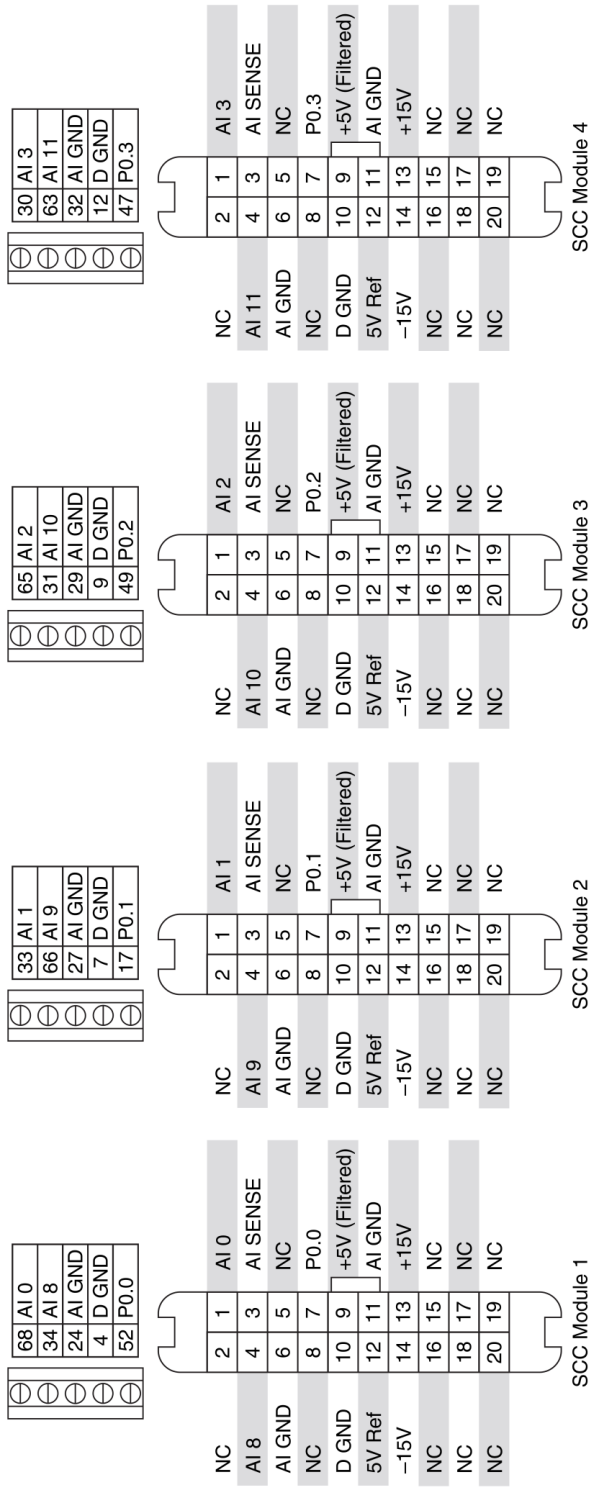

Figure A.4: SCC-68 quick reference label. No.68 and No.24 are employed in the project.

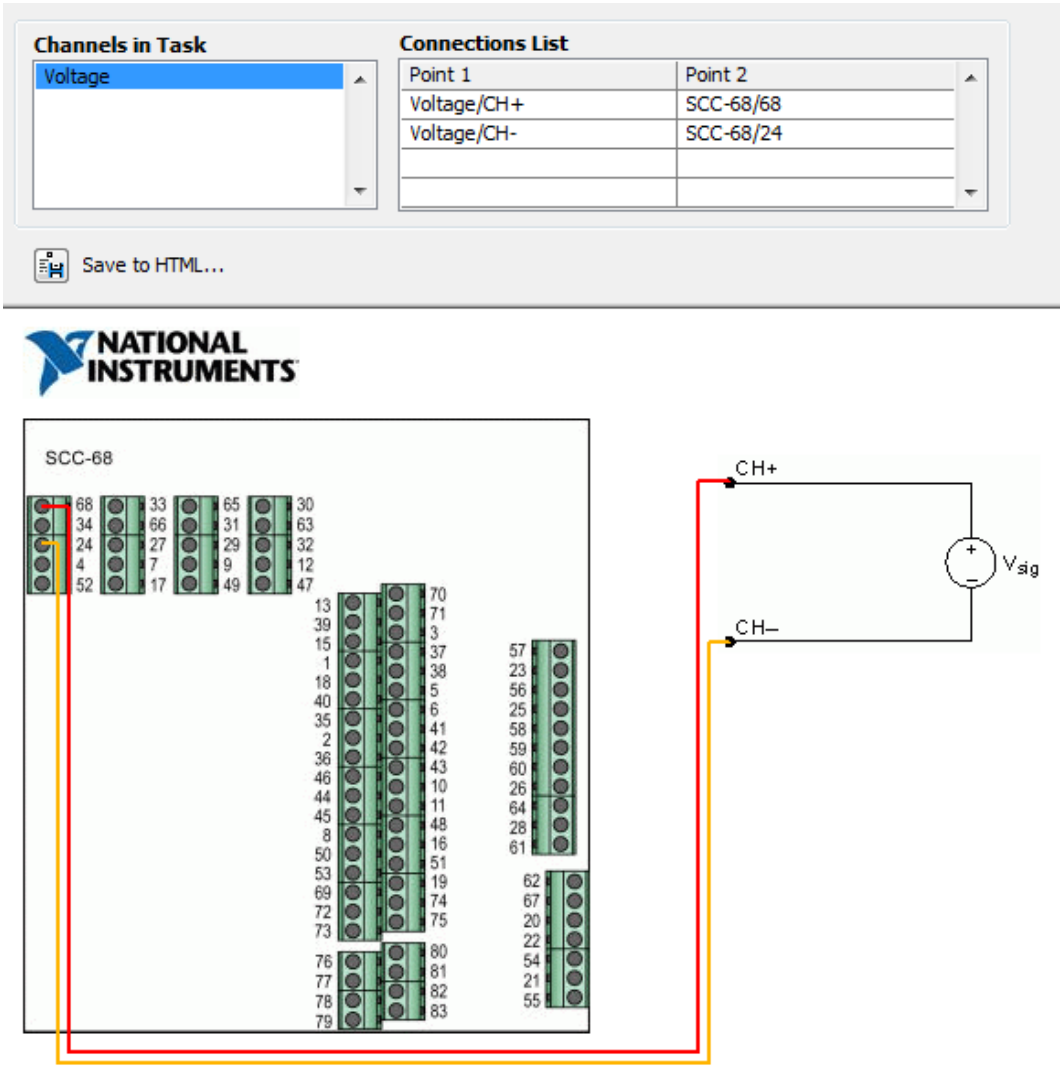

Figure A.5: DAQ assistant setting corresponding to RSS-68 terminal block.

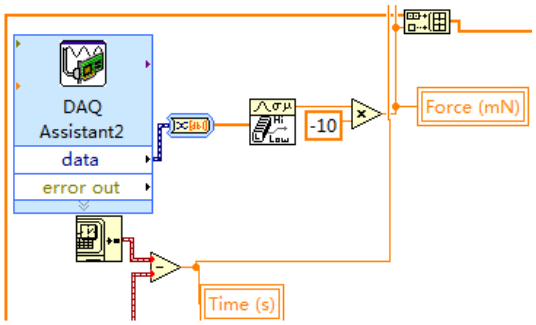

Figure A.6: DAQ setting in Labview programme.

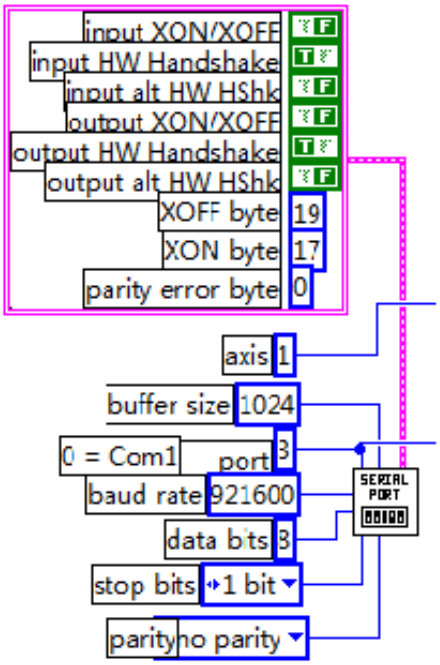

Figure A.7: USB setting in Labview programme.

Table A.3: Calibration of z-axis stage displacements. Machine provides the incremental precise at 0.001, 0.01 and 0.1 mm. Residuals are calculated by machine date minus real displacement.

Machine data (mm)	**Real displacement (mm)**	**Residuals (mm)**
0.000	0.000000	0.000000
0.001	0.000996	0.000004
0.002	0.001986	0.000014
0.003	0.002945	0.000055
0.004	0.003959	0.000041
0.005	0.004917	0.000083
0.006	0.005917	0.000083
0.007	0.006945	0.000055
0.008	0.007858	0.000142
0.009	0.008865	0.000135
0.010	0.009846	0.000154
0.020	0.019836	0.000164
0.030	0.029722	0.000278
0.040	0.039801	0.000199
0.050	0.049601	0.000399
0.060	0.059683	0.000317
0.070	0.069503	0.000497
0.080	0.079620	0.000380
0.090	0.089413	0.000587
0.100	0.099536	0.000464
0.200	0.199483	0.000517
0.300	0.299411	0.000589
0.400	0.399382	0.000618
0.500	0.499416	0.000584
0.600	0.599392	0.000608
0.700	0.699388	0.000612
0.800	0.799416	0.000584
0.900	0.899487	0.000513
1.000	0.999588	0.000412

Table A.4: Weight of paper strips and output voltage from force transducer.

Expected	Mass (mg)		**Average loading**	Actual output (V)		**Average**
mass(mg)	#1	#2	**force (μN)**	#1	#2	**output (V)**
0.0	0.0	0.0	0.00	0.000	0.000	0.0000
1.0	1.1	1.1	10.78	0.226	0.225	0.2255
2.0	2.1	2.1	20.58	0.428	0.422	0.4250
3.0	3.2	3.1	30.87	0.627	0.611	0.6190
4.0	3.9	3.8	37.73	0.735	0.751	0.7430
5.0	4.9	4.8	47.53	0.924	0.916	0.9200
6.0	5.8	5.7	56.35	1.184	1.166	1.1750
7.0	6.8	6.8	66.64	1.375	1.423	1.3990
8.0	7.8	7.9	76.93	1.621	1.606	1.6135
9.0	9.0	9.0	88.20	1.832	1.792	1.8120
10.0	9.9	9.8	96.53	2.081	2.053	2.0670
11.0	11.1	11.3	109.76	2.321	2.326	2.3235
20.0	19.2	19.3	188.65	4.232	4.306	4.2690
30.0	29.7	29.8	291.55	7.168	7.141	7.1545
40.0	38.2	38.0	373.38	9.683	9.664	9.6735

Table A.5: Hysteresis calibration of z-axis stage. Machine generate two types of increment steps, 0.0002 and 0.002 mm. Corresponding real displacement readings are recorded.

Machine output	**Real reading**	**Machine output**	**Real reading**
0.0000	0.000005	0.0000	0.000050
0.0002	0.000190	0.0020	0.001990
0.0004	0.000415	0.0040	0.003987
0.0006	0.000596	0.0060	0.005939
0.0008	0.000801	0.0080	0.007967
0.0010	0.000963	0.0100	0.009902
0.0010	0.001010	0.0100	0.009980
0.0008	0.000856	0.0080	0.008036
0.0006	0.000661	0.0060	0.006028
0.0004	0.000460	0.0040	0.003962
0.0002	0.000275	0.0020	0.002033
0.0000	0.000080	0.0000	0.000040

Table A.6: Repeatability calibration data of z-axis stage. Machine generates five different increment steps, 0.0002, 0.0004, 0.0006, 0.0008 and 0.001 mm five times. Corresponding real displacement readings are recorded.

0.0002	**0.0004**	**0.0006**	**0.0008**	**0.0010**
0.000217	0.000410	0.000592	0.000805	0.000983
0.000206	0.000411	0.000580	0.000820	0.000981
0.000212	0.000399	0.000583	0.000820	0.001023
0.000219	0.000407	0.000588	0.000794	0.001006
0.000202	0.000405	0.000587	0.000792	0.001002

Bibliography

[1] Ahearne, M. Introduction to cell-hydrogel mechanosensing. *Interface Focus 4*, 2 (2014), 20130038.

[2] Ahearne, M., Wilson, S. L., Liu, K. K., Rauz, S., El Haj, A. J., and Yang, Y. Influence of cell and collagen concentration on the cell-matrix mechanical relationship in a corneal stroma wound healing model. *Experimental Eye Research 91*, 5 (nov 2010), 584–591.

[3] Ahearne, M., Yang, Y., Then, K. Y., and Liu, K. K. An indentation technique to characterize the mechanical and viscoelastic properties of human and porcine corneas. *Annals of Biomedical Engineering 35*, 9 (2007), 1608–1616.

[4] Alonso, J. L., and Goldmann, W. H. Feeling the forces: Atomic force microscopy in cell biology. *Life Sciences 72*, 23 (2003), 2553–2560.

[5] Baron, M., Norman, D., Willis, A., and Campbell, I. D. Structure of the fibronectin type 1 module. *Nature 345*, 6276 (1990), 642–646.

[6] Bell, E., Ivarsson, B., and Merrill, C. Production of a tissue-like structure by contraction of collagen lattices by human fibroblasts of different proliferative potential in vitro. *Proceedings of the National Academy of Sciences of the United States of America 76*, 3 (1979), 1274–1278.

[7] Bella, J., Eaton, M., Brodsky, B., and Berman, H. M. Crystal and molecular structure of a collagen-like peptide at 1.9 A resolution. *Science 266*, 5182 (oct 1994), 75–81.

[8] Beningo, K. A., Dembo, M., Kaverina, I., Small, J. V., and Wang, Y. L. Nascent focal adhesions are responsible for the generation of strong propulsive forces in migrating fibroblasts. *Journal of Cell Biology 153*, 4 (2001), 881–887.

[9] Bers, D. M. Calcium fluxes involved in control of cardiac myocyte contraction. *Circulation Research 87*, 4 (2000), 275–281.

[10] Bershadsky, A. D., Balaban, N. Q., and Geiger, B. Adhesion-dependent cell mechanosensitivity. *Annual Review of Cell and Developmental Biology 19* (jan 2003), 677–695.

[11] Binnig, G., and Quate, C. F. Atomic Force Microscope. *Physical Review Letters 56*, 9 (1986), 930–933.

[12] Bittner, K., Liszio, C., Blumberg, P., Schönherr, E., and Kresse, H. Modulation of collagen gel contraction by decorin. *The Biochemical Journal 314* (1996), 159–166.

[13] Bottomley, L. A. Scanning probe microscopy. *Analytical Chemistry 70* (1998), 425R–475R.

[14] Brown, R. Enhanced Fibroblast Contraction of 3D Collagen Lattices and Integrin Expression by TGF-β1 and -β3: Mechanoregulatory Growth Factors? *Experimental Cell Research 274*, 2 (2002), 310–322.

[15] Brown, R. A., Prajapati, R., McGrouther, D. A., Yannas, I. V., and Eastwood, M. Tensional homeostasis in dermal fibroblasts: Mechanical

responses to mechanical loading in three-dimensional substrates. *Journal of Cellular Physiology 175*, 3 (1998), 323–332.

[16] Burton, K., and Taylor, D. L. Traction forces of cytokinesis measured with optically modified elastic substrata. *Nature 385*, 6615 (1997), 450–454.

[17] Butler, J. P., Tolić-Nørrelykke, I. M., Fabry, B., and Fredberg, J. J. Traction fields, moments, and strain energy that cells exert on their surroundings. *American Journal of Physiology Cell Physiology 282*, 3 (2002), C595–C605.

[18] Campbell, B. H., Agarwal, C., and Wang, J. H. TGF-β1, TGF-β3, and PGE2 regulate contraction of human patellar tendon fibroblasts. *Biomechanics and Modeling in Mechanobiology 2*, 4 (jun 2004), 239–245.

[19] Campbell, B. H., Clark, W. W., and Wang, J. H. C. A multi-station culture force monitor system to study cellular contractility. *Journal of Biomechanics 36*, 1 (2003), 137–140.

[20] Chambers, A. F., Groom, A. C., and MacDonald, I. C. Dissemination and growth of cancer cells in metastatic sites. *Nature Reviews. Cancer 2*, 8 (2002), 563–572.

[21] Chan, C. E., and Odde, D. J. Traction dynamics of filopodia on compliant substrates. *Science (New York, N.Y.) 322*, 5908 (2008), 1687–1691.

[22] Chen, J., Li, H., SundarRaj, N., and Wang, J. H.-C. Alpha-smooth muscle actin expression enhances cell traction force. *Cell Motility and the Cytoskeleton 64*, 4 (2007), 248–257.

[23] Chu, P. S., Ma, W., Wong, S. C., Chu, R. W., Cheng, C., Wong, S., Tse, J. M., Lau, F., Yiu, M., and Man, C. The destruction of the lower

urinary tract by ketamine abuse: a new syndrome? *BJU International 102*, 11 (2008), 1616–1622.

[24] Cross, S. E., Jin, Y.-S., Rao, J., and Gimzewski, J. K. Nanomechanical analysis of cells from cancer patients. *Nature Nanotechnology 2*, 12 (2007), 780–783.

[25] Cross, S. E., Jin, Y.-S., Tondre, J., Wong, R., Rao, J., and Gimzewski, J. K. AFM-based analysis of human metastatic cancer cells. *Nanotechnology 19*, 38 (2008), 384003.

[26] Curtze, S., Dembo, M., Miron, M., and Jones, D. B. Dynamic changes in traction forces with DC electric field in osteoblast-like cells. *Journal of Cell Science 117*, Pt 13 (2004), 2721–2729.

[27] Dallon, J. C., and Ehrlich, H. P. A review of fibroblast-populated collagen lattices. *Wound Repair and Regeneration 16*, 4 (2008), 472–479.

[28] Darby, I. A., Laverdet, B., Bonté, F., and Desmoulière, A. Fibroblasts and myofibroblasts in wound healing. *Clinical, Cosmetic and Investigational Dermatology 7* (2014), 301–311.

[29] Davis, G. E., Pintar-Allen, K. A., Salazar, R., and Maxwell, S. A. Matrix metalloproteinase-1 and -9 activation by plasmin regulates a novel endothelial cell-mediated mechanism of collagen gel contraction and capillary tube regression in three-dimensional collagen matrices. *Journal of Cell Science 114*, Pt 5 (2001), 917–930.

[30] Delanoë-Ayari, H., Iwaya, S., Maeda, Y. T., Inose, J., Rivière, C., Sano, M., and Rieu, J. P. Changes in the magnitude and distribution of forces at different dictyostelium developmental stages. *Cell Motility and the Cytoskeleton 65*, 4 (2008), 314–331.

[31] Delanoe-Ayari, H., Rieu, J. P., and Sano, M. 4D traction force microscopy reveals asymmetric cortical forces in migrating dictyostelium cells. *Physical Review Letters 105*, 24 (2010), 2–5.

[32] Delvoye, P., Wiliquet, P., Levêque, J. L., Nusgens, B. V., and Lapière, C. M. Measurement of mechanical forces generated by skin fibroblasts embedded in a three-dimensional collagen gel. *Journal of Investigative Dermatology 97*, 5 (1991), 898–902.

[33] Dembo, M., and Wang, Y. L. Stresses at the cell-to-substrate interface during locomotion of fibroblasts. *Biophysical Journal 76*, 4 (1999), 2307–2316.

[34] Doyle, A. D., and Lee, J. Cyclic changes in keratocyte speed and traction stress arise from Ca2+-dependent regulation of cell adhesiveness. *Journal of Cell Science 118*, Pt 2 (2005), 369–379.

[35] DuFort, C. C., Paszek, M. J., and Weaver, V. M. Balancing forces: architectural control of mechanotransduction. *Nature Reviews. Molecular Cell Biology 12*, 5 (may 2011), 308–319.

[36] Eastwood, M., McGrouther, D. A., and Brown, R. A. A culture force monitor for measurement of contraction forces generated in human dermal fibroblast cultures: evidence for cell-matrix mechanical signalling. *BBA - General Subjects 1201*, 2 (1994), 186–192.

[37] Eastwood, M., Porter, R., Khan, U., McGrouther, G., and Brown, R. Quantitative analysis of collagen gel contractile forces generated by dermal fibroblasts and the relationship to cell morphology. *Journal of Cellular Physiology 166*, 1 (1996), 33–42.

[38] Ehrentraut, S., Frede, S., Stapel, H., Mengden, T., Grohé, C., Fandrey, J., Meyer, R., and Baumgarten, G. Antagonism of

lipopolysaccharide-induced blood pressure attenuation and vascular contractility. *Arteriosclerosis, Thrombosis, and Vascular Biology 27*, 10 (2007), 2170–2176.

[39] Ehrlich, H. P., and Rittenberg, T. Differences in the Mechanism for High-Versus Moderate-Density Fibroblast-Poplulated Collagen Lattice Contraction. *Journal of Cellular Physiology 185*, February (2000), 432–439.

[40] Ehrlich, H. P., Rockwell, W. B., Cornwell, T. L., and Rajaratnam, J. B. Demonstration of a direct role for myosin light chain kinase in fibroblast-populated collagen lattice contraction. *Journal of Cellular Physiology 146*, 1 (1991), 1–7.

[41] Engel, A., and Gaub, H. E. Structure and mechanics of membrane proteins. *Annual Review of Biochemistry 77* (2008), 127–148.

[42] Fang, Q., Liu, X., Abe, S., Kobayashi, T., Wang, X. Q., Kohyama, T., Hashimoto, M., Wyatt, T., and Rennard, S. I. Thrombin induces collagen gel contraction partially through PAR1 activation and PKC-E. *European Respiratory Journal 24*, 6 (2004), 918–924.

[43] Farris, A. B., and Colvin, R. B. Renal Interstitial fibrosis: mechanisms and evaluation in: current opinion in nephrology and hypertension. *Current Opinion in Nephrology and Hypertension 21*, 3 (2012), 289–300.

[44] Fitts, R. H. The cross-bridge cycle and skeletal muscle fatigue. *Journal of Applied Physiology (Bethesda, Md. : 1985) 104*, 2 (2008), 551–558.

[45] Fouchard, J., Bimbard, C., Bufi, N., Durand-Smet, P., Proag, A., Richert, A., Cardoso, O., and Asnacios, A. Three-dimensional cell body shape dictates the onset of traction force generation and growth of focal adhesions. *Proceedings of the National Academy of Sciences of the United States of America 111*, 36 (2014), 13075–13080.

[46] Franck, C., Maskarinec, S. A., Tirrell, D. A., and Ravichandran, G. Three-Dimensional Traction Force Microscopy: A New Tool for Quantifying Cell-Matrix Interactions. *PLoS ONE 6*, 3 (mar 2011), e17833.

[47] Freyman, T., Yannas, I., Pek, Y.-S., Yokoo, R., and Gibson, L. Micromechanics of Fibroblast Contraction of a CollagenGAG Matrix. *Experimental Cell Research 269*, 1 (2001), 140–153.

[48] Fujimura, T., Hotta, M., Kitahara, T., and Takema, Y. Loss of contraction force in dermal fibroblasts with aging due to decreases in myosin light chain phosphorylation enzymes. *Archives of Pharmacal Research 34*, 6 (2011), 1015–1022.

[49] Galbraith, C. G., and Sheetz, M. P. A micromachined device provides a new bend on fibroblast traction forces. *Proceedings of the National Academy of Sciences of the United States of America 94*, 17 (1997), 9114–9118.

[50] Galbraith, C. G., Yamada, K. M., and Sheetz, M. P. The relationship between force and focal complex development. *Journal of Cell Biology 159*, 4 (2002), 695–705.

[51] Giannone, G., Dubin-Thaler, B. J., Döbereiner, H.-G., Kieffer, N., Bresnick, A. R., and Sheetz, M. P. Periodic Lamellipodial Contractions Correlate with Rearward Actin Waves. *Cell 116*, 3 (jun 2004), 431–443.

[52] Grinnell, F. Fibroblasts, myofibroblasts, and wound contraction. *Journal of Cell Biology 124*, 4 (1994), 401–404.

[53] Grinnell, F. Mini-Review on the Cellular Mechanisms of Disease. *Journal of Cell Biology 124*, 4 (1994), 401–404.

[54] Grinnell, F. Fibroblast biology in three-dimensional collagen matrices. *Trends in Cell Biology 13*, 5 (2003), 264–269.

[55] Grinnell, F., and Petroll, W. M. Cell motility and mechanics in three-dimensional collagen matrices. *Annual Review of Cell and Developmental Biology 26* (2010), 335–361.

[56] Hansma, H. G., Kasuya, K., and Oroudjev, E. Atomic force microscopy imaging and pulling of nucleic acids. *Current Opinion in Structural Biology 14*, 3 (2004), 380–385.

[57] Harris, A., K, Wild, P., and Stopak, D. Silicone rubber substrata: a new wrinkle in the study of cell locomotion. *Science (New York, N.Y.) 208*, 4440 (1980), 177–179.

[58] Harris, A. K., Stopak, D., and Wild, P. Fibroblast traction as a mechanism for collagen morphogenesis. *Nature 290*, 5803 (1981), 249–251.

[59] Hersen, P., and Ladoux, B. Biophysics: Push it, pull it. *Nature 470*, 7334 (2011), 340–341.

[60] Hertz, H. Über die Berührung fester elastischer Körper. *Journal für die reine und angewandte Mathematik 92* (1882), 156–171.

[61] Hills, C. E., Bland, R., Bennett, J., Ronco, P. M., and Squires, P. E. TGF-β1 mediates glucose-evoked up-regulation of connexin-43 cell-to-cell communication in HCD-cells. *Cellular Physiology and Biochemistry 24*, 3-4 (2009), 177–186.

[62] Hills, C. E., and Squires, P. E. TGF-β1-induced epithelial-to-mesenchymal transition and therapeutic intervention in diabetic nephropathy. *American Journal of Nephrology 31*, 1 (2009), 68–74.

[63] Hills, C. E., and Squires, P. E. The role of TGF-β and epithelial-to mesenchymal transition in diabetic nephropathy. *Cytokine & Growth Factor Reviews 22*, 3 (2011), 131–139.

[64] Hirano, Y., Takahashi, H., Kumeta, M., Hizume, K., Hirai, Y., Otsuka, S., Yoshimura, S. H., and Takeyasu, K. Nuclear architecture and chromatin dynamics revealed by atomic force microscopy in combination with biochemistry and cell biology. *Pflügers Archiv-European Journal of Physiology 456*, 1 (2008), 139–153.

[65] Hirokawa, S., Shimanuki, T., Kitajima, H., Nishimori, Y., and Shimosaka, M. Knockdown of electron transfer flavoprotein β subunit reduced TGF-β-induced α-SMA mRNA expression but not COL1A1 in fibroblast-populated three-dimensional collagen gel cultures. *Journal of Dermatological Science 68*, 3 (2012), 179–186.

[66] Horie, M., Saito, A., Yamauchi, Y., Mikami, Y., Sakamoto, M., Jo, T., Nakajima, J., Takizawa, H., Nagase, T., and Kohyama, T. Histamine induces human lung fibroblast-mediated collagen gel contraction via histamine H1 receptor. *Experimental Lung Research 40*, 5 (2014), 222–236.

[67] Hu, K., Shi, H., Zhu, J., Deng, D., Zhou, G., Zhang, W., Cao, Y., and Liu, W. Compressed collagen gel as the scaffold for skin engineering. *Biomedical Microdevices 12*, 4 (2010), 627–635.

[68] Huet, E., Vallée, B., Szul, D., Verrecchia, F., Mourah, S., Jester, J. V., Hoang-Xuan, T., Menashi, S., and Gabison, E. E. Extracellular matrix metalloproteinase inducer/CD147 promotes myofibroblast differentiation by inducing alpha-smooth muscle actin expression and collagen gel contraction: implications in tissue remodeling. *The FASEB journal : official publication of the Federation of American Societies for Experimental Biology 22*, 4 (2008), 1144–1154.

[69] Hutter, J. L., and Bechhoefer, J. Calibration of atomic-force microscope tips. *Review of Scientific Instruments 64*, 7 (1993), 1868–1873.

[70] Huxley, A. F., and Niedergerke, R. Structural changes in muscle during contraction; interference microscopy of living muscle fibres. *Nature 173*, 4412 (1954), 971–973.

[71] Huxley, H., and Hanson, J. Changes in the Cross-Striations of Musle during Contraction and Stretch and their Structural interpretation. *Nature 173* (1954), 973–976.

[72] Huxley, H. E. The Mechanism of Muscular Contraction. *Science 164*, 3886 (1969), 1356–1366.

[73] Hynes, R. O. Integrins: versatility, modulation, and signaling in cell adhesion. *Cell 69*, 1 (1992), 11–25.

[74] Irwin, C. R., Myrillas, T., Smyth, M., Doogan, J., Rice, C., and Schor, S. L. Regulation of fibroblast-induced collagen gel contraction by interleukin-1beta. *Journal of Oral Pathology & Medicine 27*, 6 (1998), 255–259.

[75] Iwadate, Y., and Yumura, S. Actin-based propulsive forces and myosin-II-based contractile forces in migrating Dictyostelium cells. *Journal of Cell Science 121*, Pt 8 (2008), 1314–1324.

[76] Jacobs, C. R., Temiyasathit, S., and Castillo, A. B. Osteocyte mechanobiology and pericellular mechanics. *Annual Review of Biomedical Engineering 12* (aug 2010), 369–400.

[77] Jeng, J.-H., Lan, W.-H., Wang, J.-S., Chan, C.-P., Ho, Y.-S., Lee, P.-H., Wang, Y.-J., Wang, T.-M., Chen, Y.-J., and Chang, M.-C. Signaling mechanism of thrombin-induced gingival fibroblast-populated collagen gel contraction. *British Journal of Pharmacology 147*, 2 (2006), 188–98.

[78] Jin, T., Li, L., Siow, R. C. M., and Liu, K.-K. A novel collagen gel-based measurement technique for quantitation of cell contraction force. *Journal of The Royal Society Interface 12*, 106 (2015), 20141365.

[79] Johnson, C. L., Johnson, C. G., Bazan, E., Garver, D., Gruenstein, E., and Ahluwalia, M. Histamine receptors in human fibroblasts: inositol phosphates, Ca2+, and cell growth. *The American Journal of Physiology 258*, 3 Pt 1 (1990), C533–C543.

[80] Johnson, K. L. *Contact Mechanics*. Cambridge University Press, Cambridge, 1985.

[81] Kalluri, R., and Weinberg, R. A. The basics of epithelial-mesenchymal transition. *The Journal of Clinical Investigation 119*, 6 (2009), 1420–1428.

[82] Kanno, Y., Sasaki, Y., Shiba, Y., Yoshida-Noro, C., and Takeichi, M. Monoclonal antibody ECCD-1 inhibits intercellular communication in teratocarcinoma PCC3 cells. *Experimental Cell Research 152*, 1 (1984), 270–274.

[83] Karamichos, D., Brown, R. A., and Mudera, V. Collagen stiffness regulates cellular contraction and matrix remodeling gene expression. *Journal of Biomedical Materials Research Part A 83A*, 3 (2007), 887–894.

[84] Khetan, S., Guvendiren, M., Legant, W. R., Cohen, D. M., Chen, C. S., and Burdick, J. a. Degradation-mediated cellular traction directs stem cell fate in covalently crosslinked three-dimensional hydrogels. *Nature Materials 12*, 5 (2013), 458–465.

[85] Kol, N., Gladnikoff, M., Barlam, D., Shneck, R. Z., Rein, A., and Rousso, I. Mechanical properties of murine leukemia virus particles: effect of maturation. *Biophysical Journal 91*, 2 (2006), 767–774.

[86] Kolodney, M. S., and Wysolmerski, R. B. Isometric contraction by fibroblasts and endothelial cells in tissue culture: A quantitative study. *Journal of Cell Biology 117*, 1 (1992), 73–82.

[87] Kress, H., Stelzer, E. H. K., Holzer, D., Buss, F., Griffiths, G., and Rohrbach, A. Filopodia act as phagocytic tentacles and pull with discrete steps and a load-dependent velocity. *Proceedings of the National Academy of Sciences of the United States of America 104*, 28 (2007), 11633–11638.

[88] Kurosaka, H., Kurosaka, D., Kato, K., Mashima, Y., and Tanaka, Y. Transforming growth factor-β1 promotes contraction of collagen gel by bovine corneal fibroblasts through differentiation of myofibroblasts. *Investigative Ophthalmology and Visual Science 39*, 5 (1998), 699–704.

[89] Langholz, O., Rockel, D., Mauch, C., Kozlowska, E., Bank, I., Krieg, T., and Eckes, B. Collagen and collagenase gene expression in three-dimensional collagen lattices are differentially regulated by alpha 1 beta 1 and alpha 2 beta 1 integrins. *Journal of Cell Biology 131*, 6 (1995), 1903–1915.

[90] Leader, W. M., Stopak, D., and Harris, a. K. Increased contractile strength and tightened adhesions to the substratum result from reverse transformation of CHO cells by dibutyryl cyclic adenosine monophosphate. *Journal of Cell Science 64* (1983), 1–11.

[91] Lee, K. Y., and Mooney, D. J. Hydrogels for tissue engineering. *Chemical Reviews 101*, 7 (2001), 1869–1879.

[92] Legant, W. R., Choi, C. K., Miller, J. S., Shao, L., Gao, L., Betzig, E., and Chen, C. S. Multidimensional traction force microscopy reveals out-

of-plane rotational moments about focal adhesions. *Proceedings of the National Academy of Sciences of the United States of America 110*, 3 (2013), 881–866.

[93] Legant, W. R., Miller, J. S., Blakely, B. L., Cohen, D. M., Genin, G. M., and Chen, C. S. Measurement of mechanical tractions exerted by cells in three-dimensional matrices. *Nature Methods 7*, 12 (2010), 969–71.

[94] Li, B., Lin, M., Tang, Y., Wang, B., and Wang, J. H. C. A novel functional assessment of the differentiation of micropatterned muscle cells. *Journal of Biomechanics 41*, 16 (2008), 3349–3353.

[95] Li, B., and Wang, J. H. C. Application of sensing techniques to cellular force measurement. *Sensors (Switzerland) 10*, 11 (2010), 9948–9962.

[96] Li, B., and Wang, J. H. C. Fibroblasts and myofibroblasts in wound healing: Force generation and measurement. *Journal of Tissue Viability 20*, 4 (2011), 108–120.

[97] Li, F., Li, B., Wang, Q. M., and Wang, J. H. C. Cell shape regulates collagen type I expression in human tendon fibroblasts. *Cell Motility and the Cytoskeleton 65*, 4 (2008), 332–341.

[98] Liang, W., McDonald, P., McManus, B., van Breemen, C., and Wang, X. Histamine-induced Ca2+ signaling in human valvular myofibroblasts. *Journal of Molecular and Cellular Cardiology 35*, 4 (2016), 379–388.

[99] Lim, C. T., Zhou, E. H., Li, A., Vedula, S. R. K., and Fu, H. X. Experimental techniques for single cell and single molecule biomechanics. *Materials Science and Engineering C 26*, 8 (2006), 1278–1288.

[100] Lin, D. C., and Horkay, F. Nanomechanics of polymer gels and biological tissues: A critical review of analytical approaches in the Hertzian regime and beyond. *Soft Matter 4*, 4 (2008), 669–682.

[101] Liu, K.-K. Deformation behaviour of soft particles: a review. *Journal of Physics D: Applied Physics 39*, 11 (2006), R189–R199.

[102] Lo, C. M., Wang, H. B., Dembo, M., and Wang, Y. L. Cell movement is guided by the rigidity of the substrate. *Biophysical Journal 79*, 1 (2000), 144–152.

[103] Lombardi, M. L., Knecht, D. a., Dembo, M., and Lee, J. Traction force microscopy in Dictyostelium reveals distinct roles for myosin II motor and actin-crosslinking activity in polarized cell movement. *Journal of Cell Science 120* (2007), 1624–1634.

[104] Maksym, G. N., Fabry, B., Butler, J. P., Navajas, D., Tschumperlin, D. J., Laporte, J. D., and Fredberg, J. J. Mechanical properties of cultured human airway smooth muscle cells from 0.05 to 0.4 Hz. *Journal of Applied Physiology 89*, 4 (2000), 1619–1632.

[105] Marenzana, M., Wilson-Jones, N., Mudera, V., and Brown, R. A. The origins and regulation of tissue tension: Identification of collagen tension-fixation process in vitro. *Experimental Cell Research 312*, 4 (2006), 423–433.

[106] Marganski, W. A., De Biase, V. M., Burgess, M. L., and Dembo, M. Demonstration of altered fibroblast contractile activity in hypertensive heart disease. *Cardiovascular Research 60*, 3 (2003), 547–556.

[107] Maskarinec, S. a., Franck, C., Tirrell, D. a., and Ravichandran, G. Quantifying cellular traction forces in three dimensions. *Proceedings of the National Academy of Sciences of the United States of America 106*, 52 (2009), 22108–22113.

[108] Masszi, A., Fan, L., Rosivall, L., McCulloch, C. A., Rotstein, O. D., Mucsi, I., and Kapus, A. Integrity of cell-cell contacts is a critical

regulator of TGF-β1-induced epithelial-to-myofibroblast transition: role for β-catenin. *The American Journal of Pathology 165*, 6 (2004), 1955–1967.

[109] Matsumoto, H., Moir, L. M., Oliver, B. G. G., Burgess, J. K., Roth, M., Black, J. L., and McParland, B. E. Comparison of gel contraction mediated by airway smooth muscle cells from patients with and without asthma. *Thorax 62*, 10 (2007), 848–854.

[110] Moraes, C., Sun, Y., and Simmons, C. a. (Micro)managing the mechanical microenvironment. *Integrative Biology: Quantitative Biosciences from Bano to Macro 3*, 10 (2011), 959–971.

[111] Morales, S. A., Mareninov, S., Prasad, P., Wadehra, M., Braun, J., and Gordon, L. K. Collagen gel contraction by ARPE-19 cells is mediated by a FAK-Src dependent pathway. *Experimental Eye Research 85*, 6 (2007), 790–798.

[112] Moreno, A. P., Berthoud, V. M., Pérez-Palacios, G., and Pérez-Armendariz, E. M. Biophysical evidence that connexin-36 forms functional gap junction channels between pancreatic mouse β-cells. *American Journal of Physiology-Endocrinology And Metabolism 288*, 5 (2005), E948–E956.

[113] Morgan, C. J. A., Muetzelfeldt, L., and Curran, H. V. Consequences of chronic ketamine selfadministration upon neurocognitive function and psychological wellbeing: a one year longitudinal study. *Addiction 105*, 1 (2010), 121–133.

[114] Moser, T., Neef, A., and Khimich, D. Mechanisms underlying the temporal precision of sound coding at the inner hair cell ribbon synapse. *The Journal of Physiology 576*, 1 (2006), 55–62.

[115] Muller, D. J. AFM: A nanotool in membrane biology. *Biochemistry 47*, 31 (2008), 7986–7998.

[116] Munevar, S., Wang, Y. L., and Dembo, M. Distinct roles of frontal and rear cell-substrate adhesions in fibroblast migration. *Molecular Biology of the Cell 12*, 12 (2001), 3947–3954.

[117] Munevar, S., Wang, Y.-L., and Dembo, M. Traction Force Microscopy of Migrating Normal and H-ras Transformed 3T3 Fibroblasts. *Biophysical Journal 80*, 4 (2001), 1744–1757.

[118] Mutsaers, S. E., Bishop, J. E., McGrouther, G., and Laurent, G. J. Mechanisms of tissue repair: From wound healing to fibrosis. *International Journal of Biochemistry and Cell Biology 29*, 1 (1997), 5–17.

[119] Nakamura, Y., Hirano, S., Suzuki, K., Seki, K., Sagara, T., and Nishida, T. Signaling Mechanism of TGF-b1Induced Collagen Contraction Mediated by Bovine Trabecular Meshwork Cells. *Investigative Opthalmology & Visual Science 43*, 11 (2002), 3465–3472.

[120] Ngo, P., Ramalingam, P., Phillips, J. A., and Furuta, G. T. Collagen gel contraction assay. In *Cell-Cell Interactions: Methods and Protocols*. Springer, 2006, pp. 103–109.

[121] Nishiyama, T., Tominaga, N., Nakajima, K., and Hayashi, T. Quantitative Evaluation of the Factors Affecting the Process of Fibroblast-Mediated Collagen Gel Contraction by Separating the Process into Three Phases. *Collagen and Related Research 8*, 3 (1988), 259–273.

[122] Norman, L. L., Oetama, R. J., Dembo, M., Byfield, F., Hammer, D. A., Levitan, I., and Aranda-Espinoza, H. Modification of cellular cholesterol content affects traction force, adhesion and cell spreading. *Cellular and Molecular Bioengineering 3*, 2 (2010), 151–162.

[123] Oliver, T., Dembo, M., and Jacobson, K. Separation of propulsive and adhesive traction stresses in locomoting keratocytes. *Journal of Cell Biology 145*, 3 (1999), 589–604.

[124] Orgel, J. P. R. O., Miller, A., Irving, T. C., Fischetti, R. F., Hammersley, A. P., and Wess, T. J. The in situ supermolecular structure of type I collagen. *Structure 9*, 11 (2001), 1061–1069.

[125] Paul H. Ehrlich, Sun, B., Kainth, K. S., and Kromah, F. Elucidating the mechanism of wound contraction: Rapid versus sustained myosin ATPase activity in attached-delayed-released compared with free-floating fibroblast-populated collagen lattices. *Wound Repair and Regeneration 14*, 5 (2006), 625–632.

[126] Pelham, R. J., and Wang, Y.-l. Cell locomotion and focal adhesions are regulated by substrate flexibility. *Proceedings of the National Academy of Sciences 94*, 25 (1997), 13661–13665.

[127] Peperzak, K. A., Gilbert, T. W., and Wang, J. H. C. A multi-station dynamic-culture force monitor system to study cell mechanobiology. *Medical Engineering and Physics 26*, 4 (2004), 355–358.

[128] Pesen, D., and Hoh, J. H. Micromechanical architecture of the endothelial cell cortex. *Biophysical Journal 88*, 1 (2005), 670–679.

[129] Phillips, J. A., Vacanti, C. A., and Bonassar, L. J. Fibroblasts regulate contractile force independent of MMP activity in 3D-collagen. *Biochemical and Biophysical Research Communications 312*, 3 (2003), 725–732.

[130] Pollard, T. D. The cytoskeleton, cellular motility and the reductionist agenda. *Nature 422*, 6933 (2003), 741–745.

[131] Powell, C. a., Smiley, B. L., Mills, J., and Vandenburgh, H. H. Mechanical stimulation improves tissue-engineered human skeletal muscle. *American Journal of Physiology. Cell Physiology 283*, 5 (2002), C1557–C1565.

[132] Raymond, M. C., and Thompson, J. T. RPE-mediated collagen gel contraction. Inhibition by colchicine and stimulation by TGF-beta. *Investigative Ophthalmology and Visual Science 31*, 6 (1990), 1079–1086.

[133] Rodriguez, M., McGarry, P., and Sniadecki, N. Review on cell mechanics: Experimental and modeling approaches. *Applied Mechanics Reviews 65*, 6 (2013), 060801.

[134] Rösel, D., Brábek, J., Tolde, O., Mierke, C. T., Zitterbart, D. P., Raupach, C., Bicanová, K., Kollmannsberger, P., Panková, D., Vesely, P., Folk, P., and Fabry, B. Up-regulation of Rho/ROCK signaling in sarcoma cells drives invasion and increased generation of protrusive forces. *Molecular Cancer Research : MCR 6*, 9 (2008), 1410–1420.

[135] Rotsch, C., Jacobson, K., and Radmacher, M. Dimensional and mechanical dynamics of active and stable edges in motile fibroblasts investigated by using atomic force microscopy. *Proceedings of the National Academy of Sciences 96*, 3 (1999), 921–926.

[136] Schoen, I., Hu, W., Klotzsch, E., and Vogel, V. Probing cellular traction forces by micropillar arrays: Contribution of substrate warping to pillar deflection. *Nano Letters 10*, 5 (2010), 1823–1830.

[137] Sethi, K. K., Yannas, I. V., Mudera, V., Eastwood, M., McFarland, C., and Brown, R. A. Evidence for sequential utilization of fibronectin, vitronectin, and collagen during fibroblast-mediated collagen contraction. *Wound Repair and Regeneration 10*, 6 (2002), 397–408.

[138] Sharma, K., and Ziyadeh, F. N. Hyperglycemia and diabetic kidney disease: the case for transforming growth factorβ as a key mediator. *Diabetes 44*, 10 (1995), 1139–1146.

[139] Siamantouras, E., Hills, C. E., Squires, P. E., and Liu, K.-K. Quantifying cellular mechanics and adhesion in renal tubular injury using single cell force spectroscopy. *Nanomedicine: Nanotechnology, Biology and Medicine 12*, 4 (2016), 1013–1021.

[140] Silva, L. P. Imaging proteins with atomic force microscopy: an overview. *Current Protein and Peptide Science 6*, 4 (2005), 387–395.

[141] Solon, J., Levental, I., Sengupta, K., Georges, P. C., and Janmey, P. A. Fibroblast adaptation and stiffness matching to soft elastic substrates. *Biophysical Journal 93*, 12 (2007), 4453–4461.

[142] Spudich, J. The myosin swinging cross-bridge model. *Nature Reviews. Molecular Cell Biology 2*, 5 (2001), 387–392.

[143] Srirangam, S., and Mercer, J. Ketamine bladder syndrome: an important differential diagnosis when assessing a patient with persistent lower urinary tract symptoms. *BMJ Case Reports 2012* (2012), bcr2012006447.

[144] Steinberg, B. M., Smith, K., Colozzo, M., and Pollack, R. Establishment and transformation diminish the ability of fibroblasts to contract a native collagen gel. *Journal of Cell Biology 87*, 1 (1980), 304–308.

[145] Sun, Y., Chen, C. S., and Fu, J. Forcing stem cells to behave: a biophysical perspective of the cellular microenvironment. *Annual Review of Biophysics 41* (2012), 519–542.

[146] Suresh, S. Biomechanics and biophysics of cancer cells. *Acta Materialia 55*, 12 (2007), 3989–4014.

[147] Tan, J. L., Tien, J., Pirone, D. M., Gray, D. S., Bhadriraju, K., and Chen, C. S. Cells lying on a bed of microneedles: an approach to isolate mechanical force. *Proceedings of the National Academy of Sciences of the United States of America 100*, 4 (2003), 1484–1489.

[148] Tatara, Y. On Compression of Rubber Elastic Sphere Over a Large Range of DisplacementsPart 1: Theoretical Study. *Journal of Engineering Materials and Technology 113*, 3 (1991), 285–291.

[149] Tee, S.-Y., Fu, J., Chen, C. S., and Janmey, P. A. Cell shape and substrate rigidity both regulate cell stiffness. *Biophysical Journal 100*, 5 (2011), L25–L27.

[150] Tingström, a., Heldin, C. H., Rubin, K., Tingstrom, A., Heldin, C. H., and Rubin, K. Regulation of fibroblast-mediated collagen gel contraction by platelet-derived growth factor, interleukin-1 alpha and transforming growth factor-beta 1. *Journal of Cell Science 102* (1992), 315–322.

[151] Tolić-Nørrelykke, I. M., and Wang, N. Traction in smooth muscle cells varies with cell spreading. *Journal of Biomechanics 38*, 7 (2005), 1405–1412.

[152] Tomasek, J. J., Haaksma, C. J., Eddy, R. J., and Vaughan, M. B. Fibroblast contraction occurs on release of tension in attached collagen lattices: dependency on an organized actin cytoskeleton and serum. *The Anatomical record 232*, 3 (1992), 359–368.

[153] Travis, J. a., Hughes, M. G., Wong, J. M., Wagner, W. D., and Geary, R. L. Hyaluronan enhances contraction of collagen by smooth muscle cells and adventitial fibroblasts: Role of CD44 and implications for constrictive remodeling. *Circulation Research 88*, 1 (2001), 77–83.

[154] Tsai, T., Cha, T., Lin, C., Tsao, C., Tang, S., Chuang, F., Wu, S., Sun, G., Yu, D., and Chang, S. Ketamineassociated bladder dysfunction. *International Journal of Urology 16*, 10 (2009), 826–829.

[155] Unal, M., Alapan, Y., Jia, H., Varga, A. G., Angelino, K., Aslan, M., Sayin, I., Han, C., Jiang, Y., Zhang, Z., and Gurkan, U. A. Micro and Nano-scale Technologies for Cell Mechanics. *Nanobiomedicine 1*, 5 (2014), 1–29.

[156] Van Vliet, K. J., Bao, G., and Suresh, S. The biomechanics toolbox: Experimental approaches for living cells and biomolecules. *Acta Materialia 51*, 19 (2003), 5881–5905.

[157] Wang, H.-b. B., Dembo, M., Wang, Y.-l. L., Ghassemi, S., Meacci, G., Liu, S., Gondarenko, A. a., Mathur, A., Roca-cusachs, P., Sheetz, M. P., Hone, J., Leight, J. L., Wozniak, M. a., Chen, S., Lynch, M. L., and Christopher, S. Substrate flexibility regulates growth and apoptosis of normal but not transformed cells. *American Journal of Physiology. Cell Physiology 279*, 5 (2013), C1345–1350.

[158] Wang, N., Tolić-Nørrelykke, I. M., Chen, J., Mijailovich, S. M., Butler, J. P., Fredberg, J. J., and Stamenović, D. Cell prestress. I. Stiffness and prestress are closely associated in adherent contractile cells. *American Journal of Physiology. Cell Physiology 282*, 3 (2002), C606–C616.

[159] Wang, Y., Botvinick, E. L., Zhao, Y., Berns, M. W., Usami, S., Tsien, R. Y., and Chien, S. Visualizing the mechanical activation of Src. *Nature 434*, 7036 (2005), 1040–1045.

[160] Webster, K. D., Crow, A., and Fletcher, D. A. An AFM-based stiffness clamp for dynamic control of rigidity. *PLoS One 6*, 3 (2011), e17807.

[161] Weder, G., Vörös, J., Giazzon, M., Matthey, N., Heinzelmann, H., and Liley, M. Measuring cell adhesion forces during the cell cycle by force spectroscopy. *Biointerphases 4*, 2 (2009), 27–34.

[162] Wiesendanger, R. Scanning Probe Microscopy and Spectroscopy, 1994.

[163] Wood, D., Cottrell, A., Baker, S. C., Southgate, J., Harris, M., Fulford, S., Woodhouse, C., and Gillatt, D. Recreational ketamine: from pleasure to pain. *BJU International 107*, 12 (2011), 1881–1884.

[164] Wright, M. Pharmacologic effects of ketamine and its use in veterinary medicine. *Journal of the American Veterinary Medical Association 180*, 12 (1982), 1462–1471.

[165] Wu, M., Fannin, J., Rice, K. M., Wang, B., and Blough, E. R. Effect of aging on cellular mechanotransduction. *Ageing Research Reviews 10*, 1 (jan 2011), 1–15.

[166] Wynne, B. M., Chiao, C.-W., and Webb, R. C. Vascular smooth muscle cell signaling mechanisms for contraction to angiotensin II and endothelin-1. *Journal of the American Society of Hypertension 3*, 2 (may 2016), 84–95.

[167] Yanase, M., Ikeda, H., Ogata, I., Matsui, A., Noiri, E., Tomiya, T., Arai, M., Inoue, Y., Tejima, K., Nagashima, K., Nishikawa, T., Shibata, M., Ikebe, M., Rojkind, M., and Fujiwara, K. Functional diversity between Rho-kinase- and MLCK-mediated cytoskeletal actions in a myofibroblast-like hepatic stellate cell line. *Biochemical and Biophysical Research Communications 305*, 2 (2003), 223–228.

[168] Yang, Z., Lin, J. S., Chen, J., and Wang, J. H. C. Determining substrate displacement and cell traction fields-a new approach. *Journal of Theoretical Biology 242*, 3 (2006), 607–616.

[169] Zagai, U., Skold, C. M., Trulson, A., Venge, P., and Lundahl, J. The effect of eosinophils on collagen gel contraction and implications for tissue remodelling. *Clinical and Experimental Immunology 135*, 3 (2004), 427–433.

[170] Zaidel-Bar, R., Cohen, M., Addadi, L., and Geiger, B. Hierarchical assembly of cell-matrix adhesion complexes. *Biochemical Society transactions 32*, Pt3 (2004), 416–420.

[171] Zeisberg, M., and Kalluri, R. The role of epithelial-to-mesenchymal transition in renal fibrosis. *Journal of Molecular Medicine 82*, 3 (2004), 175–181.

[172] Zhang, H., Dai, S., Bi, J., and Liu, K.-K. Biomimetic three-dimensional microenvironment for controlling stem cell fate. *Interface Focus 1*, 5 (oct 2011), 792–803.

[173] Zhu, Y. K., Umino, T., Liu, X. D., Wang, H. J., Romberger, D. J., Spurzem, J. R., and Rennard, S. I. Contraction of Fibroblast-Containing Collagen Gels: Initial Collagen Concentration Regulates the Degree of Contraction and Cell Survival. *In Vitro Cellular & Developmental Biology - Animal 37*, 1 (2001), 10–16.